

# Interpretation of ab initio Calculations of Cerium Compounds and Predictive Power of Density Functional Theory Calculations for Iodine Catalysis

INAUGURAL-DISSERTATION

zur  
Erlangung des Doktorgrades  
der Mathematisch-Naturwissenschaftlichen Fakultät  
der Universität zu Köln

vorgelegt von  
  
OLIVER MOOSSEN  
  
aus Hagen

Köln 2018

Gutachter: 1. Prof. Dr. Michael Dolg  
2. PD Dr. Michael Hanrath

Datum der Einreichung:	15.03.2018
Datum der mündlichen Prüfung:	16.05.2018

---

*Ein schlauer Satz*

Ein schlauer Mensch





# Abstract

This thesis is divided into two parts, the investigation of the electronic structure of cerium complexes paying special attention on the relevance of the cerium 4f orbitals in order to assign the oxidation state of cerium and the quality of density functional theory (DFT) computations and their consistency with experimental data in order to investigate the reliability of such calculations and their predictive credibility for reactions.

In the first part, the electronic structure of the ground state of several cerium complexes,  $\text{Ce}(\text{C}_8\text{H}_8)_2$ ,  $\text{Ce}(\text{C}_8\text{H}_6)_2$ ,  $\text{Cp}_2\text{CeZ}$  ( $\text{Z} = \text{CH}_2, \text{CH}^-, \text{NH}, \text{O}, \text{F}^+$ ) as well as  $\text{CH}_2\text{CeF}_2$  and  $\text{OCeF}_2$  were investigated. Using CASSCF computations including orbital rotations of the active orbitals, the underlying reason for the different interpretations of the cerium oxidation state ( $\text{Ce(III)}$  and  $\text{Ce(IV)}$ ) of cerocene was found. By orbital rotation nearly pure cerium 4f and ligand  $\pi$  orbitals were obtained for cerocene. The CASSCF wavefunction based on these localized orbitals was analyzed and a leading  $f^1\pi^3$  was obtained. Therefore, cerocene was classified as a  $\text{Ce(III)}$  compound. This result is in agreement to spectroscopic XANES data. Using the same computational technique, the electronic structure of all other cerium compounds was investigated. Similar to cerocene, nearly pure Ce 4f and ligand orbitals were obtained for  $\text{Ce}(\text{C}_8\text{H}_6)_2$ ,  $\text{Cp}_2\text{CeCH}_2$ ,  $\text{Cp}_2\text{CeCH}^-$  and  $\text{CH}_2\text{CeF}_2$  resulting in a leading  $f^1\pi^1$  or  $f^1p^1$  configuration. Therefore these systems were classified as  $\text{Ce(III)}$  compounds. In contrast the complexes  $\text{Cp}_2\text{CeNH}$ ,  $\text{Cp}_2\text{CeO}$  and  $\text{OCeF}_2$  should be described as mixed valent  $\text{Ce(III)/Ce(IV)}$  compounds, whereas the  $\text{Cp}_2\text{CeF}^+$  complex can be categorized as a  $\text{Ce(IV)}$  compound. It can be shown that the most compact wavefunction, which correctly describes the influence of the Ce 4f orbitals can be obtained for all molecules, except cerocene, at the CASSCF(2,2) level. These compact wavefunctions based on localized orbitals were used to investigate the nature of the orbital interactions of the active orbitals. The results revealed that the 4f- $\pi$  orbital interaction of  $\text{Ce}(\text{C}_8\text{H}_6)_2$  as well as the 4f-p orbital interaction of  $\text{CH}_2\text{CeCp}_2$ ,  $\text{CH}^-\text{CeCp}_2$  and  $\text{CH}_2\text{CeF}_2$  of the Ce- $\text{CH}_2$  or Ce-CH bonds can be classified as covalent interactions. The mixed valent systems revealed an increased ionic character of the active orbital interactions for the Ce-NH and Ce-O bonds, whereas the Ce-F bond can be clearly described as ionic. These results are in a good agreement to the assigned

---

oxidation states.

In the second part of this thesis, the quality and reliability of DFT computations of reactions compared to experimental results was investigated. The energies of the starting materials, the products as well as the transition states of several iodine catalyzed reactions were computed using various DFT methods. The results revealed that experimental outcomes (reaction time and product yields) can not be computed reliably for the whole set of investigated reactions. Additionally, it revealed that modern and older functionals possess the same predictive credibility. Nevertheless it was shown that all experimental outcomes of the reactions between methyl acrylate and aniline derivatives were reproduced by DFT methods. Therefore a reliable reaction prediction using DFT methods is not generally performable, but based on experimental results, DFT computations can predict reaction trends of very similar systems correctly. These correct predictions were obtained by all used functionals, which emphasizes that for a specific application modern and older functionals might possess the same quality.

# Kurzzusammenfassung

Diese Arbeit untergliedert sich in zwei große Themenbereiche, die Untersuchung der Elektronenstruktur von Cer Komplexen im Hinblick auf die Bedeutung der 4f-Orbitale und der Klassifizierung des Oxidationszustandes des Cer-Ions in den chemischen Verbindungen, sowie der Untersuchung der Qualität von DFT Rechnungen im Hinblick auf die korrekte Reproduktion von experimentellen Ergebnissen und ihrer Einsatzfähigkeit im Bereich der Reaktionsprädiktion.

Im ersten Teil dieser Arbeiten wurde die Elektronenstruktur von verschiedenen Cer-Verbindungen,  $\text{Ce}(\text{C}_8\text{H}_8)_2$ ,  $\text{Ce}(\text{C}_8\text{H}_6)_2$ ,  $\text{Cp}_2\text{CeZ}$  ( $\text{Z} = \text{CH}_2, \text{CH}^-, \text{NH}, \text{O}, \text{F}^+$ ), sowie  $\text{CH}_2\text{CeF}_2$  und  $\text{OCeF}_2$  untersucht. Zunächst konnte mithilfe von CASSCF-Rechnungen in Kombination mit einer Orbitalrotation der aktiven Orbitale, die Ursache für die verschiedenen Interpretationen des Cer-Oxidationszustandes ( $\text{Ce}(\text{III})$  und  $\text{Ce}(\text{IV})$ ) im Cerocen aufgeklärt werden. Anschließend konnten durch Entmischung der Molekülorbitale von Cerocen, Orbitale erzeugt werden, die entweder nahezu ausschließlich 4f-Charakter des Cers oder  $\pi$ -Charakter der Liganden aufwiesen. Auf der Basis dieser Orbitale konnte die CASSCF-Wellenfunktion analysiert werden, wodurch sich eine führende  $f^1\pi^3$  zeigte und somit die Klassifizierung dieser Verbindung als  $\text{Ce}(\text{III})$ -Komplex ermöglichte, welche konsistent zu den spektroskopischen XANES-Daten ist. An die Erkenntnisse des Cerocens anschließend, wurde die Elektronenstruktur weiterer, bereits genannter, Cer Komplexe analysiert. Es konnte hierbei gezeigt werden, dass vergleichbar zum Cerocen, die Molekülorbitale von  $\text{Ce}(\text{C}_8\text{H}_6)_2$ ,  $\text{Cp}_2\text{CeCH}_2$ ,  $\text{Cp}_2\text{CeCH}^-$  und  $\text{CH}_2\text{CeF}_2$  ebenfalls in nahezu reine Cer 4f- und  $\pi$ - bzw. p-Ligandenorbitale überführt werden können. Durch eine folgende CASSCF-Wellenfunktionanalyse konnten diese Verbindungen ebenfalls als  $\text{Ce}(\text{III})$ -Komplexe klassifiziert werden. Die weiteren Verbindungen zeigten ein abweichendes Verhalten. Die Komplexe  $\text{Cp}_2\text{CeNH}$ ,  $\text{Cp}_2\text{CeO}$  und  $\text{OCeF}_2$  konnten als gemischt-valente  $\text{Ce}(\text{III})/\text{Ce}(\text{IV})$ -Verbindungen klassifiziert werden. Die einzige Verbindung, die als  $\text{Ce}(\text{IV})$ -Verbindung eingestuft werden konnte ist  $\text{Cp}_2\text{CeF}^+$ , bei der die Bedeutung der Cer 4f-Orbitale vernachlässigbar war. Darüber hinaus konnte für alle Moleküle, außer Cerocen, eine kompakte CASSCF(2,2)-Wellenfunktion erhalten werden, ohne die korrekte Beschreibung der 4f-Orbitale zu verlieren. Diese Wellenfunk-

---

tion ermöglichte eine Untersuchung der Orbitalwechselwirkungen der aktiven Orbitale, wodurch gezeigt werden konnte, dass die 4f- $\pi$  Orbitalwechselwirkung im  $\text{Ce}(\text{C}_8\text{H}_6)_2$ , sowie die 4f-p-Wechselwirkung der Ce-CH<sub>2</sub>- bzw. Ce-CH-Bindungen in  $\text{CH}_2\text{CeCp}_2$ ,  $\text{CH}^-\text{CeCp}_2$  und  $\text{CH}_2\text{CeF}_2$  als kovalent eingestuft werden können. Die gemischt valenten Cer Komplexe zeigten einen erhöhten ionischen Orbitalwechselwirkungscharakter bei den Ce-NH- bzw. Ce-O-Bindungen. Der  $\text{Cp}_2\text{CeF}^+$  Komplex zeigte eine eindeutige ionische Wechselwirkung der Ce-F-Bindung. Somit ist ebenfalls die Wechselwirkungsklassifizierung in Übereinstimmung mit den berechneten Oxidationszuständen.

Im zweiten Teil dieser Arbeit wurde die Qualität von DFT-Rechnungen und experimentellen Ergebnissen der organischen Synthese untersucht. Als Beispielsystem dienten verschiedene durch Iod katalysierte Reaktionen, deren Edukte, Produkte und Übergangszustände mit verschiedenen Methoden berechnet wurden. Es konnte hierbei gezeigt werden, dass eine verlässliche Übereinstimmung mit den experimentellen Ergebnissen (Reaktionszeit und Ausbeute) nicht über die gesamte Anzahl an untersuchten Ergebnissen erhalten werden kann. Weiterhin konnte gezeigt werden, dass moderne und ältere Funktionale eine ähnliche Aussagekraft auf die Prädiktion haben. Eindeutige verlässliche Übereinstimmung mit den experimentellen Ergebnissen konnten nur innerhalb der Reaktionen erhalten werden, die Anilinderivate mit Methacrylat umsetzten. Somit konnte geschlussfolgert werden, dass eine richtige Vorhersage von Reaktionsausgängen nicht uneingeschränkt möglich ist, jedoch ausgehend von experimentellen Erkenntnissen ist es möglich chemisch sehr ähnliche Reaktionen richtig vorherzuberechnen. Diese Vorhersage ist mit allen verwendeten Funktionalen möglich, wodurch gezeigt wurde, dass moderne Funktionale bei einer spezifischen Anwendung keine bessere Qualität als ältere Funktionale aufweisen müssen.

# Contents

<b>1</b>	<b>Introduction</b>	<b>3</b>
<b>2</b>	<b>Theory</b>	<b>5</b>
2.1	Schrödinger Equation and the Form of the Hamiltonian . . . . .	5
2.2	The Hartree-Fock Method . . . . .	8
2.3	Correlation Methods . . . . .	12
2.3.1	Configuration Interaction . . . . .	12
2.3.2	Multi-configurational Self-consistent Field . . . . .	16
2.3.3	Multi-reference Configuration Interaction . . . . .	18
2.3.4	Coupled Cluster . . . . .	19
2.4	Relativistic Quantum Chemistry . . . . .	22
2.4.1	Foundations of the Special Theory of Relativity . . . . .	22
2.4.2	Dirac Equation . . . . .	24
2.5	Pseudopotentials . . . . .	26
2.6	Population analysis . . . . .	29
2.7	Density Functional Theory . . . . .	31
2.7.1	Fundamentals of DFT . . . . .	31
2.7.2	Functional Types . . . . .	33
<b>3</b>	<b>Results</b>	<b>35</b>
3.1	Cerocene . . . . .	35
3.1.1	Introduction . . . . .	35
3.1.2	Computational Details . . . . .	37
3.1.3	Electronic Structure . . . . .	38
3.1.4	Conclusions . . . . .	40
3.2	Bis( $\eta^8$ -pentalene)cerium . . . . .	41
3.2.1	Introduction . . . . .	41
3.2.2	Computational Details . . . . .	42
3.2.3	Ground State Geometry . . . . .	43

3.2.4	Electronic Structure and Active Orbital Rotation . . . . .	45
3.2.5	Occupation Number Fluctuation Analysis . . . . .	48
3.2.6	Conclusions . . . . .	49
3.3	Bis(cyclopentadienyl)cerium Compounds . . . . .	50
3.3.1	Introduction . . . . .	50
3.3.2	Computational Details . . . . .	51
3.3.3	Ground State Geometries . . . . .	52
3.3.4	Bond Distances and Force Constants . . . . .	56
3.3.5	Electronic Structure . . . . .	58
3.3.6	Active Orbital Rotation . . . . .	70
3.3.7	Occupation Number Fluctuation Analysis . . . . .	75
3.3.8	Conclusions . . . . .	77
3.4	Cerium Fluorine Compounds . . . . .	78
3.4.1	Introduction . . . . .	78
3.4.2	Computational Details . . . . .	79
3.4.3	Ground State Geometries . . . . .	81
3.4.4	Spin-Multiplicity of the Ground State . . . . .	83
3.4.5	Electronic Structure and the Relevance of the 4f Orbitals . . . . .	84
3.4.6	Active Orbital Rotation . . . . .	87
3.4.7	Occupation Number Fluctuation Analysis . . . . .	91
3.4.8	Vibrational Frequencies . . . . .	92
3.4.9	Conclusions . . . . .	95
3.5	Density Functional Theory Investigations . . . . .	96
3.5.1	Introduction . . . . .	96
3.5.2	Computational Details . . . . .	96
3.5.3	Iodine Catalysis . . . . .	97
3.5.4	Unbenchmarked iodine catalysis . . . . .	99
3.5.5	The Effect of the Dispersion Correction . . . . .	102
3.5.6	Barrierless Decomposition . . . . .	103
3.5.7	Computational Validation . . . . .	105
3.5.8	Experimental Benchmarking . . . . .	107
3.5.9	Iodine Catalysis in CH <sub>2</sub> Cl <sub>2</sub> at 25°C . . . . .	109
3.5.10	R-NH and R-NH <sub>2</sub> Compounds . . . . .	112
3.5.11	Reaction of Aniline and Methyl Acrylate . . . . .	114
3.5.12	Height Consistency for the Iodine Catalysis in CH <sub>2</sub> Cl <sub>2</sub> at 25 °C . . . . .	116
3.5.13	Iodine Catalysis in Toluene at 70°C . . . . .	118

3.5.14 Iodine Catalysis at 100°C . . . . .	122
3.5.15 Experimentally Undescribed Iodine Catalyzed Systems . . . . .	123
3.5.16 Catalyzed and Uncatalyzed Transition States . . . . .	125
3.5.17 Statistically Derived Shifts Based on Experimental Data . . . . .	127
3.5.18 Iodine Catalyzed Transition States including Shifts . . . . .	129
3.5.19 Conclusions . . . . .	130
<b>A Appendix</b>	<b>131</b>
A.1 Electronic Structure of 4f Element Compounds . . . . .	131
A.2 Experimental Benchmark . . . . .	136
A.3 Reaction Energies of the Iodine Catalysis . . . . .	140
A.3.1 Dichlormethane at 25 °C . . . . .	140
A.3.2 Toluene at 70 °C . . . . .	148
A.3.3 Toluene at 100 °C . . . . .	156
<b>References</b>	<b>175</b>





# 1 Introduction

Over the last decades computational chemistry became an important part of the chemical scientific community in general. A huge variety of computational methods arised, which can be mainly divided into wave function-based methods, density functional theory methods and molecular mechanics. These methods are used in all fields of chemistry, e.g. simulating spectra, computing bond distances, finding the most stable conformer of a molecule or investigating reaction mechanisms. In principle, any measurable value can be calculated by computational methods. According to the physical complexity of chemical systems, all developed and applied methods are approximations of the exact description. Therefore, the results obtained by computations as well as conclusions based on these results should be treated with caution and need to be checked. Nevertheless, quantum chemistry can be used to support experimental research and to derive insights for chemical systems, where suitable experiments are not available.

In this work, computational methods are used to investigate the electronic structure of cerium complexes in order to assign reasonable oxidation states to cerium and to point out the relevance of the 4f orbitals in these compounds. The concept of oxidation states is fundamental in chemistry, but especially for multi-reference systems it is not well defined. Therefore, a suitable procedure for the assignment of oxidation states for such systems, using wave function-based methods, will be presented and discussed.

For large systems density functional theory methods have to be used, according to the huge computational demand of highly accurate wave function-based methods. Many DFT computations are performed to support an experimental outcome and are performed after the experimental results were obtained. Predictive DFT computations are rare. However, one target of computational chemistry is to develop methods, which can be used to correctly predict reaction outcomes. In order to investigate the correctness of DFT computations, several iodine catalyzed reactions were computed with a variety of available standard DFT functionals. The results, paying special attention on the correctly computed experimentally observed outcomes and trends, will be discussed.



## 2 Theory

For not explicitly time-dependant Hamiltonians the fundamental task of theoretical chemistry is to solve the Schrödinger equation for a specific quantum mechanical system. An exact solution of this equation is solely possible for the hydrogen atom or hydrogen-like systems, whereas more complex quantum chemical systems have to be solved approximately. This difficulty lead to various approaches and methods for the approximate solution of the Schrödinger equation. In the following sections, the concepts of quantum chemistry and main aspects of common approaches will be outlined. The discussions and fundamental formulas given in the following chapter mainly follow the book of Szabo and Ostlund [1], Jensen [2] as well as the book of Levine and Helgaker [3]. For a compact description of the corresponding equations, atomic units are used, implying that the reduced Planck's constant, the elementary charge, the rest mass of the electron as well as the Coulomb force constant are set to the numerical value of one (i.e.  $\hbar = e = m_e = \frac{1}{4\pi\epsilon_0} = 1$ ).

### 2.1 Schrödinger Equation and the Form of the Hamiltonian

The most basic equation of nonrelativistic quantum chemistry is the time-dependent Schrödinger equation. For an hydrogen atom it can be written as

$$i\hbar\frac{\partial}{\partial t}|\Psi(\vec{x},t)\rangle = \hat{H}|\Psi(\vec{x},t)\rangle. \quad (2.1)$$

$\hat{H}$ : Hamiltonian

$\Psi$ : Wave function

$\vec{x}$ : Vector of the spatial coordinates and the spin of the electron

t: Time

Equation (2.1) describes the state of a quantum chemical system at any time t entirely. Any property can be derived by applying the corresponding operator to the wave function, e.g.  $\hat{H}$  for the energy of the system.

The time dependency can be separated by using a product ansatz of the wave function with a time-dependent function  $\Theta(t)$  and function  $\Psi(\vec{x})$ , which depends on the spatial coordinates and the spin of the electrons

$$|\Psi(\vec{x}, t)\rangle = \Theta(t)|\Psi(\vec{x})\rangle. \quad (2.2)$$

Combining the equations (2.1) and (2.2) leads to the differential equation

$$i\hbar \frac{\partial}{\partial t} \Theta(t) = E \Theta(t), \quad (2.3)$$

where  $E$  is the energy of the system and which has to be solved to obtain the time-dependent part of the wave function. The resulting formula is given by

$$\Theta(t) \propto \exp\left(-i \frac{Et}{\hbar}\right). \quad (2.4)$$

After applying this separation ansatz, the time-independent Schrödinger equation is obtained as

$$\hat{H}|\Psi(\vec{x})\rangle = E|\Psi(\vec{x})\rangle, \quad (2.5)$$

constituting the most important equation in the field of non-relativistic quantum chemistry according to the fact that most applications treat stationary states and properties.

The Hamiltonian includes the physics of a system, for instance in the case of a molecule in the non-relativistic case the operator is constructed from the kinetic energy of the electrons  $E_{\text{kin}}(\text{e})$ , the kinetic energy of the nuclei  $E_{\text{kin}}(\text{nuc})$ , the electron-electron repulsion  $E_{\text{pot}}(\text{e}, \text{e})$ , the electron-nuclei attraction  $E_{\text{pot}}(\text{e}, \text{nuc})$  and the repulsion of all nuclei  $E_{\text{pot}}(\text{nuc}, \text{nuc})$  and is given by following equation (2.6)

$$\begin{aligned} \hat{H} &= E_{\text{kin}}(\text{e}) + E_{\text{pot}}(\text{e}, \text{e}) + E_{\text{pot}}(\text{e}, \text{nuc}) + E_{\text{pot}}(\text{nuc}, \text{nuc}) + E_{\text{kin}}(\text{nuc}) \\ &= -\frac{1}{2} \sum_{i=1}^n \Delta_i + \sum_{i<j}^n \frac{1}{r_{ij}} - \sum_{i=1}^n \sum_{I=1}^N \frac{Z_I}{r_{iI}} + \sum_{I<J}^N \frac{Z_I Z_J}{r_{IJ}} - \frac{1}{2} \sum_{I=1}^N \frac{1}{M_I} \Delta_I. \end{aligned} \quad (2.6)$$

$n$ : Number of electrons

$i, j$ : Electron indices

$N$ : Number of nuclei

$I, J$ : Nuclei indices

$Z_I$ : Nuclear charge of atom  $I$

$r_{ij}$ : Distance of the particles  $i$  and  $j$

In principle the Schrödinger equation (2.5), using the Hamiltonian shown in equation (2.6), has to be solved for the electrons and the nuclei for a molecular quantum system. As a consequence, the total wave function is a function constructed from an electronic and a nuclear part. The Born-Oppenheimer approximation states that the wave function of the nuclei and the wave function of the electrons can be separated by applying a product ansatz

$$\Psi_{total} = \Psi_{elec} \cdot \Psi_{nuc}. \quad (2.7)$$

Since the mass of the nuclei in comparison to the electron's is much larger, the nuclei are assumed to be fixed at their local coordinates. Therefore the kinetic energy of all nuclei can be assumed to be zero and the repulsion energy of the nuclei can be added as a constant for a specific geometrical arrangement of the investigated molecule. This results in the following equation, that constitutes a simplified form of the Hamiltonian,

$$\hat{H}_{el} = -\frac{1}{2} \sum_{i=1}^n \Delta_i + \sum_{i<j}^n \frac{1}{r_{ij}} - \sum_{i=1}^n \sum_{I=1}^N \frac{Z_I}{r_{iI}}, \quad (2.8)$$

that is often referred to as the electronic Hamiltonian  $\hat{H}_{el}$  and is used in many computational methods in quantum chemistry.

## 2.2 The Hartree-Fock Method

Due to the interaction of electrons in instantaneous motion, the Schrödinger equation can not be solved exactly for many-electron systems. According to this problem, many computational methods intend to calculate an approximate solution of the Schrödinger equation. One fundamental approach is the Hartree-Fock (HF) method that nowadays is the basis for many so-called correlation or post Hartree-Fock methods and approaches, e.g. configuration interaction (CI) or coupled cluster (CC).

The wave function ansatz of the HF approach is a single determinant composed of one electron wavenfunctions named spin orbitals. This wave function ansatz is usually called Slater determinant [4] and can be written as

$$|\Psi(\vec{x}_1, \vec{x}_2, \dots, \vec{x}_n)\rangle = |\Psi(1, 2, \dots, n)\rangle = \frac{1}{\sqrt{n!}} \begin{vmatrix} \phi_1(1) & \dots & \phi_1(n) \\ \vdots & \ddots & \vdots \\ \phi_n(1) & \dots & \phi_n(n) \end{vmatrix}. \quad (2.9)$$

$n$ : Number of electrons

$\phi_i$ :  $i$ -th spin orbital

The Pauli exclusion principle states that the wave function of electrons, fermions in general, has to be antisymmetric under the exchange of two arbitrary particles

$$\Psi(1, \dots, i, \dots, j, \dots, n) = -\Psi(1, \dots, j, \dots, i, \dots, n). \quad (2.10)$$

The Slater determinant satisfies this antisymmetry requirement.s

The Schrödinger equation (2.5) is solved approximately in the HF approach[1] by using one Slater determinant and the electronic Hamiltonian presented in equation (2.8)

$$\hat{H}|\tilde{\Psi}\rangle \approx E|\Psi\rangle. \quad (2.11)$$

To obtain the approximate solution, the expectation value of the energy  $\langle E \rangle$ , defined by

$$\langle E \rangle = \frac{\langle \Psi | \hat{H}_{\text{el}} | \Psi \rangle}{\langle \Psi | \Psi \rangle}, \quad (2.12)$$

is minimized by variation of the spin orbitals

$$E = \min \frac{\langle \Psi | \hat{H}_{\text{el}} | \Psi \rangle}{\langle \Psi | \Psi \rangle} \geq E_{\text{exact}}. \quad (2.13)$$

The variation principle guarantees that the approximate solution and the resulting energy is an upper bound to the exact energy. This also ensures that a solution with a lower energy provides a more accurate solution and description for the quantum chemical system.

The minimization process is performed using the method of Lagrange multipliers under the additional restriction of orthonormalized spin orbitals

$$\langle \phi_i | \phi_j \rangle = \delta_{ij} \quad (2.14)$$

and leads to the so-called canonical Fock equations

$$\hat{f}_1 \phi_i(1) = \varepsilon_i \phi_i(1). \quad (2.15)$$

The main advantage of this method is that the Schrödinger equation with an  $n$ -particle wave function is reduced to  $n$  one particle equations, which can be solved more easily.

The Fock operator  $\hat{f}_1$

$$\hat{f}_1 = -\frac{1}{2}\Delta_1 - \sum_{I=1}^N \frac{Z_I}{r_{1I}} + \sum_{j=1}^n \left[ \hat{J}_j(1) - \hat{K}_j(1) \right], \quad (2.16)$$

$\hat{J}_j$ : Coulomb operator

$\hat{K}_j$ : Exchange operator

is an effective one-electron Hamiltonian that computes the spin orbital energy  $\varepsilon_i$  for the corresponding spin orbital  $\phi_i$ . The Fock operator is constructed by an one-particle part

$$\hat{h}(1) = -\frac{1}{2}\Delta_1 - \sum_{I=1}^N \frac{Z_I}{r_{1I}} \quad (2.17)$$

and a two-particle part, containing the Coulomb and exchange operators, which describes the electron-electron interaction in an averaged way.

The Coulomb operator can be interpreted as the classical Coulomb interaction, whereas the exchange operator has no classical analogue and is mathematically derived from the antisymmetry requirement of the wave function, resulting from the Pauli exclusion principle. These operators are defined by acting on an orbital in the following form:

$$\hat{J}_j \phi_i(1) = \int \phi_j^*(2) \frac{1}{r_{12}} \phi_j(2) d\tau_2 \phi_i(1) \quad (2.18)$$

$$\hat{K}_j \phi_i(1) = \int \phi_j^*(2) \frac{1}{r_{12}} \phi_i(2) d\tau_2 \phi_j(1). \quad (2.19)$$

$J_j$ : Coulomb operator

$K_j$ : Exchange operator

Expectation values of these operators occur as the so-called Coulomb- and exchange integrals. These integrals are calculated as [1]

$$J_{ij} = \langle \phi_i | \hat{J}_j | \phi_i \rangle = \int \int \phi_i^*(1) \phi_j^*(2) \frac{1}{r_{12}} \phi_i(1) \phi_j(2) d\tau_1 d\tau_2 \quad (2.20)$$

$$K_{ij} = \langle \phi_i | \hat{K}_j | \phi_i \rangle = \int \int \phi_i^*(1) \phi_j^*(2) \frac{1}{r_{12}} \phi_j(1) \phi_i(2) d\tau_1 d\tau_2. \quad (2.21)$$

$J_{ij}$ : Coulomb integral

$K_{ij}$ : Exchange integral

After deriving the Fock equations (2.15), this set of integro-differential equations needs to be solved in the HF approach. Therefore each orbital has to be expanded in a linear combination of basis functions. This ansatz is related to the mathematical fact that each function can be, in principle, approximated as a linear combination of different functions. A specific amount of basis functions defines a basis set. This ansatz is exact in case of a complete basis set.

The spin orbitals  $\phi_i$  are generally constructed by a spatial function  $\varphi_i$  and a spinfunction  $\omega_i$ , which is given by

$$\phi_i(\vec{x}) = \varphi_i(x, y, z) \cdot \omega_i(\{\alpha, \beta\}). \quad (2.22)$$

The integration over the spin coordinates is computed as

$$\langle \alpha | \alpha \rangle = \langle \beta | \beta \rangle = 1 \quad (2.23)$$

$$\langle \alpha | \beta \rangle = \langle \beta | \alpha \rangle = 0. \quad (2.24)$$

The spatial part of the spin orbitals is approximated by a linear combination of the basis functions  $\chi_i$ , for which Gaussian functions are most commonly used

$$\varphi_i = \sum_{\alpha=1}^{m_{basis}} c_{\alpha i} \chi_{\alpha}. \quad (2.25)$$

Inserting this ansatz into the Fock equations (2.15) yields

$$\hat{f}_1 \sum_{\alpha=1}^{m_{basis}} c_{\alpha i} \chi_{\alpha}(1) = \varepsilon_i \sum_{\alpha=1}^{m_{basis}} c_{\alpha i} \chi_{\alpha}(1). \quad (2.26)$$



The orbital coefficients  $c_{\alpha i}$  need to be optimized with respect to the energy to finally solve the Schrödinger equation approximately. By multiplication from the left with an additional basis function  $\chi_\beta$  and formulating an expectation value for each orbital leads to a matrix representation named Roothaan-Hall equation

$$FC = SC\varepsilon. \quad (2.27)$$

$F$ : Fockmatrix with matrix elements  $F_{\alpha\beta} = \langle \chi_\alpha | \hat{f} | \chi_\beta \rangle$

$C$ : Coefficient matrix (i-th column corresponds to the coefficients for the i-th orbital)

$S$ : Overlap matrix with matrix elements  $S_{\alpha\beta} = \langle \chi_\alpha | \chi_\beta \rangle$

$\varepsilon$ : Matrix of the spinorbital energies  $\varepsilon_{ii} = \varepsilon_i$  in the canonical HF

Under the constraint of orthonormalized basis functions

$$\langle \chi_i | \chi_j \rangle = \delta_{ij}, \quad (2.28)$$

the overlap matrix transforms into the identity matrix and the Roothall-Hall equation simplifies to the following form

$$FC = C\varepsilon, \quad (2.29)$$

which is usually solved in an iterative manner by the self-consistent field (SCF) procedure. The iterative computation of the orbital coefficients is needed, because the Coulomb- and exchange operators in the Fock operator depend on the orbitals themselves. The total HF energy is calculated by

$$E_{\text{HF}} = \sum_{i=1}^n \varepsilon_i - \sum_{i>j} (J_{ij} - K_{ij}) + E_{\text{pot}}(\text{nuc}, \text{nuc}). \quad (2.30)$$

The summation of the orbital energies double counts the electron-electron interaction, which is corrected by the second term in equation (2.30) and the nuclear repulsion energy has to be taken into account for a specific geometry. The HF method does not deliver the exact energy, even for an infinite or complete basis set, the energy reaches the so-called Hartree-Fock limit. The HF method computes approximately 99% of the exact energy for a quantum chemical system. This accuracy is not sufficient for many applications and therefore the HF approach is only the basis for many more elaborate computational methods, which are described in the following section.

## 2.3 Correlation Methods

As discussed, the HF method can not deliver the exact energy. This is caused by approximating the wave function as a single determinant and describing the electron-electron interaction by means of an averaged field. In order to obtain the exact nonrelativistic energy, the interaction of every electron pair has to be described correctly, which is called electron correlation and the missing energy amount is named correlation energy. The correlation energy is always a negative value, because the HF energy is an upper bound to the exact energy. It is defined by the difference of the HF energy and the exact energy

$$E_{\text{corr}} = E_{\text{exact}} - E_{\text{HF}}, \quad (2.31)$$

and can be computed using different approaches. The fundamental concepts of the correlation methods as well as the advantages and disadvantages of these methods are discussed in the following subsections.

### 2.3.1 Configuration Interaction

An elaborate approach of computing the correlation energy is the configuration interaction (CI) method. The basic idea is to choose a linear combination of Slater determinants as the wave function ansatz to approximately solve the Schrödinger equation. This wave function ansatz can be mathematically written in the following form

$$|\Psi_{\text{CI}}\rangle = k_{\text{ref}} |\Psi_{\text{ref}}\rangle + \sum_{ia} k_i^a |\Psi_i^a\rangle + \sum_{\substack{i < j \\ a < b}} k_{ij}^{ab} |\Psi_{ij}^{ab}\rangle + \dots \quad (2.32)$$

This type of wave function ansatz is conceptionally very similar to the basis set approximation in the Hartree-Fock method described in equation (2.25). Therefore, the common nomenclature of the one particle basis, which is the basis set  $\{\phi_i\}$  and the many-particle basis, which contains the Slater determinants  $\{|\Psi_i\rangle\}$  in the CI expansion, is often used. The many-particle basis consists of a reference determinant  $|\Psi_{\text{ref}}\rangle$ , which normally corresponds to the HF determinant  $\Psi_{\text{HF}}$ , also often referred to as  $\Psi_0$  and a specific set of substituted Slater determinants. These determinants are systematically ordered with respect to the occupied orbital from which an electron is excited to the orbital that is occupied afterwards, i.e.  $\Psi_i^a$  is the substitution of the  $i$ -th orbital by the  $a$ -th orbital. Determinants with one excited electron are called single excited determinants or singles ( $|S\rangle$ ), whereas doubly excited determinants are called doubles ( $|D\rangle$ ) and so forth. This

terminology is used to categorize different CI approaches by their substitution order, e.g. a CI calculation which includes all singles and doubles is therefore called CISD. Inserting this ansatz into the Schrödinger equation leads to the equation

$$H\vec{k}_\nu = E_{\text{CI},\nu}\vec{k}_\nu, \quad (2.33)$$

$H$ : Hamilton matrix with matrix elements  $H_{ij} = \langle \Psi_i | \hat{H} | \Psi_j \rangle$

$\vec{k}$ : Coefficient vector for the  $\nu$ -th state

$E_{\text{CI}}$ : Ground state energy of the CI approach

for the ground state. The variation principle is also valid for the CI method, so a reduction of the energy guarantees a better solution of the Schrödinger equation and a higher quality of the approximate wave function. The Hamilton matrix in the CI approach can be visualized in the following way

	$ \Psi_0\rangle$	$ S\rangle$	$ D\rangle$	$ T\rangle$	$ Q\rangle$	$\dots$
$\langle \Psi_0  $	$\langle \Psi_0   \hat{H}   \Psi_0 \rangle$	0	$\langle \Psi_0   \hat{H}   D \rangle$	0	0	$\dots$
$\langle S  $		$\langle S   \hat{H}   S \rangle$	$\langle S   \hat{H}   D \rangle$	$\langle S   \hat{H}   T \rangle$	0	$\dots$
$\langle D  $			$\langle D   \hat{H}   D \rangle$	$\langle D   \hat{H}   T \rangle$	$\langle D   \hat{H}   Q \rangle$	$\dots$
$\langle T  $				$\langle T   \hat{H}   T \rangle$	$\langle T   \hat{H}   Q \rangle$	$\dots$
$\langle Q  $					$\langle Q   \hat{H}   Q \rangle$	$\dots$
$\vdots$						$\vdots$

(2.34)

In this form a few rules, which are simplifying the computation can be seen. First, there is no coupling between the reference determinant and the single excitations, which was stated by the Brillouin's theorem for HF orbitals. Due to the fact that singles mix with the double excitations and the doubles interact with the reference determinant, the singles can not be neglected in a CI calculation. The effect of the singly excited Slater determinants on the total energy is indirect. The second rule which can be observed is that all matrix elements between determinants differing in more than two orbitals also vanishes. This is an enormous reduction of the elements, which need to be determined, especially in CI calculations including a high substitution level. The third and last simplification is the consequence of the hermiticity of this matrix, which states that  $H_{ij}^* = H_{ji}$  are equal. Therefore only the upper triangle of this matrix has to be determined. In principle, the CI method is able to compute the exact nonrelativistic energy of a quantum chemical system. This can be achieved by using an infinite one particle basis and including all possible determinants in the CI wave function ansatz, which is named full configuration interaction (FCI). For a finite one particle basis, the maximum reachable quality by using the FCI method is called the FCI limit. According

to the huge number of upcoming determinants, that are determined by

$$N_{\text{dets}} = \binom{K}{n} = \frac{K!}{n!(K-n)!}, \quad (2.35)$$

$K$ : number of spin orbitals

$n$ : number of electrons

the FCI method is only applicable for about 10 electron systems, while using a double zeta basis set. Therefore the wave function has to be truncated. The most used CI method is the already mentioned CISD, but also CISDT or CISDTQ methods can be used for small systems nowadays.

The CI method can compute good results for specific tasks where the HF approach is conceptionally failing. A famous example is the dissociation of the  $\text{H}_2$  molecule. In this homonuclear diatomic compound the molecular orbitals (MOs) are linear combinations of the  $1s$  orbitals of the hydrogen atoms given by

$$\sigma_g = 1s_A + 1s_B \quad (2.36)$$

$$\sigma_u = 1s_A - 1s_B, \quad (2.37)$$

if the normalization constants are neglected. The Slater determinant for the  $\text{H}_2$  molecule, composed of two hydrogen atoms  $\text{H}_A$  and  $\text{H}_B$  can be constructed from the binding  $\sigma_g$  MO for the ground state

$$|\Psi_{\text{H}_2}\rangle \propto \sigma_g^\alpha(1)\sigma_g^\beta(2) - \sigma_g^\alpha(2)\sigma_g^\beta(1). \quad (2.38)$$

Separating the spin and the spatial function of this wave function results in

$$|\Psi_{\text{H}_2}\rangle \propto \sigma_g(1)\sigma_g(2)(\alpha(1)\beta(2) - \alpha(2)\beta(1)). \quad (2.39)$$

From the spatial part of the wave function the inability of the HF ansatz to describe the dissociation can be seen. Inserting equation (2.37) into the spatial part results in

$$\sigma_g(1)\sigma_g(2) = (1s_A(1) + 1s_B(1))(1s_A(2) + 1s_B(2)) \quad (2.40)$$

$$= 1s_A(1)1s_A(2) + 1s_B(1)1s_B(2) + 1s_A(1)1s_B(2) + 1s_B(1)1s_A(2) \quad (2.41)$$

In equation (2.41) the first two terms are called ionic and the last two covalent. The single determinant ansatz of the HF approach leads to a wave function that is composed of 50% ionic and 50% covalent terms. For the dissociation of the dimer this ionic character should vanish, which is not possible in this ansatz. Therefore the dissociation

energy will have a low quality using the HF method. The CID method has the ability to describe this phenomenon correctly. The doubly excited determinant constructed from the antibonding  $\sigma_u$  orbitals results in

$$\sigma_u(1)\sigma_u(2) = 1s_A(1)1s_A(2) + 1s_B(1)1s_B(2) - 1s_A(1)1s_B(2) - 1s_B(1)1s_A(2). \quad (2.42)$$

The CID wave function can then be written as

$$|\Psi_{\text{CID}}\rangle = (k_1\sigma_g(1)\sigma_g(2) + k_2\sigma_u(1)\sigma_u(2))(\alpha(1)\beta(2) - \alpha(2)\beta(1)), \quad (2.43)$$

and by choosing the coefficients as

$$k_1 = -k_2, \quad (2.44)$$

the ionic terms in the wave function vanish and the wave function will only be composed of the covalent terms, which are needed at the dissociation limit of the  $\text{H}_2$  dimer

$$|\Psi_{\text{CID}}\rangle = k_1(1s_A(1)1s_B(2) + 1s_B(1)1s_A(2))(\alpha(1)\beta(2) - \alpha(2)\beta(1)). \quad (2.45)$$

The CI ansatz is not size-consistent in general if the excitation level is truncated. This is the main disadvantage of this approach, because size-consistency is an important attribute for a correlation method in general. Therefore, the basic idea of size-consistency will be illustrated briefly. For a system  $AB$  composed of two non-interacting subsystems  $A$  and  $B$  the Hamiltonian is separable

$$\hat{H}_{AB} = \hat{H}_A + \hat{H}_B, \quad (2.46)$$

as a logical consequence of the absent interaction. Therefore the total energy should be the summation of the two energies of the subsystems  $A$  and  $B$

$$E_{AB} = E_A + E_B. \quad (2.47)$$

Considering the CISD method for such a case reveals that double excitations are included in the separated calculations for the subsystems  $A$  and  $B$ , which results in the inclusion of quadruple excitations for the summation of these two systems. The CISD method applied to the combined system  $AB$  however, uses only the double excitations, which results in a different quality. According to this it can be concluded that the CISD method is not size-consistent, which can be problematic for several applications, e.g. reaction energies. The fundamental size-consistency problem has been overcome by the well known and often used coupled cluster ansatz that will also be presented and discussed in throughout the following sections.

### 2.3.2 Multi-configurational Self-consistent Field

Electron correlation is generally divided into two different types, dynamic and static correlation. The previously explained CI approach is in general suitable for quantum chemical systems that have one dominant leading Slater determinant. This type of electron correlation is named dynamic correlation. Static correlation is of special importance for multi-reference (MR) compounds, in which no single determinant is leading in the wave function. Well known examples are open-shell systems, transition states or excited states. The optimized orbitals of the HF method are not appropriate for these kinds of MR systems and the orbitals have to be generated using a different approach. The multi-configurational self-consistent field (MCSCF) approach overcomes this problem and is suitable for MR systems. The general wave function ansatz is a linear combination of determinants, which is analogue to the CI wave function

$$|\Psi_{\text{MCSCF}}\rangle = \sum_I k_I |\Psi_I\rangle. \quad (2.48)$$

In contrast to the CI method, where the orbitals are not optimized, the MCSCF method optimizes the coefficients of the determinants and the orbital coefficients. The MCSCF method becomes identical to the HF approach, if only one Slater determinant is used. As well as the CI method the MCSCF approach, except CASSCF, is not size-consistent entailing the same problems, which were already highlighted for the CI method. Nevertheless MCSCF can be used for many applications, e.g. excitation energies for atoms and molecules, delivering very accurate results. The main disadvantage and problem of MCSCF is the choice of the determinants that are included in the wave function ansatz. The determinants need to be carefully selected, motivated by chemical or physical understanding of the investigated systems. An unbalanced or uncarefully picked set of determinants can lead to inaccurate results or wrong insights.

In the beginning of the MCSCF method, the determinants were individually selected. Nowadays more systematic approaches, e.g. complete active space self-consistent field (CASSCF) or restricted active space self-consistent field (RASSCF), are used. In these methods the determinants are chosen systematically, defined by the so-called active space. In this systematic approach the orbital space is partitioned into three different subspaces which are namely the inactive, virtual and active orbitals. This partitioning is normally executed with respect to the computed HF orbital energies of the system.

In general the orbitals are categorized in the following way:

- **inactive orbitals:** Orbitals that are usually energetically low and are therefore always occupied in all used determinants of the wave function expansion.
- **virtual orbitals:** Orbitals that are, in contrast to the inactive orbitals, energetically high and therefore always unoccupied in all determinants that are used in the wave function expansion.
- **active orbitals:** These orbitals define the varying occupation patterns of the determinants which are included in the CI expansion of the MCSCF method. Commonly these orbitals correspond to the highest occupied molecular orbitals (HOMOs) and the lowest unoccupied molecular orbitals (LUMOs) determined by the HF method.

The active orbitals can and should be selected by a rational understanding of the system and not only according to the HF orbital energies, especially for open-shell systems. For a quantum chemical open-shell system, e.g. vanadium, that has an electron configuration of  $[\text{Ar}]3d^34s^2$ , all determinants resulting from the  $d$ -orbitals should be included in the wave function regardless of the HF orbital energies of the  $d$ -orbitals. Such a procedure is the basic idea of the CASSCF method. After dividing the orbital space to the already mentioned subspace, all determinants which arise from the active orbitals and electron will be included in the CI expansion to construct the wave function. The resulting number of determinants can be calculated according to the FCI approach

$$N_{\text{dets}} = \binom{K_{\text{act}}}{n_{\text{act}}} = \frac{K_{\text{act}}!}{n_{\text{act}}!(K_{\text{act}} - n_{\text{act}})!}. \quad (2.49)$$

$K_{\text{act}}$ : Number of spin orbitals included in the active space

$n_{\text{act}}$ : Number of electrons included in the active space

Therefore the CASSCF method is often described as a FCI approach in the active orbital space and the qualitatively correct energies for specific applications like excitation energies becomes clear. For small active spaces this approach should be the best method to derive accurate electronic energies and corresponding results, but for systems where larger active spaces are needed a different approach might be needed.

The RASSCF approach is such a method and the basic idea of this procedure is to divide the whole orbital space into more subspaces. The virtual and inactive orbitals are defined equivalently to the already given definition. In the RASSCF approach, the active space is partitioned into three subspaces. In contrast to the CASSCF method not

all determinants arising from this space will be constructed. The subspaces are normally numbered and named RAS1, RAS2 and RAS3.

- **RAS1:** Active orbital space with a lower limit for the number of electrons in this space.
- **RAS2:** Active orbital space where all determinants are constructed similar to the CASSCF scheme.
- **RAS3:** Active orbital space with an upper limit for the number of electrons in this space.

The RASSCF scheme allows more control about the active space and can in principle be applied to more complex systems and tasks than the CASSCF approach, if the important occupation patterns and determinants are well understood and known. The discussed multi-reference computational methods in this section are accurate for problems where the static correlation is the dominant effect of the investigated system. For situations where a large amount of dynamic correlation is also needed, these methods might be failing, leading to inaccurate results. Therefore methods are needed that are able to deal with static and dynamic correlation, which will be presented in the following section.

### 2.3.3 Multi-reference Configuration Interaction

Since the MCSCF method covers static correlation and the CI approach can treat dynamic correlation, a combination of these two approaches was developed. The combination of these two methods is called multi-reference configuration interaction (MRCI). MRCI covers static and dynamic correlation, which results in accurate electronic energies, especially for multi-reference compounds. The wave function ansatz of the MRCI approach is also a linear combination of determinants similar to the CI expansion, but in contrast to this method more than one reference determinant is included from which all excited determinants are constructed

$$|\Psi_{\text{MRCI}}\rangle = \sum_I k_I |\Psi_I\rangle \quad \text{with} \quad \{\Psi_I\} = \bigcup_{\text{ref}} \{\Psi_I^{\text{ref}}\}. \quad (2.50)$$

The normal procedure is to generate reference determinants using the MCSCF approach and then perform a MRCI calculation where the truncated excitation level is applied to all reference determinants for constructing the wave function. The orbitals were optimized in the MCSCF calculation and will not be reoptimized in the corresponding MRCI approach. This method optimizes only the coefficients of the determinants, equivalent



to the CI approach. The nomenclature of the different MRCI methods is analogue to CI, e.g. MRCISD includes all singles and doubles for every reference determinant. From this ansatz very accurate wave functions and energies can be computed, but for a truncated MRCI approach the size-consistency is also not fulfilled, which can be a problem for the computation of reaction energies for growing system size.

### 2.3.4 Coupled Cluster

The most important disadvantage of all previously discussed correlation methods, except CASSCF, is the size-inconsistency. This property guarantees the same quality of the wave function for systems of different size, which will be needed for the calculation of reaction energies. To overcome the problem of size-inconsistency the coupled cluster (CC) method was developed. This approach is the most accurate wave function based method in the field of computational chemistry for single reference molecules. According to this, the basic concept of CC will be explained and discussed in this section. This section mainly follows the work of Crawford and Schaefer [5].

For size-consistency the wave function ansatz has to be a product ansatz, which is used in the CC method. Typically the wave function ansatz of this method is written in an exponential form

$$|\Psi_{CC}\rangle = \exp(\hat{T})|\Psi_{\text{ref}}\rangle, \quad (2.51)$$

which consists of the cluster operator  $\hat{T}$  and a reference determinant. Analogue to the CI method this reference determinant is usually the Hartree-Fock determinant. The cluster operator, given by

$$\hat{T} = \hat{T}_1 + \hat{T}_2 + \dots + \hat{T}_n, \quad (2.52)$$

creates the excited determinants with respect to the reference determinant and therefore constructs the whole wave function in this approach. The term  $\hat{T}_n$  is the sum of all possible  $n$ -electron excitations and is often defined in the formalism of second-quantization as

$$\hat{T}_n = \left(\frac{1}{n!}\right)^2 \sum_{ij\dots ab\dots}^n t_{ij\dots}^{ab\dots} \hat{a}_a^\dagger \hat{a}_b^\dagger \dots \hat{a}_j \hat{a}_i. \quad (2.53)$$

$a_a^\dagger$ : Creation operator, which occupies the  $i$ -th spin orbital with respect to the reference determinant

$a_i$ : Annihilation operator, which unoccupies the  $a$ -th spin orbital with respect to the

reference determinant

$t_{ij\dots}^{ab\dots}$ : Coefficient of the CC approach, named amplitude

In a CC calculation the amplitudes are the coefficients which are optimized to find the best approximation of the wave function.

The exponential of the cluster operator in the wave function can be expanded in a Taylor series.

$$\exp(\hat{T}) = 1 + \hat{T} + \frac{1}{2!}\hat{T}^2 + \frac{1}{3!}\hat{T}^3 + \frac{1}{4!}\hat{T}^4 + \dots \quad (2.54)$$

From this representation, the product ansatz of the wave function, which is the reason of the size-consistency, can be extracted. The different CC methods are also categorized with respect to the excitation level of the cluster operator  $\hat{T}$ .

$$\text{CCS} \quad : \hat{T} = \hat{T}_1 \quad (2.55)$$

$$\text{CCSD} \quad : \hat{T} = \hat{T}_1 + \hat{T}_2 \quad (2.56)$$

$$\text{CCSDT} : \hat{T} = \hat{T}_1 + \hat{T}_2 + \hat{T}_3 \quad (2.57)$$

Normally, the coupled cluster method is realized via the so-called projective similarity transformed CC ansatz instead of using a variational CC approach. The mathematical equations for this approach can be written as

$$\langle \Psi_{\text{ref}} | e^{-\hat{T}} \hat{H} e^{\hat{T}} | \Psi_{\text{ref}} \rangle = E \quad (2.58)$$

$$\langle \Psi_{ij\dots}^{ab\dots} | e^{-\hat{T}} \hat{H} e^{\hat{T}} | \Psi_{\text{ref}} \rangle = 0, \quad (2.59)$$

where the equation (2.58) describes the energy and the equation (2.59) defines the amplitude equations. From this ansatz two main advantages are obtained. The first advantage is the decoupling of the energy equation (2.58) from the amplitude equations (2.59). The second advantage is that the similarity transformed Hamiltonian can be simplified as

$$\begin{aligned} e^{-\hat{T}} \hat{H} e^{\hat{T}} = & \hat{H} + [\hat{H}, \hat{T}] + \frac{1}{2!} [[\hat{H}, \hat{T}], \hat{T}] + \frac{1}{3!} [[[\hat{H}, \hat{T}], \hat{T}], \hat{T}] \\ & + \frac{1}{4!} [[[[\hat{H}, \hat{T}], \hat{T}], \hat{T}], \hat{T}] + \dots \end{aligned} \quad (2.60)$$

which is named Campbell-Baker-Hausdorff formular or the Hausdorff expansion.

A variational coupled cluster approach

$$\frac{\langle \Psi_{\text{ref}} | (e^{\hat{T}})^{\dagger} \hat{H} (e^{\hat{T}}) | \Psi_{\text{ref}} \rangle}{\langle \Psi_{\text{ref}} | (e^{\hat{T}})^{\dagger} (e^{\hat{T}}) | \Psi_{\text{ref}} \rangle} = E \geq E_{\text{exact}} \quad (2.61)$$

is more complex than the projective ansatz. The variation principle does not hold for the projective CC ansatz, which implies that it is possible to calculate a lower energy than the exact one, but according to the fact that the error of the CC ansatz is systematically lowered by increasing the excitation level, the CC method can be used. The CC method is the most accurate computational method, which is known and can be used for electronic energies for any quantum chemical single reference system. CC can be used for many small and medium sized molecules and the CCSD(T) method combined with the cc-pVTZ basis set is nowadays referred to as the gold standard of quantum chemistry. The CCSD(T) approach includes singles and doubles in the wave function ansatz and adds energy corrections of triples from Møller-Plesset perturbation theory.

The convenient CC approach is, just like the CI approach not suitable for MR systems. Therefore multi-reference coupled cluster (MRCC) theory, which will deliver very accurate electronic energies for MR systems is an important research field and is needed for high quality computational investigations of reaction mechanisms, excited states, transition metal and  $f$ -block element chemistry in the future.

## 2.4 Relativistic Quantum Chemistry

The already discussed methods do not include the physics of special relativity. For many systems and applications relativistic effects can be neglected, but especially for heavy or super heavy elements the relativistic effects are relevant for an accurate computation of the electronic structure. Therefore the fundamentals of relativistic quantum chemistry are briefly described in the following section. The discussion and formulas follow the book of Dyall and Faegri [6].

### 2.4.1 Foundations of the Special Theory of Relativity

The classical Newtonian description delivers relations between the spatial coordinates and the time in two different inertial frames  $K$  and  $K'$ . This relation can be expressed in terms of the Galilean transformations. Assuming the coordinate axes of two inertial frames  $K$  and  $K'$  are parallel and  $K'$  is moving with constant speed  $v$  along the positive  $x$  axis, the Galilean transformations are

$$x' = x - vt \quad (2.62)$$

$$x = x' + vt \quad (2.63)$$

$$y' = y \quad (2.64)$$

$$z' = z \quad (2.65)$$

$$t' = t. \quad (2.66)$$

This transformation holds for ordinary classical mechanics for low speeds. It was shown that the Galilean transformation is inadequate for electromagnetic phenomena and a proper physical description was developed. The solution was presented by Einstein in 1905 based on the following two postulates:

- The laws of physics are identical in all inertial frames.
- In empty space, light signals propagate in straight lines with speed  $c$  in all inertial frames.

Using a set of linear transformations

$$x = ax' + bt \quad (2.67)$$

$$x' = ax - bt, \quad (2.68)$$

appeared to be reasonable. Following this idea and the postulates of special relativity the so-called Lorentz transformation was derived. These transformations can be expressed in the following form

$$x = \gamma (x' + vt') \quad (2.69)$$

$$x' = \gamma (x - vt) \quad (2.70)$$

$$y' = y \quad (2.71)$$

$$z' = z \quad (2.72)$$

$$t = \gamma \left( t' + \frac{vx'}{c^2} \right) \quad (2.73)$$

$$t' = \gamma \left( t - \frac{vx}{c^2} \right), \quad (2.74)$$

for the previously described situation of two inertial systems  $K$  and  $K'$ . The introduced factor  $\gamma$  has the form

$$\gamma = \frac{1}{\sqrt{1 - \frac{v^2}{c^2}}}. \quad (2.75)$$

For high velocities  $v \approx c$  the resulting effects of this transformation are significant. In the case of low velocities  $v \ll c$ , the transformation becomes equal to the Galilean transformation, because the Lorentz factor is approximately 1. These transformations are also resulting in a transformation of the mass

$$m = \gamma m', \quad (2.76)$$

which reveals that the mass is not constant for a particle and it changes in moving frames. According to this insight the rest mass  $m_0$  (mass at zero speed), that is constant in all inertial frames, was introduced and from the presented relations the following energy equation was derived

$$E = mc^2 = T + m_0c^2, \quad (2.77)$$

where  $T$  is the kinetic energy and  $m_0c^2$  is called the rest energy. The relation reveals that non-moving particles have an energy and there is a connection between mass and energy. It also revealed the possibility to transform mass into outgoing energy, which is relevant in the research field of nuclear fusion or fission.

### 2.4.2 Dirac Equation

After deriving the fundamentals of relativity, this theory was applied to the field of quantum mechanics. For a free electron in the nonrelativistic case the Hamiltonian is given as

$$\hat{H} = \hat{T} = \frac{\hat{\vec{p}}^2}{2m_e} \quad (2.78)$$

and using atomic units the time-dependent Schrödinger equation of this system becomes

$$-\frac{1}{2} \left( \frac{\partial^2}{\partial x^2} + \frac{\partial^2}{\partial y^2} + \frac{\partial^2}{\partial z^2} \right) |\Psi\rangle = i \frac{\partial}{\partial t} |\Psi\rangle. \quad (2.79)$$

In general and especially for atomic or molecular systems the electrons are not free. They are described by the Coulomb interaction with the nuclei and all other electrons. These interactions can be treated by introducing the scalar potential  $\phi$ , obtaining the following equation for electrons

$$\hat{H} = \hat{T} + \hat{V} = \frac{\hat{\vec{p}}^2}{2} - \phi. \quad (2.80)$$

Considering the Lorentz invariance of the time-dependent Schrödinger equation, it becomes clear that the vector potential  $\vec{A}$  has to be included too, because the scalar potential is only one component of the four vector  $\mathbf{A} = \left( \vec{A}, \frac{i\phi}{c} \right)$ . It is also convenient to introduce the mechanical momentum  $\vec{\pi}$  given as an operator by

$$\hat{\vec{\pi}} = \hat{\vec{p}} + \vec{A}, \quad (2.81)$$

known as minimal coupling. Applying the scalar and vector potential to the energy equation (2.77) delivers the expression

$$(E + \phi)^2 = m^2 c^4 + c^2 \left( \hat{\vec{p}} + \vec{A} \right)^2, \quad (2.82)$$

which can be rewritten using the mechanical momentum as

$$E = c\vec{\alpha} \cdot \hat{\vec{\pi}} + \beta mc^2 - \phi. \quad (2.83)$$

Using the quantum mechanical definition for the operators and further transformation results in the time-dependent Dirac equation

$$\left( i \frac{\partial}{\partial t} + \phi \right) |\Psi\rangle = [c\vec{\alpha} \cdot (-i\nabla + \vec{A}) + \beta mc^2] |\Psi\rangle. \quad (2.84)$$

Separating the time-dependent part of this expression finally leads to the time-independent Dirac equation

$$\hat{H}_D|\Psi\rangle = [c\vec{\alpha} \cdot (-i\nabla + A) + \beta mc^2 - \phi] |\Psi\rangle = E|\Psi\rangle. \quad (2.85)$$

The term  $\vec{\alpha}$  is given as a three component vector of matrices

$$\vec{\alpha} = \begin{pmatrix} \alpha_x \\ \alpha_y \\ \alpha_z \end{pmatrix}, \quad \alpha_i = \begin{pmatrix} 0_2 & \sigma_i \\ \sigma_i & 0_2 \end{pmatrix}, i = x, y, z, \quad (2.86)$$

including the Pauli spin matrices

$$\sigma_x = \begin{pmatrix} 0 & 1 \\ 1 & 0 \end{pmatrix}, \quad \sigma_y = \begin{pmatrix} 0 & -i \\ i & 0 \end{pmatrix}, \quad \sigma_z = \begin{pmatrix} 1 & 0 \\ 0 & -1 \end{pmatrix}, \quad (2.87)$$

and  $0_2$ , which is the  $2 \times 2$  null matrix. The  $4 \times 4$  matrix  $\beta$  can be written as

$$\beta = \begin{pmatrix} I_2 & 0_2 \\ 0_2 & I_2 \end{pmatrix}, \quad (2.88)$$

where  $I_2$  is the  $2 \times 2$  unit matrix. As a consequence of including relativistics into quantum mechanics, the wave function has to be a four component vector given as

$$|\Psi\rangle = \begin{pmatrix} \psi_\alpha^L \\ \psi_\beta^L \\ \psi_\alpha^S \\ \psi_\beta^S \end{pmatrix} = \begin{pmatrix} \psi^L \\ \psi^S \end{pmatrix}. \quad (2.89)$$

$\psi^L$ : Large components of the wave function

$\psi^S$ : Small components of the wave function

The large component and the small component are named after their relevance for the electronic solutions of the Dirac equation. In the case of electrons the large component is large and the small component is small, but for the positronic solutions, which are also obtained by solving the Dirac equation, this behavior is inverted.

The derived results elucidate that relativistic quantum chemistry is significantly more complex and computationally demanding than nonrelativistic quantum chemistry.

## 2.5 Pseudopotentials

For computational quantum chemical methods, e.g. HF, CI or CC, the number of electrons is an important factor that effects the calculation time significantly. The specific scaling of the computation time is dependent on the basis set and the resulting virtual orbitals as well and it is different for every method. Especially, the increasing computational effort with respect to the electron number is a problem, if the investigated system includes heavy elements. For many interesting applications heavy elements need to be calculated, e.g. metal-organic complexes have an important relevance in the field of catalysis and therefore such complexes are also subjects of quantum chemical investigations. Additionally, relativistic effects have a significant relevance for the electronic structure of heavy elements and should be included in quantum chemical investigations, too. Including the effects of relativity is also very computationally demanding, as described in the previous section.

To reduce the number of electrons of specific elements in computations, effective core potentials (ECPs) were developed. This allows quantum chemical investigations for molecules including heavy elements with a moderate computational effort and additionally these potentials can cover relativistic effects in an implicit way. The ECPs are nowadays an important aspect in the field of computational chemistry and therefore the concepts are described in the following part.

The basic idea of the ECP approach is to divide the electrons of an atom into the valence electrons and the core electrons

$$n = n_c + n_v. \quad (2.90)$$

$n$ : Total electrons

$n_c$ : Core electrons

$n_v$ : Valence electrons

The valence electrons  $n_v$  are explicitly included in the computational method, while the effect of the core electrons, which are not treated explicitly, are described by the ECP. This reduces the electron number of the system and a faster computation can be performed. Therefore the Hamiltonian has to be redefined in this approach. The Hamiltonian only acts on the valence electrons and is therefore often referred to as the valence only Hamiltonian [7] and is given by

$$\hat{H}_v = -\frac{1}{2} \sum_{i=1}^{n_v} \Delta_i + \sum_{i < j}^{n_v} \frac{1}{r_{ij}} + \sum_{i=1}^{n_v} \hat{V}_{eff}(i). \quad (2.91)$$



This Hamiltonian is similar to the normal nonrelativistic Hamiltonian, but acts only on the valence electrons and not on the core electrons. The effective one electron potential  $\hat{V}_{eff}(i)$  consists of the potential energy of the cores and a correction term for the electron-electron interaction called pseudopotential  $\hat{V}_{PP}(i)$ . This effective one electron potential corrects the energy of the reduced electron system in this ansatz and can be written as

$$\hat{V}_{eff}(i) = -\frac{Q}{r_i} + \hat{V}_{PP}(i). \quad (2.92)$$

The potential energy of the electron nuclei interaction is realized by reducing the nuclear charge  $Z$  by the number of core electron  $n_c$  that is called core charge  $Q$

$$Q = Z - n_c. \quad (2.93)$$

The pseudopotential of an atom can then be mathematically described by [8–10]

$$\hat{V}_{PP}(i) \approx V_L(r_i) + \sum_{l=0}^{L-1} \hat{P}_l(i) [V_l(r_i) - V_L(r_i)]. \quad (2.94)$$

The potential  $V_L(r_i)$  acts on all orbital angular momenta  $l \geq L$ . The term  $[V_l(r_i) - V_L(r_i)]$  acts on all occurring orbital angular momentum quantum numbers  $l$  in the core, where  $L - 1$  defines the largest upcoming momentum.  $\hat{P}_l(i)$  is the projection operator of the orbital angular momentum and given by

$$\hat{P}_l(i) = \sum_{m=-l}^{m=l} |lm\rangle \langle lm|. \quad (2.95)$$

The potentials  $V_l(r_i)$  and  $V_L(r_i)$  are realized, according to the work of *Kahn et al.* [11], as linear combinations of Gaussian functions that are multiplied by powers of  $r$

$$V_m(r_i) = \sum_k A_{km} r_i^{n_{km}} e^{-a_{km} r_i^2}. \quad (2.96)$$

These linear combinations have to be adjusted to reference energies of all electron (AE) computations for every atom. The reference calculation can be performed with non-relativistic or scalar relativistic methods. The convenient approach is to use scalar relativistic computed energies for heavy elements, because these scalar relativistic effects are then implicitly included in the ECP and are therefore also included in every calculation that is performed using this ECP. Most commonly the coefficients  $A_{kL}$  are set to zero, which results in a simplification of the pseudopotential to the form

$$\hat{V}_{PP}(i) = \sum_{l=0}^{L-1} \hat{P}_l(i) V_l(r_i). \quad (2.97)$$

For relativistic two-component calculations the already derived equations have to be modified. The total angular momentum  $j$  has to be introduced. The relativistic pseudopotential is then given by [7]

$$\hat{V}_{PP}(i) = \sum_{l=0}^{L-1} \sum_{j=|l-\frac{1}{2}|}^{j=l+\frac{1}{2}} V_{lj}(r_i) \hat{P}_{lj}, \quad (2.98)$$

and the projection operator transforms to the expression

$$\hat{P}_{lj}(i) = \sum_{m=-j}^{m=j} |ljm\rangle \langle lj m|. \quad (2.99)$$

According to the work of *Ermler*[12], the pseudopotential can be separated into two different terms described by the following expression

$$\hat{V}_{PP}(i) = \hat{V}_{PP}^{SA}(i) + \hat{V}_{PP}^{SO}(i), \quad (2.100)$$

where the two individual parts are given by

$$\hat{V}_{PP}^{SA}(i) = \sum_{l=0}^{L-1} \frac{1}{2l+1} \hat{P}_l \left[ l V_{l,|l-\frac{1}{2}|}(r_i) + (l+1) V_{l,l+\frac{1}{2}}(r_i) \right] \quad (2.101)$$

and

$$\hat{V}_{PP}^{SO}(i) = \sum_{l=1}^{L-1} \frac{V_l(r_i)}{2l+1} \left[ l \hat{P}_{l,l+\frac{1}{2}} - (l+1) \hat{P}_{l,|l-\frac{1}{2}|} \right]. \quad (2.102)$$

This splitting into a spin-free averaged (SA) term  $\hat{V}_{PP}^{SA}$  and a spin-dependent or spin-orbit (SO) term  $\hat{V}_{PP}^{SO}$ , results in the advantage that it is possible to perform one-component calculations via SA-ECP and afterwards to compute the spin-orbit coupling effects in a perturbative manner via SO-ECP. The ECP approach is nowadays the most important quantum chemical approach in the field of  $f$ -block chemistry, metal-organic chemistry and in general for the computational investigations of heavy and super-heavy elements.

## 2.6 Population analysis

The fundamental concept of orbitals is in general very important in chemical science. Atoms, ions and molecules are classified and characterized according to their available, occupied and unoccupied orbitals from which physical as well as chemical properties of these systems are derived. This characterization is possible with computational methods nowadays, even for systems with a complicated electronic structure, e.g. lanthanides, actinides or transition metals. The experimental investigations and classifications of such molecules are often demanding, expensive or not accessible. Therefore, computational chemistry can deliver qualitative insights in this area.

A convenient opportunity for this classification is the analysis of the basis functions subsequent to a suitable quantum chemical calculation of the molecule. A common approach is the *Mulliken* population analysis, which was applied in this work and is therefore described in the following [13]. As already mentioned, orbitals are constructed from basis functions, due to equation (2.25)

$$\varphi_i = \sum_{\alpha=1}^{m_{basis}} c_{\alpha i} \chi_{\alpha}.$$

The one electron density arising from an orbital of a molecule, can be written as

$$|\varphi_i|^2 = \sum_{\alpha\beta}^{m_{basis}} c_{\alpha i}^* c_{\beta i} \chi_{\alpha}^* \chi_{\beta}. \quad (2.103)$$

The summation and integration over all occupied orbitals, described in the previous equation, delivers the number of electrons  $n_{el}$  in the system

$$\begin{aligned} n_{el} &= \sum_{i=1}^{n_{occ}} \int |\varphi_i|^2 dr \\ &= \sum_{i=1}^{n_{occ}} \sum_{\alpha\beta}^{m_{basis}} c_{\alpha i}^* c_{\beta i} \langle \chi_{\alpha} | \chi_{\beta} \rangle \\ &= \sum_{i=1}^{n_{occ}} \sum_{\alpha\beta}^{m_{basis}} c_{\alpha i}^* c_{\beta i} S_{\alpha\beta}. \end{aligned} \quad (2.104)$$

Introducing the orbital occupation number  $n_i$ , this approach can be generalized for every

occupation pattern, according to the following equation

$$\begin{aligned}
 n_{\text{el}} &= \sum_{i=1}^{n_{\text{occ}}} n_i \int |\varphi_i|^2 dr \\
 &= \sum_{\alpha\beta}^{m_{\text{basis}}} \left( \sum_{i=1}^{n_{\text{occ}}} n_i c_{\alpha i}^* c_{\beta i} \right) S_{\alpha\beta} \\
 &= \sum_{\alpha\beta}^{m_{\text{basis}}} D_{\alpha\beta} S_{\alpha\beta}.
 \end{aligned} \tag{2.105}$$

The matrix  $D$ , which was derived in equation (2.105) is called density matrix. Based on this matrix, the electron density at a specific nucleus  $X$ , can be computed via

$$\rho_X = \sum_{\alpha \in X}^{m_{\text{basis}}} \sum_{\beta}^{m_{\text{basis}}} D_{\alpha\beta} S_{\alpha\beta}. \tag{2.106}$$

$\rho_X$ : Electronic charge corresponding to nucleus  $X$

During the procedure all atomic orbitals (AOs) of the nucleus  $X$  are used for the computation of the density. In this analysis the diagonal elements  $D_{\alpha\alpha} S_{\alpha\alpha}$  directly correspond to the atomic orbital  $\alpha$ . The off-diagonal elements of the form  $D_{\alpha\beta} S_{\alpha\beta}$  are parted between the two involved centers or nuclei in the *Mulliken* population analysis. The procedure can be extended by dividing the analysis with respect to the atomic orbitals, which results in the ability to investigate the relevance and the occupation of every orbital type for any atom of the molecule, separately. In this work the Mulliken population analysis is used to investigate the relevance and the occupation of the 4*f*-orbitals for several lanthanide compounds in their molecular electronic structure.

Additionally, the charge of every nuclei in the molecule can be calculated from the electron density computation of every atom. The charge is given by the following equation

$$Q_X = Z_X - \rho_X. \tag{2.107}$$

$Q_X$ : Gross charge at the nucleus  $X$

$Z_X$ : Nuclear charge of the atom  $X$

## 2.7 Density Funtional Theory

### 2.7.1 Fundamentals of DFT

Density functional theory (DFT) is probably the most frequently used and dominating method in the field of computational chemistry. Therefore the fundamental aspects of DFT are presented and discussed in this section, mainly following the book of Cramer [14]. The name density functional theory arises from the mapping of a given electron density, that is a function of the spatial coordinates onto the real numbers, especially the energy. In the field of theoretical, wave function based chemistry the electron density can be calculated from the wave function in the following form

$$\rho(\vec{r}) = n \int \dots \int |\Psi(\vec{r}_1, \vec{r}_2, \dots \vec{r}_n)|^2 d\vec{r}_2 \dots d\vec{r}_n. \quad (2.108)$$

An additional integration of the density delivers the electron number of the system

$$n = \int \rho(\vec{r}) d\vec{r}. \quad (2.109)$$

The complexity of a  $n$ -electron wave function is  $3n$  (or  $4n$  including the spin), whereas the density has only a complexity of three and in contrast to the wave function, the density is an observable. Early DFT methods were completely orbital free, but due to their inaccurate results in many cases the Kohn-Sham self-consistent field method was developed and is nowadays the standard for DFT computations in the field of computational quantum chemistry.

The main idea of the Kohn-Sham ansatz was to reintroduce orbitals to the DFT approach and derive the Kohn-Sham equations

$$\hat{h}_1^{\text{KS}} \phi_i(1) = \epsilon_i \phi_i(1), \quad (2.110)$$

which are very similar to the HF equations. These equations can be solved in a self-consistent approach, equivalent to the solution in the HF method, by approximating the orbitals as a linear combination of basis functions. The Kohn-Sham operator is, equivalent to the Fock operator, an one-electron operator and is given by

$$\hat{h}_1^{\text{KS}} = -\frac{1}{2}\Delta_1 - \sum_I^N \frac{Z_I}{r_{1I}} + \int \frac{\rho(r')}{|r_1 - r'|} dr' + V_{\text{XC}}. \quad (2.111)$$

$V_{\text{XC}}$  is the so-called functional derivative, which can be written as

$$V_{\text{XC}} = \frac{\partial E_{\text{XC}}}{\partial \rho}. \quad (2.112)$$

The density in modern DFT methods is derived by the occupied orbitals themselves in the following way

$$\rho = \sum_{i=1}^{n_{occ}} |\phi_i|^2, \quad (2.113)$$

which shows that an iterative procedure is needed, because the Kohn-Sham operator is depending on the orbitals. The total electronic energy computed by a DFT calculation can be written as

$$E_{\text{DFT}}[\rho(r)] = T[\{\phi_i\}] + E_{ne}[\rho(r)] + J[\rho(r)] + E_{XC}[\rho(r)]. \quad (2.114)$$

The kinetic energy is computed from the orbitals in the same procedure as is HF theory,

$$T[\{\phi_i\}] = \sum_{i=1}^n \langle \phi_i | -\frac{1}{2} \Delta | \phi_i \rangle \quad (2.115)$$

which was a huge improvement of the orbital-free DFT approaches, because the inaccurate results of these methods were most notably connected to the inaccurately computed kinetic energies. The energy term  $E_{XC}[\rho(r)]$  is unknown and is provided by the chosen density functional. This term is often referred to as the correlation and exchange energy or the functional is called correlation and exchange functional, but in fact the functional and the energy arising from it also include the correction for the kinetic energy  $\Delta T[\rho(r)]$  and the correction for the electron-electron interaction  $\Delta V_{ee}[\rho(r)]$ . The mathematical form of the functional is the remaining problem in the field of density functional theory and therefore a huge research area.

### 2.7.2 Functional Types

All available functionals can be categorized by their main ansatz for the functional. In the following several functional approaches will be described. The simplest model for a correlation and exchange functional is the local density approximation (LDA). LDA approaches are based on the assumption of an homogenous electron gas for the system. The energy is then calculated in the following form

$$E_{XC}[\rho(r)] = \int \rho(r) \epsilon_{xc}[\rho(r)] dr, \quad (2.116)$$

where the  $\epsilon_{xc}[\rho(r)]$  is referred to as the energy density. This density is a per particle density. Normally it is divided in a pure correlation and a pure exchange part

$$\epsilon_{xc}[\rho(r)] = \epsilon_c[\rho(r)] + \epsilon_x[\rho(r)]. \quad (2.117)$$

The exchange part can be written as

$$\epsilon_x^{LDA}[\rho(r)] = -C_x \int \rho^{\frac{4}{3}}(r) dr. \quad (2.118)$$

For a general case of non identical spin densities the local spin density approximation (LSDA) was introduced resulting in an energy density of the form

$$\epsilon_x^{LSDA}[\rho(r)] = -2^{\frac{1}{3}} C_x \int \rho^{\frac{4}{3}\alpha}(r) + \frac{4}{3}\beta(r) dr, \quad (2.119)$$

which becomes equal to the LDA approach for a closed-shell system. For both approaches the parameter  $C_x$  is given by

$$C_x = \frac{3}{4} \left( \frac{3}{\pi} \right)^{\frac{1}{3}}. \quad (2.120)$$

In the literature this ansatz is called Slater exchange. There is no known mathematical form for the correlation part in the LDA and LSDA approaches and therefore the different LDA or LSDA functionals have a differing correlation energy term, which becomes equal to the LDA approach for a closed-shell system.

For molecular systems the electron density is rather far from a homogenous density and the applicability of LDA approaches revealed limitations. To overcome this problem the generalized gradient approximation (GGA) was introduced and gradient-corrected functionals were developed. Most GGA functionals are constructed from a LDA or LSDA functional and an additional gradient corrected term, which can be written as

$$\epsilon_{x/c}^{GGA}[\rho(r)] = \epsilon_{x/c}^{LSD}[\rho(r)] + \Delta \epsilon_{x/c} \left[ \frac{|\nabla \rho(r)|}{\rho^{4/3}(r)} \right]. \quad (2.121)$$

A further developed functional category are the so-called hybrid functionals. The basic idea is to combine the HF exchange part with the correlation and exchange term of density functional approaches. One of the most used functionals, the B3-LYP functional is a famous representative for this functional type. The B3-LYP energy can be written as

$$E_{\text{XC}}^{\text{B3-LYP}} = (1 - a)E_X^{\text{LSDA}} + aE_X^{\text{HF}} + b\Delta E_X^{\text{B}} + (1 - c)E_C^{\text{LSDA}} + cE_C^{\text{LYP}}, \quad (2.122)$$

including the three parameters  $a, b$  and  $c$  which were fitted to experimental data. By introducing fitting parameters in the density functionals, accurate results can be obtained from these calculations, while the general applicability might be lost. Additionally, computations from these functionals are not *ab initio*. Therefore this class of functionals delivers semi-empirical methods and investigations. Nowadays further conceptionally improved DFT functionals, e.g. meta-GGA or double hybrid functionals, are available.



## 3 Results

### 3.1 Cerocene

#### 3.1.1 Introduction

The bis- $\eta^8$ -annulene cerium, also called cerocene, was first synthesized by Greco et al. in 1976 [15].  $\text{Ce}(\text{C}_8\text{H}_8)_2$  is a lanthanide analogue to the actinide sandwich compound uranocene, which was synthesized in 1968 by Streitwieser and Müller-Westerhoff [16]. The electronic structure of cerocene, especially the oxidation state of cerium was discussed controversially for over three decades [17–28]. The absence of a low-energy peak arising from an occupied f orbital as observed for uranocene and the similarity to thorocene resulted in the conclusion that cerocene is a Ce(IV) complex composed of  $\text{Ce}^{4+}$  and two anionic aromatic  $\text{C}_8\text{H}_8^{2-}$  ligands. However, Fulde and Neumann concluded that the ground state of cerocene might be a molecular Kondo system with a  $\text{Ce}^{3+}$  and two  $\text{C}_8\text{H}_8^{1.5-}$  rings, where the unpaired electrons in the cerium 4f orbital and the ligand  $\pi$  orbital are coupled [18]. This view was confirmed by Dolg et al. in 1991 by multi-configuration self-consistent field (MCSCF) computations [19]. These computations included relativistic effects by using a pseudopotential (PP) for cerium and resulted in a wavefunction, which showed a leading  $4f^1\pi^3$  configuration for the open-shell  $^1\text{A}_{1g}$  ground state. In 1995 multi-reference configuration interaction (MRCI) and multi-reference averaged coupled-pair functional (MRACPF) delivered first *ab initio* computations for the electronic spectrum, the metal-ring vibrations and the metal-ligand distance for cerocene and thorocene [20]. For the ground state of  $\text{Ce}(\text{C}_8\text{H}_8)_2$  a Mulliken population analysis revealed an f electron count of 1.08, which would support a Ce(III) compound. According to the low energy of a cerium 4f orbital, it was argued that a peak in the photoelectron spectrum of cerocene resulting from an occupied f orbital should be observed at higher energies compared to the ligand  $\pi$  orbitals. For uranocene it was additionally argued that due to the strong influence of relativistic effects the uranium 5f shell is destabilized and a peak in the photoelectron spectra arising from a  $5f^2$  occupation shows at lower energy compared to the  $\pi$  orbitals. Therefore the absence of a peak located at low energies indicates a Th(IV) oxidation state for thorocene, but it is not the case

for cerocene and therefore this compound should be viewed as a Ce(III) system. This view was additionally supported by a X-ray absorption near-edge structure (XANES) study [21]. For two cerocene derivatives the measured spectra were closer to Ce(III) systems than to a Ce(IV) compound. The view of cerocene as a Ce(III) complex was further supported by additional experimental studies[22, 23] and finally in 2009 Walter et al.[24] published an extensive experimental study including magnetic measurements, extended X-ray absorption fine structure (EXAFS) as well as XANES measurements on the unsubstituted cerocene supporting the Ce(III) oxidation state in cerocene. However, in 2004 and 2007 articles were published supporting a Ce(IV) oxidation state [25, 26]. In 2009 Kerridge et al. presented the results of all-electron (AE) complete active space second-order perturbation theory (CASPT2) calculations applying the DKH2 hamiltonian for cerocene [27]. In contrast to the MRCI and MRACPF computations supporting a Ce(III) system the computed metal-ring distance of Kerridge et al. of 1.964 Å was in a good agreement with the experimental value of 1.969 Å [29]. An f electron count of 0.90 was computed, but the analysis of the state-averaged computation including the ground and first excited state revealed a leading  $f^0$  configuration contributing by about 58% to the ground state, whereas the  $f^1$  configuration only showed 23%. Therefore it was concluded that cerocene is best described as a Ce(IV) complex, where the transfer of electron density from the ring ligands to the metal ion leads to a reduction of the formal Ce(IV) oxidation state. It was also mentioned that the assignment of oxidation states for multiconfigurational ground states is not well defined and that in their view an analysis of the multiconfigurational wavefunction based on natural orbitals (NO) should be recommended. A further CASSCF study, published in 2013 by Kerridge et al. again supported this point of view [28]. However, the presented results in this section aim to show the reason for the different interpretations of the cerocene ground state. Additionally a concept of assigning oxidation states in multi-reference systems, which are in agreement to experimental spectroscopic results is presented. The presented results and discussions have already been published in 2014 [30].

### 3.1.2 Computational Details

Cerocene was studied at the complete active space self-consistent field (CASSCF) level. The following calculations were performed with the MOLPRO program package[31] at an all-electron level using the second-order Douglas-Kroll-Hess (DKH2) Hamiltonian [32–34].  $D_{2h}$  symmetry was used. For hydrogen and carbon the augmented correlation-consistent basis aug-cc-pVTZ basis set was used including up to p functions for H and d functions for C [35, 36]. For cerium a segmented contracted DKH2-optimized (23s16p12d6f3g)/[18s12p9d3f3g] basis set was applied [37]. An atomic natural orbital (ANO) basis set was also used. All calculations were performed using  $D_{2h}$  symmetry, maintaining the full  $D_{8h}$  symmetry of the system. The electronic structure calculations are based on an optimized geometry with a cerium-ligand distance of 1.971 Å, a carbon-carbon distance of 1.410 Å and carbon-hydrogen distance of 1.074 Å. The carbon-hydrogen bonds are positioned about 5.6 ° out of the ring plane towards the metal center. The used geometry is close compared to the published results by Kerrigde et al., where only the metal-ring distance was optimized and the ring ligands were assumed to be planar with a fixed C-C distance of 1.404 Å and an also fixed C-H distance of 1.087 Å.

### 3.1.3 Eletronic Structure

In order to find the underlying reason for the different interpretations and results of the former published articles investigating cerocene, CASSCF calculations were performed including the occupied doubly degenerated  $e_{2u}$  ( $D_{8h}$ )  $\pi$  orbital and the corresponding cerium 4f orbital. In the applied  $D_{2h}$  point group these orbitals are  $a_u$  and  $b_{1u}$  symmetric. The natural orbitals (NOs) in the active space showed a mixed Ce 4f and ligand  $\pi$  character and therefore these active orbitals were rotated between  $-20^\circ$  and  $70^\circ$  in steps of  $2.5^\circ$ . The f character of the active orbitals was determined by a Mulliken population analysis as well as the CI coefficients of the CASSCF wavefunction in each rotation step. In these computations only excitations within the active orbitals space were allowed. The main results of this investigation are presented in Figure 3.1, where the upper plot shows the f character of one component of the  $e_{2u}$  orbitals and the lower plot shows the corresponding configuration contribution of the CASSCF wavefunction. It should be noted that the orbital rotation has a  $90^\circ$  period, whereas the CI coefficients of a specific configuration  $a^n b^{4-n}$  has a  $180^\circ$  period for  $n=0, 1, 3, 4$  and  $90^\circ$  for  $n=2$ . The shown curves for  $n=0, 1, 3, 4$  are shifted by  $90^\circ$ , since the orbitals and their character change have such a period.

It can be seen that the active orbitals at  $0^\circ$  (NOs) are significantly mixed Ce 4f and ligand  $\pi$  orbitals. The orbital  $a$  shows about 80%  $\pi$  character and 20% f characters, whereas orbital  $b$  has about 80% f character and 20%  $\pi$  character. Using these natural orbitals it can be seen that the leading configuration is closed-shell  $a^4$ . The other configurations show small contributions. It can be seen that the contribution of the closed-shell  $a^4$  configuration can be maximized at a rotation angle about  $-4.5^\circ$ , where the corresponding contribution is about 81%. This situation of the active orbitals can be interpreted as a Ce(IV) ring-metal covalency, which Streitwieser et al. described [17, 25]. It should be emphasized that at this rotation angle the active orbitals still show a mixed character. Rotating the orbitals by about  $25^\circ$  lead to a situation where the different orbital contributions are separated, which means that a nearly pure Ce 4f orbital and a nearly pure ligand  $\pi$  orbital are obtained. Orbital  $a$  shows less than 5% f character, arising from higher f orbitals than 4f and orbital  $b$  has nearly 100% 4f character. These orbitals lead to a dominant leading  $a^3 b^1$  configuration, contributing about 83% to the CASSCF wavefunction. According to the well separated character of the active orbitals this configuration can be clearly described as  $4f^1 \pi^3$  and at this situation cerocene can be interpreted as a molecular Ce(III)-based Kondo system as it was published by Fulde and coworkers [18–20]. The applied orbital rotation is a unitary transformation and therefore the CASSCF wavefunction is invariant to the rotation. Therefore every rota-

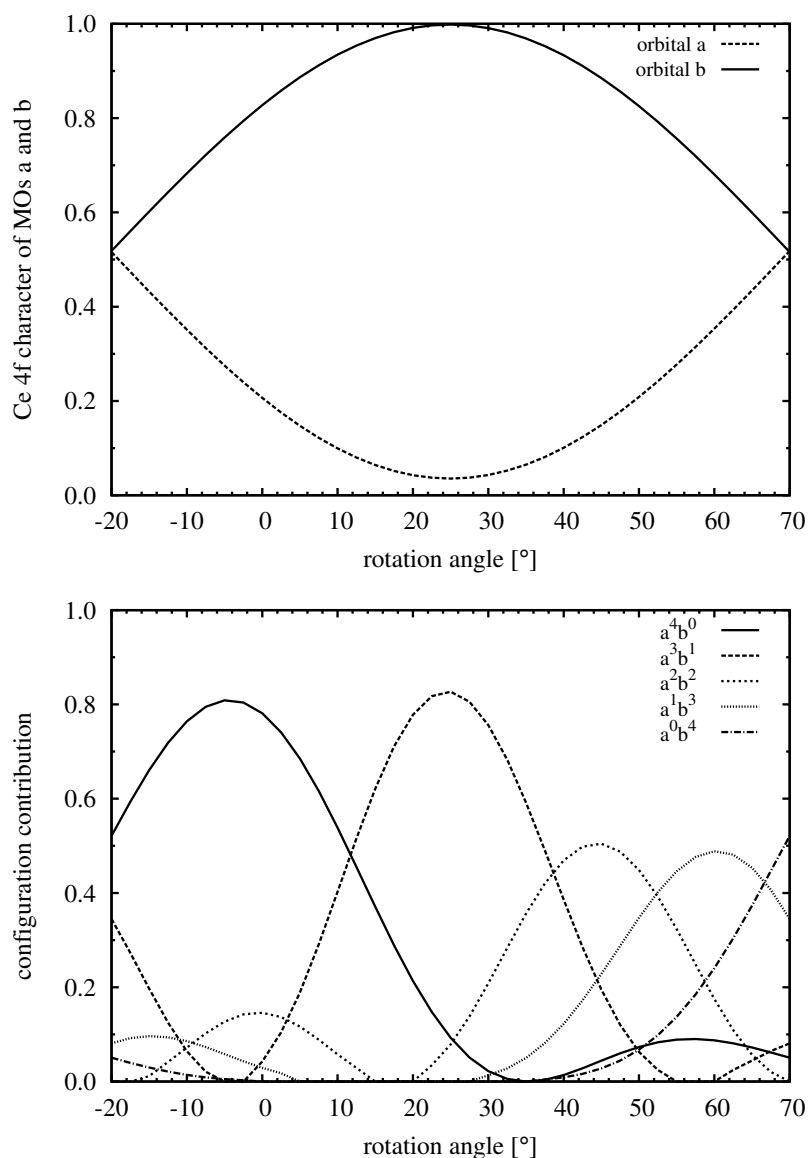


**Figure 3.1:** Orbital characters (top) and configuration contributions (bottom) of cerocene at the CASSCF level.

tion angle has the same quality and the two different situations, describing cerocene as a Ce(IV) or Ce(III) system, are equal. Nevertheless the chemical view of oxidation states arises from dividing the molecule into fragments. In this case into the ring ligands and the cerium atom. Therefore the situation, where the orbitals are demixed is the best choice for assigning the oxidation state of cerium and the categorization of cerocene as a Ce(III) compound should be recommended. In the former mentioned articles MCSCF computations were performed only considering the  $a^4b^0$  and  $a^3b^1$  configurations [19, 20].

The energy minimization of such a wavefunction lead to a unique result of orbitals and configuration contributions. As it can be seen in Figure 3.1 this situation is obtained at an rotation angle of about  $17.5^\circ$ , where the contributions of two configurations vanish and the wavefunction can be described 100% by only two configurations. At this point the orbitals are also quite well demixed and the resulting configuration contributions are 70%  $4f^1\pi^3$  and 30%  $4f^0\pi^4$ , which is in agreement to the older computations and also with the measured XANES spectrum of cerocene. This rotation angle provides the most compact description of cerocene and also leads to the Ce(III) oxidation state assignment.

### 3.1.4 Conclusions

The CASSCF wavefunction of cerocene has been analyzed with respect to the characters of the active orbitals. A full orbital rotation revealed that strongly mixed Ce 4f and ligand  $\pi$  orbitals can lead to a leading closed-shell configuration, which resulted in the conclusion that cerocene is a Ce(IV) complex. The active orbitals were demixed in order to obtain nearly pure Ce 4f and ligand  $\pi$  orbitals. The wavefunction analysis based on these localized orbitals supported a Ce(III) oxidation state. However, cerocene can be described at the same quality using wavefunction, which can be used to support both points of view. According to these results cerocene can be described as a Ce(IV) compound showing significant metal-ligand covalency between the Ce 4f and the ligand  $\pi$  orbitals or as a molecular Kondo system with an open-shell ground state with an atomic like occupied 4f orbital. However, by using nearly pure 4f and  $\pi$  orbitals the most compact wavefunction can be obtained with only two contributing configuration (about 70%  $f^1\pi^3$  and 30%  $f^0\pi^4$ ), which is in good agreement with the experimental XANES data and measured f occupation. Therefore the categorization and the assignment of oxidation states of multi-reference systems based on localized orbitals appears to be an appropriate choice and should be recommended.

## 3.2 Bis( $\eta^8$ -pentalene)cerium

### 3.2.1 Introduction

In 2007 two publications considering bis( $\eta^8$ -pentalene)cerium derivatives came to different conclusions for the oxidation state of cerium in these compounds, based on experiments and quantum chemical computations [38, 39]. Balazs *et al.* concluded that  $\text{Ce}(\text{C}_8\text{H}_4(\text{Si-}^i\text{Pr}_{3-1,4})_2)_2$  is a Ce(IV) complex [38], whereas  $\text{Ce}(\text{C}_8\text{Me}_6)_2$  was categorized as a Ce(III) compound [39]. For the latter compound L<sub>III</sub>-edge XANES measurements determined an f electron count of  $0.87 \pm 0.05$  [38], which is comparable to cerocene ( $0.89 \pm 0.03$ ) [23]. These values support a Ce(III) oxidation state, which is also supported by K-edge XANES data of  $\text{Ce}(\text{C}_8\text{Me}_6)_2$ . It was argued by Balasz *et al.* that a traditional Ce(III) complex with a localized f electron and a magnetic moment close to an expected moment of a free Ce(III) ion can be distinguished to a formal diamagnetic Ce(IV) compound, where the f electron is paired, such as cerocene. The two cerium complexes cerocene and  $\text{Ce}(\text{C}_8\text{Me}_6)_2$  have reversible one-electron reductions at -800 and -830 mV which is consistent with the Ce(IV) oxidation state and which are too low for a Ce(III)/Ce(IV) couple [38]. Based on these insights Balasz *et al.* found the Ce(IV) description appropriate. However, it was shown for cerocene that an assignment of the oxidation state of the metal in complexes can be achieved by localized orbitals and a multi-reference wavefunction analysis. For cerocene this procedure resulted in a reasonable classification of this compound compared to the experimental results obtained by XANES spectroscopy. According to the different interpretations of the different bis( $\eta^8$ -pentalene)cerium compounds, the unsubstituted bis( $\eta^8$ -pentalene)cerium complex was chosen as a model system and an CASSCF wavefunction analysis including orbital rotation was performed to derive an appropriate oxidation state assignment of cerium in this compound. The presented results and discussion have already been published in 2015 [40].

### 3.2.2 Computational Details

The ground state geometry as well as the relevance of the cerium 4f orbitals for the molecular electronic structure was studied at the complete-active space self-consistent field level (CASSCF) using the scalar relativistic second-order Douglas-Kroll-Hess (DKH2) Hamiltonian [32–34].

For cerium an atomic natural orbital (ANO) (25s18p10d8f3g)/[9s8p6d4f3g] basis set was used, whereas the correlation-consistent valence triple-zeta (cc-pVTZ) basis set (10s5p2d)/[4s3p2d] for carbon and (5s5p)/[3s2p] for hydrogen was applied [41, 42]. All computations were carried out with the program package MOLPRO [31]. To investigate the ground state geometry the compound was optimized at the CASSCF(4,4) level followed by contracted second-order Rayleigh-Schrödinger perturbation theory (RS2C)[43] for a  $D_{2d}$  and  $D_{2h}$  symmetric molecular structure. For the  $D_{2d}$  geometry all computations had to be performed in the  $C_{2v}$  subgroup, whereas the  $D_{2h}$  symmetry could be fully applied. At the RS2C level the cerium  $1s^2$  up to  $4d^{10}$  and carbon  $1s^2$  shells were treated as frozen cores. The active orbital space was constructed of the highest occupied  $\pi$  orbitals and the cerium 4f orbitals of the corresponding irreducible representation ( $a_1$  and  $a_2$  for  $D_{2d}$ ,  $b_{1u}$  and  $a_u$  for  $D_{2h}$ ). The relevance of the 4f orbitals and the corresponding interaction with the ligands was analyzed at the CASSCF(2,2) level. Additionally, the accuracy of the computation using the small active space was investigated by CASSCF(12,14)/RSPT2 calculations for the  $D_{2d}$  symmetric molecule. In order to assign the oxidation state of cerium in the bis( $\eta^8$ -pentalene)cerium molecule, the CI coefficients of the CASSCF wavefunction, as well as the orbital characters of the active orbitals by a Mulliken population analysis, were computed. The occupation number fluctuation of the active orbitals at the CASSCF(2,2) level was analyzed to investigate the nature of the metal-ligand orbital interaction [44].



### 3.2.3 Ground State Geometry

As a first step the ground state geometry was investigated for the bis( $\eta^8$ -pentalene)cerium. The previously mentioned CASSCF/RSPT2 geometry optimizations revealed that the  $D_{2d}$  structure of this compound is energetically about 0.123 eV lower compared to the  $D_{2h}$  symmetric one. The crystal structure of this compound also showed the staggered  $D_{2d}$  geometry and therefore the computation can support the experiment [39]. Selected bond distances and bond angles are presented in Table 3.1 and a graphic illustration of the optimized structures is given in Figure 3.2. The computed fold angle of the pentalene ligands is  $26.3^\circ$ , which is in good agreement compared to the experimental angle of  $24.7^\circ$ . For the two different optimized structures the bond distances and angles are quite similar and also in a good agreement with the experimental distances and angles obtained from the measured crystal structure.

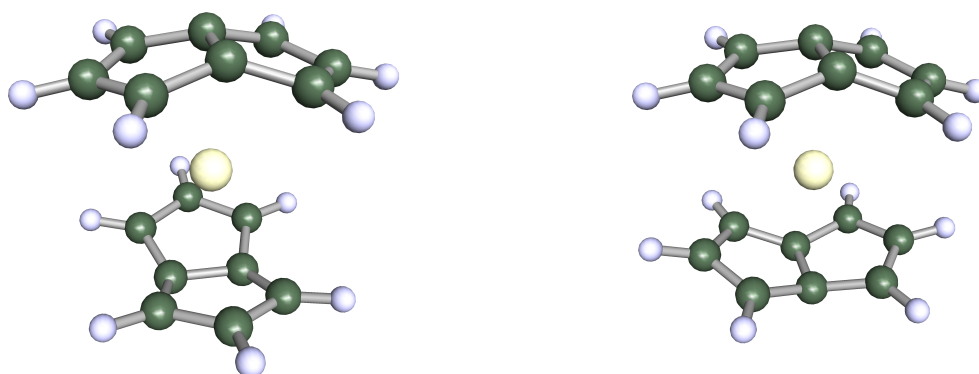


**Figure 3.2:** CASSCF(4,4)/RSPT2 optimized ground state structures of the  $D_{2d}$  (left) and  $D_{2h}$  (right) symmetric bis( $\eta^8$ -pentalene)cerium.

**Table 3.1:** Selected bond distances and bond angles of the optimized bis( $\eta^8$ -pentalene)cerium structures in  $D_{2h}$  and  $D_{2d}$  symmetry compared to averaged experimental values from a crystal structure ( $D_{2d}$ ). The atom numbering is according to IUPAC. C atoms 1,3,4,6 are equivalent as well as 2 and 5. C atoms 3a and 6a are common to the ring ligands. X describes the middle of C(3a)-C(6a).

CASSCF/RSPT2	(4,4)	(4,4)	(12,14)	Exp.
	$D_{2h}$	$D_{2d}$	$D_{2d}$	
bond distances in Å				
Ce-X	2.374	2.378	2.349	
CeC(3a)	2.485	2.488	2.462	2.469
Ce-C(1)	2.692	2.703	2.674	2.702
Ce-C(2)	2.828	2.836	2.807	2.855
C(1)-C(2)	1.418	1.420	1.417	1.416
C(1)-C(6a)	1.435	1.434	1.436	1.444
C(3a)-C(6a)	1.468	1.464	1.471	1.451
C(1)-H	1.079	1.079	1.080	
C(2)-H	1.080	1.080	1.080	
bond angles in °				
C(2)-x-C(5)	153.4	153.7	153.0	155.3
C(3a)-C(6a)-C(1)	107.4	107.5	107.4	
C(6a)-C(1)-C(2)	107.3	107.4	107.4	
C(1)-C(2)-C(3)	110.4	110.1	110.4	
x-C(2)-H	179.2	178.1	178.1	
C(6a)-C(1)-H	127.2	127.1	127.1	
C(1)-C(2)-H	124.8	124.9	124.8	

### 3.2.4 Electronic Structure and Active Orbital Rotation

As a first step the CASSCF(4,4) and CASSCF(2,2) ground state wavefunctions were analyzed for the  $D_{2d}$  and  $D_{2h}$  optimized structures. In the CASSCF(4,4) computations the two highest occupied molecular orbitals (HOMO, HOMO-1) of the pentalene ligands as well as the cerium 4f orbitals corresponding to the same irreducible representation were included in the active orbital space. The results presented in Table 3.2 reveal that a leading configuration of the wavefunction can be found at the CASSCF(4,4) level. The leading configuration contributes by about 88% ( $D_{2d}$ ) and 85% ( $D_{2h}$ ) to the complete wavefunction. The next most important configuration contributes by 7% ( $D_{2d}$ ) and 6% ( $D_{2h}$ ). Compared to the leading configuration two electrons are excited in the  $a_2$  or  $a_u$  symmetric orbitals. These two closed-shell configurations might be assigned to  $4f^0\pi^2$  and  $4f^2\pi^0$  describing the wavefunction with 95% and 91%. Therefore the active space was reduced to a compact CASSCF(2,2) wavefunction only using  $a_2$  or  $a_u$  symmetric orbitals. The energy difference between the CASSCF(4,4) and CASSCF(2,2) computations are only 0.0092 ( $D_{2d}$ ) and 0.0127 Hartree. If natural orbitals are used two closed-shell configurations, with opposite sign, contribute to the ground state wavefunction, which is comparable to the larger active space computations. Again, these configurations might be assigned to  $4f^0\pi^2$  and  $4f^2\pi^0$  and the resulting wavefunction would be written as approximately 82%  $4f^0\pi^2$ +18%  $4f^2\pi^0$  for the  $D_{2d}$  and the  $D_{2h}$  structures.

**Table 3.2:** Configuration contributions [%] to the CASSCF(4,4) and CASSCF(2,2) singlet ground state wavefunction. Localized orbitals: nearly pure cerium 4f and ligand  $\pi$  orbitals.

CASSCF(4,4)		D <sub>2d</sub>	D <sub>2h</sub>	CASSCF(2,2)		D <sub>2d</sub>	D <sub>2h</sub>
occ. pattern		config. contr.		occ. pattern		config. contr.	
a <sub>1</sub> or b <sub>1u</sub>	a <sub>2</sub> or a <sub>u</sub>	natural orbitals		a <sub>2</sub> or a <sub>u</sub>	natural orbitals		
20	20	88.44	85.12	20	82.14	82.50	
20	02	7.09	6.04	02	17.86	17.50	
11	11	2.80	5.24				
11	02	0.99	1.61		localized orbitals		
11	20	0.20	0.58	11	86.88	86.59	
02	20	0.18	0.40	02	10.63	10.82	
20	11	0.15	0.58	20	2.49	2.59	
02	11	0.15	0.36				
02	02	0.01	0.06				

Therefore the cerium oxidation state might be assigned to be Ce(IV). However, the natural molecular orbitals are mixtures of the cerium 4f and the ligand  $\pi$  orbitals, which is problematic for assigning the oxidation state of cerium based on these orbitals. According to this, the molecular orbitals were localized by a unitary transformation in the active orbitals space. The rotation angle of these orbitals were varied between  $0^\circ$  and  $90^\circ$  in steps of  $0.1^\circ$  and the orbital characters as well as the CI coefficients were monitored. The results for the most localized orbitals are explicitly given in Table 3.2 and the full orbital rotation is illustrated in Figure 3.3 compared to a hydrogen dimer at an enlarged bond distance.

First Figure 3.3 reveals that the natural orbitals ( $0^\circ$ ) are approximately 50:50 mixtures of cerium 4f and ligand  $\pi$  orbitals. Therefore the leading configuration should not be interpreted as  $f^0\pi^2$  and the compound should not be categorized as a Ce(IV) complex.

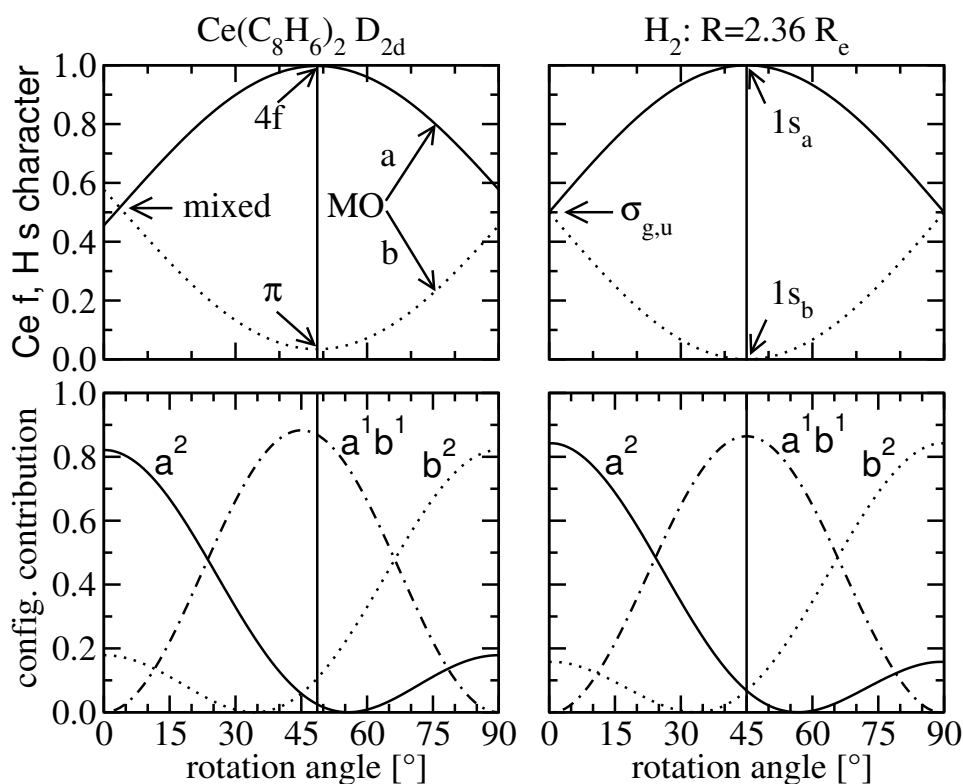


**Figure 3.3:** Orbital rotation of bis( $\eta^8$ -pentalene)cerium compared to a hydrogen dimer.

At a rotation angle of about  $48.5^\circ$  ( $D_{2d}$ ) and  $48.6^\circ$  ( $D_{2h}$ ) nearly pure cerium 4f and ligand  $\pi$  orbitals are obtained. At this rotation angle the leading configuration is open-shell and according to the pure orbital character this configuration can be described as  $4f^1\pi^1$ . The complete CASSCF(2,2) wavefunction can be written as 87%  $4f^1\pi^1$ +11%  $4f^0\pi^2$ +2%  $4f^2\pi^0$  for the  $D_{2d}$  structure. Additionally, it should be noted that the con-

tribution of the open-shell configuration using localized orbitals is higher compared to the leading closed-shell configuration using natural orbitals. The corresponding results for the  $D_{2h}$  symmetric structure are comparable, which indicates that the orientation of the two ligands does not have a significant influence on the electronic structure and the metal-ligand interaction. These results lead to the conclusion that this compound is best described as a Ce(III) compound or a mixed valent Ce(III)/Ce(IV) complex with dominant Ce(III) character. This result is in agreement with the isoelectronic cerocene compound. For a CASSCF(2,2) wavefunction it is possible to completely suppress the influence of one configuration. Using natural orbitals the open-shell configuration does not contribute to the complete wavefunction, but at a rotation angle about  $55.2^\circ$  ( $D_{2d}$ ) and  $55.8^\circ$  ( $D_{2d}$ ) one of the closed-shell configuration can be suppressed. These rotation angles are close to the angles where the orbitals are approximately fully localized, resulting in a leading open-shell configuration. Thus the most compact wavefunction is obtained analogue to a Ce(III)-based Kondo lattice system with a leading  $4f^1\pi^1$  and an admixed  $4f^0\pi^2$  configuration.

Interestingly the orbital rotation resulted in a completely comparable picture for bis( $\eta^8$ -pentalene)cerium and a hydrogen dimer at an enlarged internuclear distance at the CASSCF(2,2) level. Using natural orbitals the  $H_2$  ground state wavefunction is a linear combination of the  $\sigma_g^2$  and the  $\sigma_u^2$  configurations, where the  $\sigma$  orbitals are linear combinations of the two 1s atomic orbitals. It is well known that the hydrogen dimer has a covalent bond and it is homolytically dissociating. Therefore the leading closed-shell configuration does not lead to the classification that  $H_2$  is composed of  $H^+$  and  $H^-$ , which would be analogue to the Ce(IV) assigned oxidation state based on a leading closed-shell configuration of mixed natural orbitals for cerium complexes. Rotation of the active orbitals by  $45^\circ$  lead to two separated 1s orbitals localized on each hydrogen atom and a dominant leading  $1s_A^1 1s_B^1$  configuration. This situation is in agreement to the chemical understanding of this simple system and also supports the procedure of assigning oxidation states based on localized orbitals. However the hydrogen dimer and the behavior of its CASSCF wavefunction can be used to investigate the nature of the metal-ligand orbital interaction of the active orbitals in bis( $\eta^8$ -pentalene)cerium, which will be discussed in more detail in the following section.

### 3.2.5 Occupation Number Fluctuation Analysis

The orbital occupation number fluctuation and the local spin computed with respect to orbitals that are localized on a specific atom of a molecule can be used to characterize the orbital interactions of a specific bond based on a CASSCF wavefunction. As a reference system for covalent interaction the charge fluctuation and the local spin of a hydrogen dimer were computed at different internuclear distances at the CASSCF(2,2) level. The resulting curve, which is shown in Figure 3.4 can be used to detect covalent orbitals interactions and categorize them from strong to weak covalent. In order to investigate the nature of the metal-ligand orbital interaction in bis( $\eta^8$ -pentalene)cerium, the corresponding values were computed for the localized, nearly pure cerium 4f and ligand  $\pi$  orbitals at the CASSCF(2,2) level. Additionally, two further atomic model systems were also computed for comparison and all results are summarized in Figure 3.4.

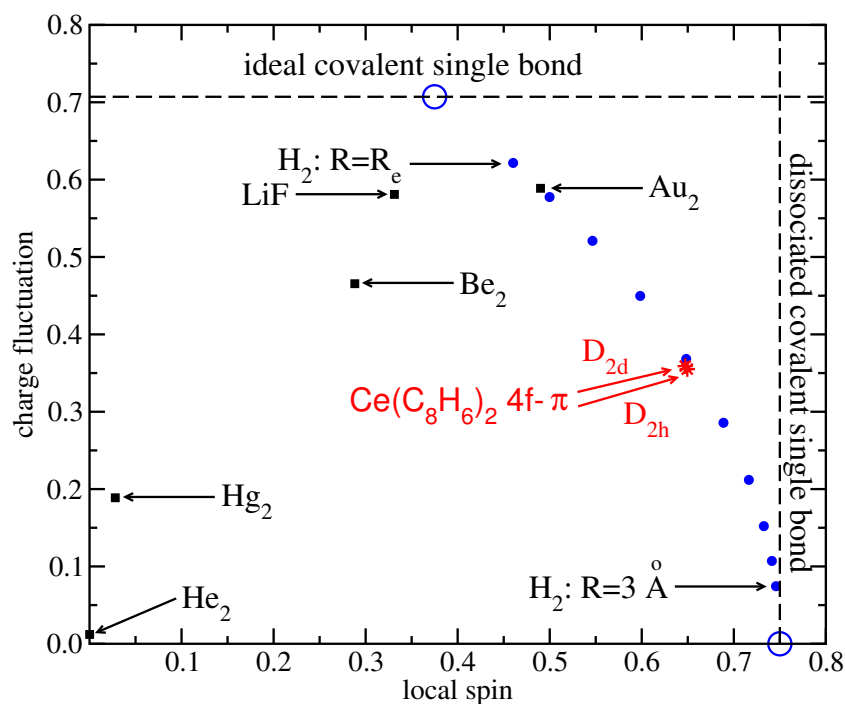


**Figure 3.4:** Occupation number fluctuation and local spin derived from CASSCF wavefunctions for bis( $\eta^8$ -pentalene)cerium and various reference systems. The  $H_2$  reference curve is given in blue.

The most expressive reference systems are  $\text{He}_2$  as a van der Waals bonded dimer,  $\text{LiF}$  as a clearly ionic bonded system and  $\text{Au}_2$  which is known to be covalent. The  $\text{Au}_2$  molecule lies exactly on the reference curve of  $\text{H}_2$ , which completely supports the covalent character of this molecule, whereas the ionic bonded  $\text{LiF}$  is shifted to left. The helium dimer shows the expected charge fluctuation and local spin with values close to zero. Interestingly the metal-ligand bonding interaction of the 4f and  $\pi$  orbitals also lies on the hydrogen dimer curve for the  $D_{2d}$  symmetric ground state geometry as well as for the  $D_{2h}$  symmetric structure. Therefore it can be concluded that the metal-ligand orbital interaction of this complex is covalent. According to the determined values, which are comparable to a stretched  $\text{H}_2$  bond, this interaction can be described as weak covalent. Based on these results, considering bis( $\eta^8$ -pentalene)cerium as a Ce(IV) compound appears to be inappropriate. The Ce(III) description seems to be more appropriate.

### 3.2.6 Conclusions

In conclusion the bis( $\eta^8$ -pentalene)cerium molecule revealed a  $D_{2d}$  symmetric ground state geometry. Similar to cerocene the CASSCF wavefunction is dominated by a leading  $4f^1\pi^1$  configuration if nearly pure cerium 4f and  $\pi$  ligand orbitals are used. Therefore this compound can be assigned to be a Ce(III) complex and is according to these results another example of a molecular Kondo system comparable to cerocene.

Additionally, the charge fluctuation analysis of the active orbitals at the CASSCF(2,2) level, which is the most compact possible description for this system, revealed that the metal-ligand orbital interaction can be classified as weak covalent.

## 3.3 Bis(cyclopentadienyl)cerium Compounds

### 3.3.1 Introduction

The assignment of oxidation states in multi-reference systems is a complex problem. As it was emphasized for cerocene quantum chemical computations can lead to different interpretations of the electronic structure and therefore lead to differently assigned oxidation states. However, it was previously shown for cerocene and bis( $\eta^8$ -pentalene)cerium that an analysis of the CASSCF wavefunction using localized orbitals results in a reasonable assignment for the oxidation state of cerium in complexes. This procedure was consistent with experimental XANES data for these compounds.

In 2005 a density functional theory study (DFT) was published by Clark *et al.* investigating the Ce-Z bonding of bis(cyclopentadienyl)cerium complexes  $\text{Cp}_2\text{CeZ}$  ( $\text{Z} = \text{CH}_2, \text{CH}^-, \text{NH}, \text{O}, \text{F}^+$ ), which have not been synthesized yet [45]. These compounds were considered as synthetic targets for cerium-main group element multiple bonding, which is in contrast to transition metal and actinide compounds quite rare for lanthanide complexes [46–48]. It was found that the Ce-Cp bonding is mainly ionic, whereas the Ce-Z interaction revealed a stronger covalent character. DFT computations might not describe multi-reference systems quite well and therefore these bis(cyclopentadienyl)cerium complexes were investigated at the CASSCF level, while applying focus on their multi-reference character and the relevance of the cerium 4f orbitals for the electronic structure of these compounds. In order to assign reasonable oxidation states for cerium in these compounds orbital rotations as well as an analysis of the CI coefficients of the CASSCF wavefunction were performed. This procedure is in agreement with the former discussed molecules cerocene and bis( $\eta^8$ -pentalene)cerium and should make the assignment of oxidation states easier for these complexes. Additionally, the most compact CASSCF wavefunction, which still describes the influence of the f orbitals correctly is presented for every complex. As it was performed for bis( $\eta^8$ -pentalene)cerium the CASSCF(2,2) wavefunctions using localized orbitals were investigated by computing the charge fluctuation and the local spin for these compounds in order to describe the nature of the Ce-Z bonding. With these computations covalent and ionic character of the Ce-Z bonds can be distinguished. The presented results and discussion of the set of molecules  $\text{Cp}_2\text{CeZ}$  ( $\text{Z} = \text{CH}_2, \text{CH}^-, \text{NH}, \text{O}, \text{F}^+$ ) have already been published in 2015 [49].



### 3.3.2 Computational Details

The geometries of the  $\text{Cp}_2\text{CeZ}$  ( $\text{Z}=\text{CH}_2$ ,  $\text{CH}^-$ ,  $\text{NH}$ ,  $\text{O}$ ,  $\text{F}^+$ ) compounds were investigated at the HF level using TURBOMOLE version 6.3 [50] in  $\text{C}_1$  and  $\text{C}_{2v}$  symmetry. The small-core ECP28MWB pseudopotential with the corresponding basis set was used for cerium [51]. For all other elements, H, C, N, O and F the def-SV(P) as well as the def2-TZVP basis sets were used [52]. These computations are abbreviated as SVP and TZVP in the following. Frequency analyses were performed to confirm minimum structures. Additional geometry optimizations imposing  $\text{C}_{2v}$  symmetry were performed at the HF, RASSCF, CASSCF [53, 54] and RSPT2 [43] level using the MOLPRO 2012.1 program package [31].

The electronic structure and the relevance of the cerium 4f orbitals for the molecular electronic structure was investigated at the CASSCF level varying the active orbital space. Mulliken population analysis[13] as well as the investigation of orbital characters of the active orbitals were performed and the CI coefficients of the CASSCF wavefunction were calculated using the MRCI code of MOLPRO [55, 56].

Wavefunction-based *ab initio* computations were performed with three different basis sets. In all calculations the ECP28MWB pseudopotential with the corresponding ANO basis set was used for cerium [51]. The smallest basis set consists of contracted s,p,d and f function for Ce and the cc-pVDZ basis set with contracted s and p functions for C, N, O, F and only s functions for H. For the second basis the same basis function types were used for all atoms, but from the cc-pVTZ basis set. The largest basis set additionally included g functions for Ce, d functions for C, N, O, F and p functions for H [57]. These three basis sets are abbreviated as VDZ,  $\text{VTZ}_a$  and  $\text{VTZ}_b$ .

### 3.3.3 Ground State Geometries

As a first step the ground state geometries were calculated at the HF level applying two different basis sets. Therefore all complexes were optimized in  $C_{2v}$  and  $C_1$  symmetry and the energies were compared and analyzed. Frequency analyses were performed to identify minimum structures for all compounds. The results of these calculations are presented in Table 3.12.

**Table 3.3:** Energy differences of the optimized  $C_{2v}$  and  $C_1$  structures in kJ/mol.

	$\Delta E(C_{2v}-C_1)$	
	SVP	TZVP
CeCp <sub>2</sub> CH <sub>2</sub>	0.002	-0.004
CeCp <sub>2</sub> CH <sup>-</sup>	-0.185	-0.028
CeCp <sub>2</sub> NH	0.076	0.235
CeCp <sub>2</sub> O	0.245	0.367
CeCp <sub>2</sub> F <sup>+</sup>	0.885	1.078

The shown energy differences of all compounds are very small ( $<1.1$  kJ/mol) for all systems. The Cp<sub>2</sub>CeCH<sub>2</sub> as well as the Cp<sub>2</sub>CeCH<sup>-</sup> compound clearly revealed a  $C_{2v}$  minimum structure. The CH<sub>2</sub> complex geometry always resulted in a  $C_{2v}$  minimum structure or very close to that in case of  $C_1$  optimizations started with an unsymmetric geometry with twisted ligands. Therefore the energy differences in Table 3.12 are extremely small (0.002 and -0.004 kJ/mol), but the ground state of this complex will be discussed later in more detail. The energy difference between the  $C_{2v}$  and  $C_1$  structures are a little higher for the Cp<sub>2</sub>CeCH<sup>-</sup> (-0.185 and -0.028 kJ/mol) compared to the CH<sub>2</sub> complex. The ground state geometries of the other bis(cyclopentadienyl) complexes differ from the two already discussed ones. As the results in Table 3.12 reveal, the unsymmetric  $C_1$  minimum structure is energetically lower compared to the corresponding lowest  $C_{2v}$  geometry. The main difference of these two structures is that the cyclopentadienyl ligands are twisted and the two types of geometries are exemplarily shown for the Cp<sub>2</sub>CeO compound in Figure 3.5. The energy differences of these optimized structures are in a range of 0.076 up to 1.078 kJ/mol for the compounds. The largest value is computed for the Cp<sub>2</sub>CeF<sup>+</sup> complex. This can be explained by the positive charge of the fluorine ligand, which leads to a negative interaction with the partial positively charged hydrogen atoms of the Cp ligands. Therefore these groups try to avoid each other, which is realised by twisting the cyclopentadienyl ligands. Nevertheless, the energy differences between symmetric and unsymmetric structures are small for all complexes and the main

difference is the orientation of the Cp ligands. This orientation should not have a significant impact on the influence of the cerium f shell in molecular electronic structure and according to this the investigation of the influence f orbitals is based on the optimized  $C_{2v}$  geometries for all systems. These structures are shown in Figure 3.7.

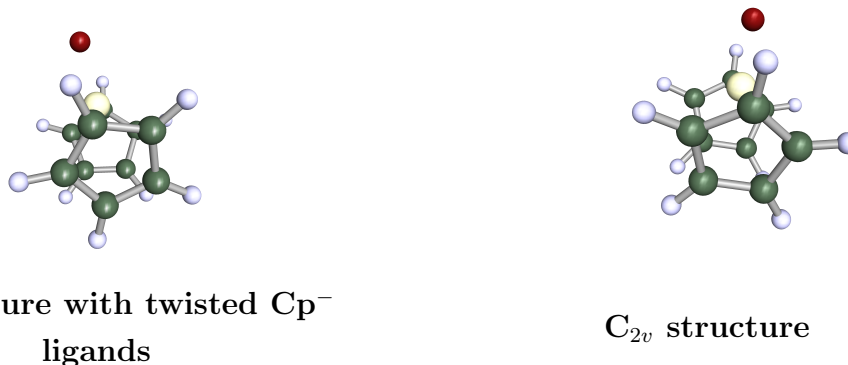


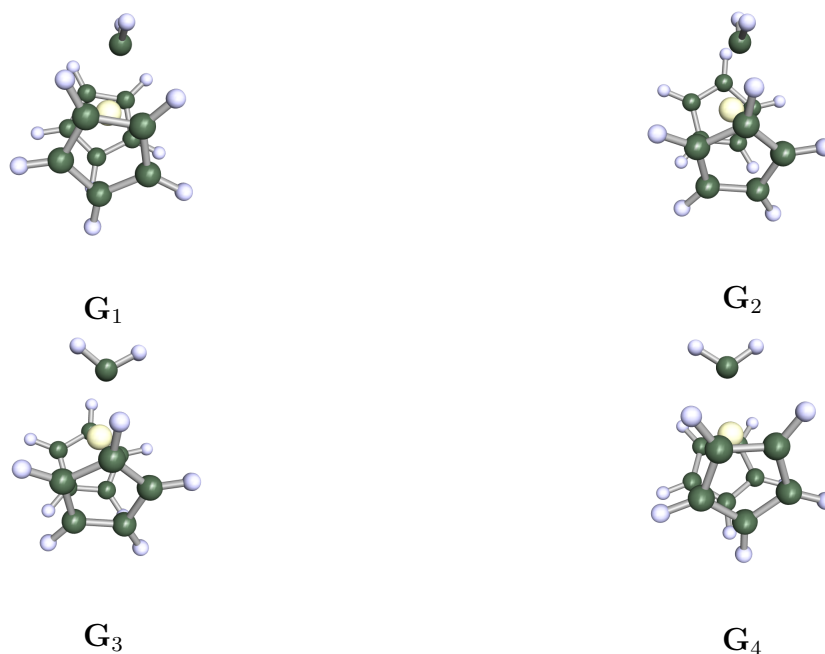
**Figure 3.5:** Different conformations of the  $Cp_2CeO$  complex.

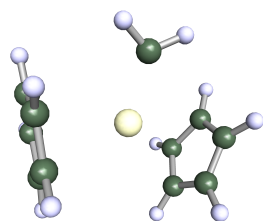
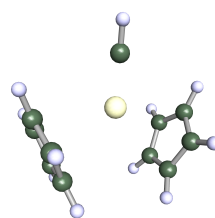
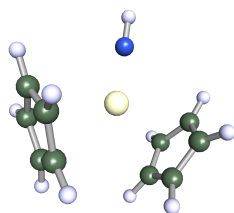
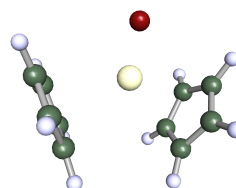
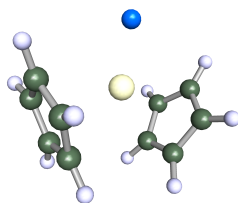
For the four complexes  $Cp_2CeZ$  ( $Z=CH^-$ ,  $NH$ ,  $O$ ,  $F^+$ ) two possible orientations of the Cp ligands exist in  $C_{2v}$  symmetry. The energetically lowest in all cases is analogue to the  $Cp_2CeO$  complex presented in Figure 3.5. Due to the different orientations of the  $CH_2$  group, four different  $C_{2v}$  structures are possible for the  $CpCeCH_2$  compound. The  $CH_2$  group can lie in the mirror plane between the Cp ligands mapping them onto each other or in the mirror plane defined by the cerium atom and one CH unit of the cyclopentadienyl ligands. The four possible conformations are shown in Figure 3.6 and will be discussed in more detail. Geometry optimizations of these structures were performed at the HF and RASSCF level and the corresponding results are presented in Table 3.4. All calculations revealed that the  $G_1$  geometry is the energetically lowest one. The possible conformations  $G_3$  and  $G_4$  are energetically clearly disfavoured. Their energies compared to the lowest structure  $G_1$  are  $\approx 55$  kJ/mol at the HF level and at least about 6 kJ/mol higher at the RASSCF level. The optimized  $G_2$  geometry is energetically closer to the  $G_1$  structure  $\approx 5$  kJ/mol higher at the HF level and 0.236 kJ/mol at the RASSCF level. However, the  $G_1$  geometry is the only confirmation which was found to be a real minimum.

**Table 3.4:** Energy differences  $\Delta E(G_i - G_1)$  in kJ/mol of the optimized  $C_{2v}$  geometries of the  $Cp_2CeCH_2$  compound.

	HF		RASSCF
	def-SV(P)	def2-TZVP	VDZ
$G_2$	5.632	4.510	0.236
$G_3$	54.566	54.071	5.785
$G_4$	56.859	56.049	6.332

For the  $Cp_2CeCH_2$  compound an equilibrium structure with a distorted  $Ce=CH_2$  group was described in a DFT study by Clark *et al.* [45] The  $\alpha$ -agostic interaction between one of the C-H bonds and the cerium resulted in a shortened cerium-hydrogen distance of 2.481 Å. Starting from such a geometry HF and CASSCF optimizations always converged to a equilibrium structure that was  $C_{2v}$  symmetric. Therefore additional DFT optimizations were performed using the B3-LYP functional, the ECP28MWB pseudo-potential with corresponding def-SV(P) basis set for cerium and the 6-31G[58] basis set for the other elements. This computation is comparable to the calculation performed by Clark *et al.* In this calculation no  $C_{2v}$  minimum structure was found and the distorted  $CH_2$  group, as a result of an  $\alpha$ -agostic interaction, can be supported.

**Figure 3.6:** Illustration of the possible  $C_{2v}$  structures of the  $Cp_2CeCH_2$  complex.

 $\text{CeCp}_2\text{CH}_2$  $\text{CeCp}_2\text{CH}^-$  $\text{CeCp}_2\text{NH}$  $\text{CeCp}_2\text{O}$  $\text{CeCp}_2\text{F}^+$ 

**Figure 3.7:** Optimized  $C_{2v}$  structures of all investigated  $\text{Cp}_2\text{CeZ}$  compounds.

### 3.3.4 Bond Distances and Force Constants

Bond distances calculated at several computational levels are presented in Table 3.5. With decreasing electronegativity of the Z group the Ce-Z bond distance increases in the series  $Z = O < NH < CH^- < CH_2$ , which agrees with the computed results of Clark *et al.*[45] Comparing the bond distances to the sum of the ionic radii reveals that these bonds are rather short. Clark *et al.* concluded that this behavior might be an indication for a covalent character of the Ce-Z interactions. The Ce-F bond distance is an exception of this overall trend. Nevertheless, the bond distance is still roughly 0.2 Å shorter than the sum of the ionic radii, which could imply weaker covalent contributions than in all other molecules.

**Table 3.5:** Ce-Z bond distances of the optimized structures given in Å.

Z	HF			RASSCF	CASSCF	RSPT2
	SVP	TZVP	VDZ		VDZ	
CH <sub>2</sub>	2.077	2.081	2.064	2.516	2.512	2.454
CH <sup>-</sup>	1.902	1.906	1.899	1.981	2.220	1.993
NH	1.867	1.872	1.870	1.900	1.925	1.946
O	1.755	1.757	1.787	1.815	1.844	1.854
F <sup>+</sup>	2.014	2.012	2.042	2.042	2.048	2.040

Additionally the strength of the Ce-Z bonds was estimated by computing a harmonic potential based on the equilibrium structure of all compounds at shortened and lengthened bond distances. The distances were deflected by 0.01 Å for each case. The resulting computed force constants of the Ce-Z bonds are presented in Figure 3.8. These constants are comparable to the single carbon-carbon bond in ethane and systematically increase with increasing electronegativity of the Z group. Again, the Cp<sub>2</sub>CeF<sup>+</sup> compound is an exception of this trend.

When optimizing the geometries using methods beyond the HF level, some significant changes occur. The energy differences between all possible C<sub>2v</sub> structures are reduced if the RASSCF method is applied (see Table 3.4). This implies a weaker interaction between the cyclopentadienyl ligands and the methylene group, which is supported by the result that the Ce-Z bond distance of this compound is increasing by about 0.4 Å using post HF methods. RASSCF, CASSCF as well as RSPT2 optimizations resulted in comparable bond distances for the CH<sub>2</sub> complex. In contrast to that, the Ce-Z bond distance of the CH<sup>-</sup> is slightly increased by about 0.1 Å at the RASSCF and RSPT2 level compared to the HF computations, whereby the CASSCF method delivers a signif-

icant enlargement of this bond by about 0.3 Å. These results indicate that  $\text{Cp}_2\text{CeCH}_2$  and  $\text{Cp}_2\text{CeCH}^-$  have significant multi-reference character. In comparison the Ce-Z bond distances are only enlarged by about 0.07 Å for the NH and O complex, whereas nearly no changes can be observed for  $\text{Cp}_2\text{CeF}^+$ . This indicates a small MR character for  $\text{Cp}_2\text{CeNH}$  and  $\text{Cp}_2\text{CeO}$  and supports a single reference description of the fluorine compound. Additionally, the force constants of the  $\text{F}^+$  complex are not changing when going from the HF to the RSP2 level, whereas they are reduced for all other compounds.

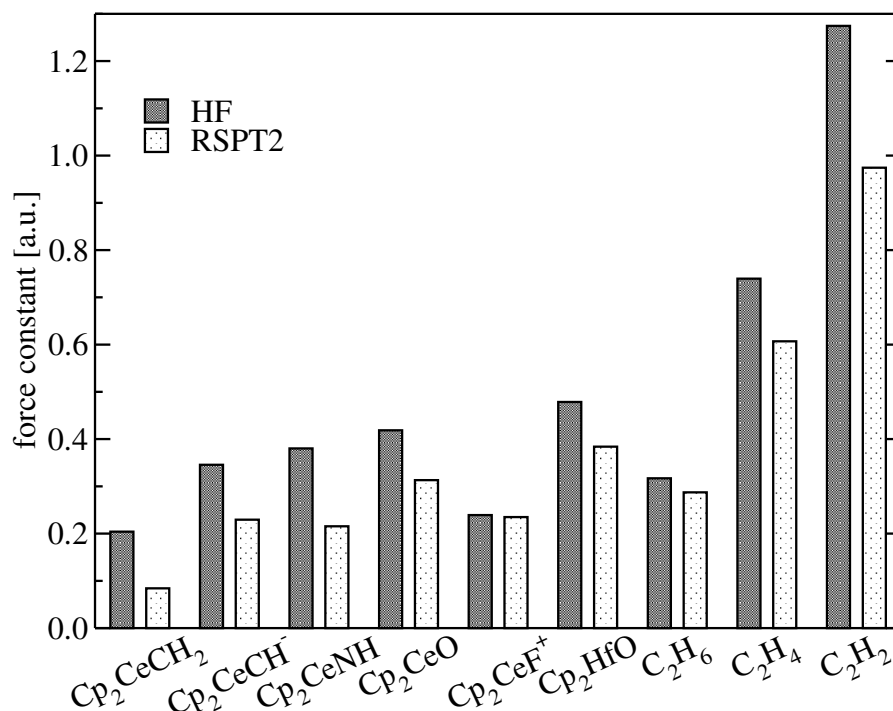


**Figure 3.8:** Force constants for the Ce-Z bond computed at the HF and RSPT2 level using the basis set given in a.u. for the  $\text{Cp}_2\text{CeZ}$  compounds compared to the Hf-O bond in  $\text{Cp}_2\text{HfO}$  and the C-C bonds of the molecular series  $\text{C}_2\text{H}_n$  ( $n=2, 4, 6$ ).

### 3.3.5 Electronic Structure

To investigate the molecular electronic structure several wave function-based methods were applied. As a first step RHF calculations were performed and afterwards MCSCF computations. In these calculations the  $C_{2v}$  symmetry was applied and the HF optimized structures, shown in Figure 3.7 were used. The active orbital space for the MCSCF computation included the seven cerium f orbitals and the HOMO of each molecule. For all molecules state-averaged calculations were performed computing all singlet and triplet states, which correspond to a  $f^0$  or  $f^1$  occupation of cerium. Afterwards the lowest singlet and triplet states were optimized separately for each compound. In this step two different calculation types were performed. In the first one, the occupation of the f orbitals was restricted from zero up to one electron and are named in the following as *restricted*. In the second computation all possible f occupations were allowed and therefore the results corresponding to this calculation type is named *unrestricted*. The results for the lowest singlet and triplet states were compared to the RHF energies and are presented in the Tables 3.6–3.10 for all investigated compounds for the *unrestricted* calculation type and three different basis sets.

It was found that the  $^1A_1$  state is the electronic ground state for all complexes and that the lowest triplet state is energetically higher compared to the singlet state for each complex. Nevertheless, the results of the five compounds differ. In case of the  $CH_2$  and  $CH^-$  complex the singlet and triplet states are lower than the RHF state, which is not obtained for the three remaining complexes. The cerium f populations determined by a Mulliken population analysis are higher than 1.0 for the  $Cp_2CeCH_2$  and the  $Cp_2CeCH^-$  compounds, which already indicates a significant relevance of the cerium 4f shell for their molecular electronic structure. The f populations of all other compounds are lower compared to these two molecules, but in case of  $Cp_2CeNH$  and  $Cp_2CeO$  the energy lowering of the singlet ground state at the MCSCF level also implies that the f orbitals are relevant for the electronic structure.

The results of  $Cp_2CeF^+$  complex differ from the other compounds. The  $^1A_1$  ground state is only lowered by about 0.7 eV at the MCSCF level and the corresponding f population is  $\approx 0.5$ , which is the lowest value of all bis(pentadienyl) cerium compounds. These results indicate that the cerium 4f shell is not as relevant for the  $F^+$  complex as for the other four compounds. The influence of these orbitals appears to be sufficiently accurate described at the closed-shell RHF level.



**Table 3.6:** Energy differences of the CASSCF states (unrestricted) of the CeCp<sub>2</sub>CH<sub>2</sub> complex compared to the RHF singlet state.

State	Basis	$\Delta E$ in eV	Ce f pop.
<sup>1</sup> A <sub>1</sub>	VDZ	-1.091	1.210
	VTZ <sub>a</sub>	-1.079	1.208
	VTZ <sub>b</sub>	-1.062	1.199
<sup>3</sup> A <sub>2</sub>	VDZ	-0.926	1.231
	VTZ <sub>a</sub>	-0.910	1.230
	VTZ <sub>b</sub>	-0.872	1.226

**Table 3.7:** As Table 3.6 but for the CeCp<sub>2</sub>CH<sup>-</sup> complex.

State	Basis	$\Delta E$ in eV	Ce f pop.
<sup>1</sup> A <sub>1</sub>	VDZ	-0.809	1.153
	VTZ <sub>a</sub>	-0.807	1.171
	VTZ <sub>b</sub>	-0.825	1.149
<sup>3</sup> B <sub>1</sub>	VDZ	-0.526	1.229
	VTZ <sub>a</sub>	-0.515	1.246
	VTZ <sub>b</sub>	-0.520	1.230

**Table 3.8:** As Table 3.6 but for the CeCp<sub>2</sub>NH complex.

State	Basis	$\Delta E$ in eV	Ce f pop.
<sup>1</sup> A <sub>1</sub>	VDZ	-0.603	0.595
	VTZ <sub>a</sub>	-0.598	0.605
	VTZ <sub>b</sub>	-0.739	0.582
<sup>3</sup> B <sub>1</sub>	VDZ	0.715	1.266
	VTZ <sub>a</sub>	0.736	1.277
	VTZ <sub>b</sub>	0.783	1.274

**Table 3.9:** As Table 3.6 but for the CeCp<sub>2</sub>O complex.

State	Basis	$\Delta E$ in eV	Ce f pop.
<sup>1</sup> A <sub>1</sub>	VDZ	-0.578	0.675
	VTZ <sub>a</sub>	-0.580	0.693
	VTZ <sub>b</sub>	-0.726	0.651
<sup>3</sup> A <sub>1</sub>	VDZ	1.548	1.330
	VTZ <sub>a</sub>	1.584	1.353
	VTZ <sub>b</sub>	1.717	1.322

**Table 3.10:** As Table 3.6 but for the CeCp<sub>2</sub>F<sup>+</sup> complex.

State	Basis	$\Delta E$ in eV	Ce f pop.
<sup>1</sup> A <sub>1</sub>	VDZ	-0.168	0.493
	VTZ <sub>a</sub>	-0.169	0.501
	VTZ <sub>b</sub>	-0.175	0.457
<sup>3</sup> A <sub>2</sub>	VDZ	0.899	1.274
	VTZ <sub>a</sub>	0.927	1.286
	VTZ <sub>b</sub>	1.011	1.251

On the basis of the already discussed MCSCF calculations the active orbital space was reduced to find the most compact wavefunction, which can still describe the electronic structure and the influence of the 4f shell correctly. Due to the low multi-reference character of the Cp<sub>2</sub>CeF<sup>+</sup> compound, this complex was not investigated in this part. First CASSCF calculations were performed with an active orbital space, where all of these orbitals have the same symmetry. There are two orbitals with symmetry a<sub>1</sub>, b<sub>1</sub> and b<sub>2</sub> and therefore these two f orbitals as well as the HOMO and HOMO-1 of each symmetry were included in the active space. The resulting active space consists of four electrons and 4 orbitals (CASSCF(4,4)). The seventh f orbital has a<sub>2</sub> symmetry and therefore these computations were carried out by including this f orbital and the HOMO in a<sub>2</sub> symmetry (CASSCF(2,2)). The <sup>1</sup>A<sub>1</sub> ground state was optimized at every computational level and for all compounds. The results of these computations are shown in the Tables 3.11–3.14.

**Table 3.11:** Energy differences of the  $^1A_1$  state of the  $CeCp_2CH_2$  complex compared to the RHF singlet state using the VDZ basis.

State	Orbital symmetry	$\Delta E$ in eV
$^1A_1$	$a_1$	-0.462
	$b_1$	-0.179
	$b_2$	-1.202
	$a_2$	-0.052

**Table 3.12:** As Table 3.11 but for the  $CeCp_2CH^-$  complex.

State	Orbital symmetry	$\Delta E$ in eV
$^1A_1$	$a_1$	-0.496
	$b_1$	-0.914
	$b_2$	-0.579
	$a_2$	-0.032

**Table 3.13:** As Table 3.11 but for the  $CeCp_2NH$  complex.

State	Orbital symmetry	$\Delta E$ in eV
$^1A_1$	$a_1$	-0.555
	$b_1$	-0.601
	$b_2$	-0.592
	$a_2$	-0.047

**Table 3.14:** As Table 3.11 but for the  $CeCp_2O$  complex.

State	Orbital symmetry	$\Delta E$ in eV
$^1A_1$	$a_1$	-0.681
	$b_1$	-0.593
	$b_2$	-0.588
	$a_2$	-0.048

These different CASSCF computations can reveal, which f orbital has the largest relevance for the molecular electronic structure of each compound. The smallest energy reduction of the ground state was obtained for all systems by the computation using orbitals with  $a_2$  symmetry. Therefore it can be concluded that the corresponding f orbital has no or at least just an insignificant influence for the molecular electronic structure. The f orbital in  $b_2$  symmetry appears to be the most relevant for the electronic structure of the  $\text{Cp}_2\text{CeCH}_2$  compound. The corresponding calculation lower the ground state by 1.202 eV, whereby it was lowered using  $a_1$  symmetric orbitals by 0.462 eV and 0.179 eV if  $b_1$  symmetric orbitals were used. For the  $\text{CH}^-$  complex the f orbital in  $b_1$  symmetry appears to be the most relevant one, showing an energy lowering of 0.914 eV (0.496 eV for  $a_1$  and 0.579 eV for  $b_2$ ). In case of  $\text{Cp}_2\text{CeNH}$  and  $\text{Cp}_2\text{CeO}$  the three f orbitals ( $a_1$ ,  $b_1$  and  $b_2$ ) showed a comparable influence on the ground state. Nevertheless, the  $b_1$  f orbital revealed to have the largest effect for the NH complex and  $a_1$  symmetric f orbital for the oxygen compound. This compound is the only molecule where the largest effect is not obtained in the symmetry, where the HOMO of the RHF calculation was found ( $b_1$  symmetric). Based on these insights the active space was reduced to two electrons and two orbitals (named *reduced* in the following). The orbitals, which resulted in the largest lowering of the ground state were chosen for each complex and the corresponding results are presented in the Tables 3.15–3.17 compared to the previously discussed CASSCF(2,8) results. It was emphasized that including the HOMO in the active orbital space resulted in a smaller energy lowering of the ground state than including the HOMO-1 ( $a_1$  symmetric). Therefore the different CASSCF(2,8) computations were performed by including this orbital instead of the HOMO and the results are presented in Table 3.18.

It can be seen that the CASSCF(2,2) level is a sufficiently accurate description for all compounds. The reduced calculation resulted in exactly the same lowering of the  $^1\text{A}_1$  ground as the restricted calculation, including all seven f orbitals. The energy difference of this restricted computation compared to the unrestricted CASSCF(2,8) is neglectable for the  $\text{CH}_2$  and the  $\text{CH}^-$  complex. In case of  $\text{Cp}_2\text{CeNH}$  and  $\text{Cp}_2\text{CeO}$  the unrestricted CASSCF computation lowered the ground state about 0.2 eV more at reduced CASSCF(2,2) level. However, reduced active space consisting of two electron and two orbitals is still a sufficiently accurate description for these compounds.

**Table 3.15:** Energy differences of the  $^1A_1$  state of the  $CeCp_2CH_2$  complex in comparison of the different performed CASSCF computations.

Basis	Type	$\Delta E$ in eV
VDZ	unrestricted	-1.091
	restricted	-1.082
	reduced $b_2$	-1.082
VTZ <sub>a</sub>	unrestricted	-1.079
	restricted	-1.068
	reduced $b_2$	-1.068
VTZ <sub>b</sub>	unrestricted	-1.062
	restricted	-1.037
	reduced $b_2$	-1.037

**Table 3.16:** As Table 3.16 but for the  $CeCp_2CH^-$  complex.

Basis	Type	$\Delta E$ in eV
VDZ	unrestricted	-0.809
	restricted	-0.786
	reduced $b_1$	-0.786
VTZ <sub>a</sub>	unrestricted	-0.807
	restricted	-0.783
	reduced $b_1$	-0.783
VTZ <sub>b</sub>	unrestricted	-0.825
	restricted	-0.775
	reduced $b_1$	-0.775

**Table 3.17:** As Table 3.16 but for the CeCp<sub>2</sub>NH complex.

Basis	Type	$\Delta E$ in eV
VDZ	unrestricted	-0.603
	restricted	-0.524
	reduced b <sub>1</sub>	-0.524
VTZ <sub>a</sub>	unrestricted	-0.598
	restricted	-0.519
	reduced b <sub>1</sub>	-0.519
VTZ <sub>b</sub>	unrestricted	-0.739
	restricted	-0.509
	reduced b <sub>1</sub>	-0.509

**Table 3.18:** As Table 3.16 but for the CeCp<sub>2</sub>O complex using the HOMO-1 instead of the HOMO.

Basis	Type	$\Delta E$ in eV
VDZ	unrestricted	-0.640
	restricted	-0.601
	reduced a <sub>1</sub>	-0.601
VTZ <sub>a</sub>	unrestricted	-0.633
	restricted	-0.590
	reduced a <sub>1</sub>	-0.590
VTZ <sub>b</sub>	unrestricted	-0.744
	restricted	-0.574
	reduced a <sub>1</sub>	-0.574

The previously discussed results showed that including the  $a_1$ ,  $b_1$  and  $b_2$  symmetric HOMOs in the active orbital space lead to a significant energy lowering of the ground state. Therefore all five compounds were investigated at the CASSCF(6,10) level, where all seven f orbitals as well as the mentioned three HOMOs were included in the active orbital space. All complexes were optimized at this level and in order to investigate the multi-reference character of these compounds the CI coefficients and the natural orbital occupation numbers were analyzed.  $C_{2v}$  symmetry was applied for these computations. This higher CASSCF level should be more appropriate to investigate the electronic structure of the five complexes than the previously discussed computations. The results are listed in the Tables A.1–A.10 in the *Appendix* for the  $^1A_1$  ground state, which was also found for every molecule at this computational level.

$Cp_2CeCH_2$  clearly showed MR character with two leading configurations. The corresponding contributions are about 56% and 41%. The analysis of the occupation pattern revealed that the first configuration corresponds to the closed-shell HF solution, whereby the second configuration is constructed by a double excitation from the  $b_2$  symmetric HOMO to the  $b_2$  symmetric LUMO. The natural orbital occupation numbers for these orbitals are 1.15 and 0.84. The occupation numbers for the other natural orbitals are higher than 1.97 or lower than 0.03 and therefore it is indicated that the wavefunction can be reduced to the CASSCF(2,2) level including two  $b_2$  symmetric orbitals. These results of the CASSCF(6,10) wavefunction are in complete agreement to the previously discussed ones. The Mulliken population analysis for two active orbitals at the CASSCF level determined cerium f contributions of about 52% and 49%, and carbon p contributions of 44% and 47%.

For the  $Cp_2CeCH^-$  compound the situation is quite comparable. Again two leading configurations were obtained contributing with about 61% and 30%. The two configurations correspond to the closed-shell HF solution and a double excitation from the  $b_1$  symmetric HOMO to the corresponding LUMO. The associated natural orbital occupation numbers are 1.32 and 0.67. The occupation numbers of these active orbitals were close to two or zero and therefore the reduction to a CASSCF(2,2) level with two  $b_1$  orbitals is indicated by these results and is also in agreement with the results presented in Table 3.16. The Mulliken population analysis of one of these active orbitals computes a cerium d/f character of 17%/27% and a carbon p contribution of 53%. The other orbital showed cerium f (65%) and carbon p contributions (33%). According to the high MR character of these two compounds they can not be well described at the HF level as well as at a standard DFT level.

For all other compounds  $\text{Cp}_2\text{CeNH}$ ,  $\text{Cp}_2\text{CeO}$  and  $\text{Cp}_2\text{CeF}^+$  a single dominant configuration (contributions: 91%, 91% and 93%) was obtained. The amount of configuration that contribute more than 0.25% is larger compared to the  $\text{CH}_2$  and  $\text{CH}^-$  compound. For the  $\text{Cp}_2\text{CeNH}$  and the  $\text{Cp}_2\text{CeO}$  complex only configurations arising from excitations of the HOMOs in  $a_1$ ,  $b_1$  and  $b_2$  symmetry to the corresponding LUMOs occur. This agrees with the results presented in the Tables 3.13 and 3.14. For  $\text{Cp}_2\text{CeF}^+$  additional excitations to the  $a_2$  symmetric LUMO can be observed. The active orbitals involved in the excitations of the  $\text{Cp}_2\text{CeNH}$  and  $\text{Cp}_2\text{CeO}$  complexes show dominant character ( $\approx 99\%$ ). Besides the leading closed-shell HF configuration, the additional configurations can be assigned to excitations of the Cp ligands. The occupation number analysis of the active orbitals revealed occupations larger than 1.92 or lower than 0.07, which is consistent with their dominant leading closed-shell determinant and therefore these compounds can not be described as compact as it is possible for the  $\text{Cp}_2\text{CeCH}_2$  and  $\text{Cp}_2\text{CeCH}^-$  compounds. However, these three compounds also show some MR character.

Mulliken population analyses were performed for the ground state at the CASSCF(6,10) level in order to investigate the relevance of the f orbitals. The corresponding results are listed in Table 3.19 and are compared to the HF computations. For the  $\text{CH}_2$  as well as for the  $\text{CH}^-$  compound the f population is significantly increased, when going from the HF to the CASSCF level, whereas the d population is lowered. For the remaining complexes the populations are not significantly differing at the CASSCF level compared to the HF calculations. These results indicate that  $\text{Cp}_2\text{CeCH}_2$  and  $\text{Cp}_2\text{CeCH}^-$  are Ce(III) systems, but a leading  $f^1$  configuration in the wavefunction should be proven in order to confirm this oxidation state. In contrast to these compounds the cerium f shell revealed a low influence for the  $\text{Cp}_2\text{CeF}^+$  complex. Considering the small MR character of this complex it might be best described as a Ce(IV) compound, whereas the other two molecules appear to be mixed valent Ce(III)/Ce(IV) systems.

**Table 3.19:** Cerium 4f and 5d populations for the  $^1A_1$  CASSCF (HF) ground state of all investigated compounds.

	VDZ		VTZ <sub>b</sub>	
	f pop.	d pop.	f pop.	d pop.
$\text{CH}_2$	1.210 (0.431)	1.341 (2.118)	1.199	1.399
$\text{CH}^-$	1.153 (0.479)	1.678 (2.386)	1.148	1.668
NH	0.595 (0.548)	1.867 (1.854)	0.582	1.899
O	0.734 (0.638)	1.720 (1.756)	0.688	1.759
$\text{F}^+$	0.493 (0.471)	1.650 (1.624)	0.457	1.645



In order to obtain a more complex and detailed picture of the multi-reference character of the discussed systems, the five molecules were reinvestigated at the CASSCF(2,2) level based on the HF optimized  $C_{2v}$  structures, varying the active orbitals. Additionally, the excitations were characterized for these computations. The included orbitals correspond to the same irreducible representation. The Ce-Z units are assumed to be quasi linear and therefore the corresponding orbitals of the bond between Ce and the Z group can be categorized as  $\sigma$  ( $a_1$ ) and  $\pi$  ( $b_1$  and  $b_2$ ). The performed calculations are an extension of the already discussed computations given in the Tables 3.11–3.18 and the results are presented in the following Tables 3.20 and 3.21.

**Table 3.20:** Energy differences of the  $^1A_1$  ground state at the CASSCF(2,2) level and the closed-shell HF ground state of the  $Cp_2CeCH_2$  and  $Cp_2CeCH^-$  complex.  $\Delta E$  values are given in eV.

Z	Orb. Sym.	Exc. type	$\Delta E_{VDZ}$	$\Delta E_{VTZ_b}$
CH <sub>2</sub>	$a_1$	Ce-C $\sigma \rightarrow \sigma^*$	-0.386	-0.392
		Ce 4d $\rightarrow$ 4f	-0.244	-0.266
	$b_1$	Ce 4d $\rightarrow$ 4f	-0.173	-0.173
		Ce-C $\pi \rightarrow \pi^*$	-1.082	-1.037
	$b_2$	Ce 4d $\rightarrow$ 4f	-0.170	-0.170
		Ce 4d $\rightarrow$ 4f	-0.091	-0.091
	$a_2$	Ce 4d $\rightarrow$ 4f	-0.091	-0.091
	$a_2$	Ce 4d $\rightarrow$ 4f	-0.091	-0.091
CH <sup>-</sup>	$a_1$	C-H $\sigma \rightarrow \sigma^*$	-0.424	-0.414
		Ce-C $\sigma \rightarrow \sigma^*$	-0.259	-0.274
		Ce 4d $\rightarrow$ 4f	-0.242	-0.263
	$b_1$	Ce-C $\pi \rightarrow \pi^*$	-0.786	-0.775
		Ce 4d $\rightarrow$ 4f	-0.167	-0.167
	$b_2$	Ce-C $\pi \rightarrow \pi^*$	-0.509	-0.491
		Ce 4d $\rightarrow$ 4f	-0.170	-0.169
	$a_2$	Ce 4d $\rightarrow$ 4f	-0.090	-0.090

The results reveal that significant MR character arise from the binding ( $\sigma$  and  $\pi$ ) and antibinding ( $\sigma^*$  and  $\pi^*$ ) orbitals of the Ce-Z unit. These orbitals are linear combinations of s, p, d, f functions centered on Ce and s, p functions centered on the Z group. Even for the  $Cp_2CeF^+$  compound MR character arises from the Ce- $F^+$  unit resulting in an energy lowering of about 0.4 eV, which was not obtained by the CASSCF(2,8) computations (see Table 3.10). These values are the overall lowest of the series  $Cp_2CeZ$  ( $Z = NH, O, F^+$ ), but they are comparable to  $Cp_2CeNH$  and  $Cp_2CeO$ . Therefore the

**Table 3.21:** As Table 3.20 but for the  $\text{Cp}_2\text{CeZ}$  ( $\text{Z} = \text{NH}, \text{O}, \text{F}^+$ ) compounds.

Z	Orb. Sym.	Exc. type	$\Delta E_{\text{VDZ}}$	$\Delta E_{\text{VTZ}_b}$
NH	a <sub>1</sub>	N-H $\sigma \rightarrow \sigma^*$	-0.481	-0.460
		Ce-N $\sigma \rightarrow \sigma^*$	-0.299	-0.317
		Ce 4d $\rightarrow$ 4f	-0.243	-0.264
	b <sub>1</sub>	Ce-N $\pi \rightarrow \pi^*$	-0.524	-0.509
		Ce 4d $\rightarrow$ 4f	-0.167	-0.167
	b <sub>2</sub>	Ce-N $\pi \rightarrow \pi^*$	-0.545	-0.535
		Ce 4d $\rightarrow$ 4f	-0.170	-0.168
	a <sub>2</sub>	Ce 4d $\rightarrow$ 4f	-0.091	-0.091
O	a <sub>1</sub>	Ce-O $\sigma \rightarrow \sigma^*$	-0.601	-0.574
		Ce 4d $\rightarrow$ 4f	-0.249	-0.274
	b <sub>1</sub>	Ce-O $\pi \rightarrow \pi^*$	-0.517	-0.498
		Ce 4d $\rightarrow$ 4f	-0.168	-0.168
	b <sub>2</sub>	Ce-O $\pi \rightarrow \pi^*$	-0.541	-0.525
		Ce 4d $\rightarrow$ 4f	-0.170	-0.170
	a <sub>2</sub>	Ce 4d $\rightarrow$ 4f	-0.091	-0.091
F <sup>+</sup>	a <sub>1</sub>	Ce-F $\sigma \rightarrow \sigma^*$	-0.429	-0.447
		Ce 4d $\rightarrow$ 4f	-0.243	-0.259
	b <sub>1</sub>	Ce-F $\pi \rightarrow \pi^*$	-0.388	-0.393
		Ce 4d $\rightarrow$ 4f	-0.169	-0.170
	b <sub>2</sub>	Ce-F $\pi \rightarrow \pi^*$	-0.407	-0.414
		Ce 4d $\rightarrow$ 4f	-0.173	-0.173
	a <sub>2</sub>	Ce 4d $\rightarrow$ 4f	-0.091	-0.091

electronic structure of these compounds is not differing as much as it was emphasized by the CASSCF(2,8) calculations. This insight was also supported by the CASSCF(6,10) results. The CASSCF(2,2) computations including a<sub>2</sub> symmetric orbitals lead to the correlation of the doubly occupied cerium 4d orbital by the empty cerium 4f orbital. Such a kind of correlation is also present in all other CASSCF(2,2) computations including a<sub>1</sub>, b<sub>1</sub> and b<sub>2</sub> symmetric orbitals. The resulting energetical lowering of the ground state is quite small (<0.25 eV) for all compounds and every active space. Therefore it can be classified as dynamic correlation. In case of  $\text{Cp}_2\text{CeCH}^-$  and  $\text{Cp}_2\text{CeNH}$  MR character also arised from the  $\sigma \rightarrow \sigma^*$  excitation of the CH or NH group and the ground state was lowered by 0.414 and 0.460 eV. Such excitation was not observed for the  $\text{CH}_2$  complex.

For comparison it should be mentioned that the energy lowering for a  $\sigma$  bond in a hydrogen dimer is 0.5 eV. The  $\sigma$  bond ( $a_1$ ) of the  $\text{Cp}_2\text{CeCH}_2$  shows a small lowering of about 0.39 eV, whereas the  $\pi$  bond ( $b_2$ ) reveals a comparatively large effect (-1.037 eV for the VTZ<sub>b</sub> basis). Since no bonding orbital is involved, the energy lowering is small for the other symmetries. Therefore the MR character mainly arises from the  $\pi$  bond. The bonding  $\sigma$  and  $\pi$  orbitals show 48% and 43% contributions from the carbon and 52% and 54% from the cerium. The corresponding contributions of the antibonding orbitals ( $\sigma$  and  $\pi$ ) are 42% and 45% for carbon and 53% and 54% for cerium. According to the analysis the Ce-C bonds of the  $\text{CH}_2$  compound are unpolar. The carbon contributions to the  $\sigma$  bond can be assigned to a  $2s2p^2$  hybrid-type orbital, whereas the cerium contributions arise mainly from 5d orbitals with a small admixture of 4f. The  $\pi$  bond is constructed by carbon 2p and cerium 4f orbitals. The 4f contributions are 49% for the bonding and 52% for the antibonding molecular orbital. Therefore about one f electron is located in the  $\pi$  bond implying a Ce(III) complex and all results are in good agreement to the CASSCF(6,10) computations.

The results of  $\text{Cp}_2\text{CeCH}^-$  are quite comparable. The energy lowering arising from the  $a_1$  symmetric  $\sigma$  bond is smaller (-0.274 eV) compared to the  $\text{CH}_2$  complex. Since the Ce-C bond distance is about 0.17 Å shorter (see Table 3.5) compared to  $\text{Cp}_2\text{CeCH}_2$ , less contributions from excited states are required for the  $\text{CH}^-$  compound. For the  $a_1$  orbitals correlation arising from the C-H and Ce-C  $\sigma$  bonds has to be distinguished. The Mulliken analysis revealed, that either only carbon and hydrogen or only cerium and carbon contributions are obtained for the active orbitals. Therefore the C-H and Ce-C bonds can be distinguished. The Ce-C  $\sigma$  bond is mainly composed of carbon  $2s2p^2$  hybrid-type and cerium 5d orbitals. In agreement to the energy lowering of the  $\sigma$  bond, the  $\pi$  bonds lower the ground state energy less compared to the  $\text{CH}_2$  complex. The  $b_1$  symmetric  $\pi$  orbitals show the largest effect. This molecular orbital is composed by cerium 4f and carbon 2p orbitals, whereas the main contributions of the  $b_2$  symmetric  $\pi$  orbital are carbon 2p and cerium 5d. Thus the most relevant contribution to the multi-reference character of this compound arises from the  $\pi$  bond where the cerium 4f orbital is involved.

In case of  $\text{Cp}_2\text{CeNH}$  the energy lowering arising from the Ce-N  $\sigma$  bond (-0.317 eV) is lower than the N-H  $\sigma$  bond (-0.460 eV), which is comparable to the  $\text{CH}^-$  compound. Almost equal energy lowerings were obtained by the  $\pi$  bonds (-0.509 eV, -0.535 eV), implying a smaller MR character of this complex compared to  $\text{Cp}_2\text{CeCH}_2$  and  $\text{Cp}_2\text{CeCH}^-$ . The energy lowering of the  $\pi$  bonds of  $\text{Cp}_2\text{CeO}$  are similar to the NH complex, but in contrast the effect of the  $\sigma$  bond is higher for the oxygen compound. All three bonds

revealed comparable energy lowerings. For the active orbitals the contributions of the N and O 2s orbitals are neglectable compared to the CH<sub>2</sub> and CH<sup>-</sup> compounds and the role of the influence of the 2p orbitals are higher. This trend can be explained by the increased electronegativity of oxygen and nitrogen compared to carbon as well as by the increased energy gap between 2s and 2p. Summarizing the results for these compounds it can be concluded that MR character is obtained for these compounds but the contributions can not be mainly assigned to a single bond.

The F<sup>+</sup> compound shows small energy lowerings arising from the three Ce-F bonds ( $\sigma$ : -0.447 eV,  $\pi$ : -0.393 eV and -0.414 eV). Dominant fluorine 2p character can be observed for these bonds. The overall contributions arising from the fluorine atom are about 86% ( $\sigma$ ) and 92–93% ( $\pi$ ) for the bonding molecular orbital and still contributions of 62% and 72–76% are computed for the antibonding ones. The cerium contributions are 13% and 7–8% for the bonding and 38% and 22–28% for antibonding orbitals. The 4f character of the bonding and antibonding orbitals are between 2 and 9%. These results support the Ce(IV) oxidation state for this compound.

### 3.3.6 Active Orbital Rotation

In the following section the relevance of the cerium 4f shell will be further investigated by using most compact MR wavefunctions in the sense of localized orbitals of Ce and the Z group. At several CASSCF levels it was shown that the Cp<sub>2</sub>CeCH<sub>2</sub> and Cp<sub>2</sub>CeCH<sup>-</sup> complexes can be accurately described at the CASSCF(2,2) level using active orbitals of the b<sub>2</sub> (CH<sub>2</sub>) or b<sub>1</sub> (CH<sup>-</sup>) irreducible representation. The corresponding natural orbitals revealed a mixed cerium and carbon character. The contributions of cerium dominantly arised from the 4f shell. Thus orbital rotation was applied to the active orbital space in order to separate these different contributions. In this procedure the rotation angle of the active orbitals was varied in steps of 1 ° between 0 ° and 90 °, while the CI coefficients as well as the orbital characters were monitored. Afterwards the steps were refined (0.1 °) to find the rotation angle with maximized Ce f or Z p character. The results for selected rotations angles are presented in the Tables 3.22 and 3.23. The full rotation is exemplarily shown for the Cp<sub>2</sub>CeCH<sub>2</sub> and Cp<sub>2</sub>CeO compounds in the Figures 3.9 and 3.10 using the orbitals that led to the largest energy lowering.

The results for the CH<sub>2</sub> and CH<sup>-</sup> compounds were similar to cerocene. A nearly pure cerium f orbitals can be created by applying the orbital rotation. The remaining orbital can be assigned to the carbon atom of the CH<sub>2</sub> or CH<sup>-</sup> group and mainly shows 2p character. If natural orbitals are used, a closed-shell configuration has the highest contribution to the wavefunction for these compounds (CH<sub>2</sub>:  $\approx$  58%, CH<sup>-</sup>: 80%), which can

mislead to the conclusion that these compounds are Ce(IV) complexes. As previously mentioned the natural orbitals are mixtures of cerium and carbon orbitals. Additionally, the coefficients of the second closed-shell configurations ( $\text{CH}_2$ :  $\approx 42\%$ ,  $\text{CH}^-$ :  $20\%$ ) have opposite sign compared to the leading ones. This is analogue to the wavefunction of the He  $1s^1 2s^1$  singlet state ( $^1S$ ), which can be written as  $0.744|1s^2\rangle - 0.633|2s^2\rangle$  (computed with MOLPRO using the aVTZ basis set). At the rotation angle, where the nearly pure f orbital is obtained the leading configuration is Ce- $f^1\text{C-p}^1$  for both compounds ( $\text{CH}_2$ :  $\approx 96\%$ ,  $\text{CH}^-$ :  $\approx 90\%$ ), revealing that these compounds are definitely Ce(III) systems with an open-shell singlet ground state. The other configuration can be neglected. In case of  $\text{CH}_2$  this analysis was also performed for the CASSCF optimized structure leading to nearly 100%  $f^1p^1$  character of the wavefunction. Figure 3.9 also emphasizes that at least one configuration ( $a^1b^1, a^0b^2$  or  $a^2b^0$ ) can be suppressed.

**Table 3.22:** Configuration contributions (in %) to the  $^1A_1$  ground state wavefunction at the CASSCF(2,2) level for the  $\text{Cp}_2\text{CeCH}_2$  and  $\text{Cp}_2\text{CeCH}^-$  compounds based on their HF optimized  $C_{2v}$  symmetric structure. The rotation angle with maximized f character of orbital a is shown for each complex and the corresponding results for the CASSCF(6,10) optimized geometry are written in parentheses.

	Basis set	rotation angle	config. contribution			Ce f character of orbital a	Z p character of orbital b
			$a^1b^1$	$a^2b^0$	$a^0b^2$		
$\text{CH}_2$	VDZ	45.9 °	95.97	1.41	2.63	0.996	0.893
	VTZ <sub>b</sub>	46.0 °	95.87	1.38	2.75	0.996	0.879
	(VTZ <sub>b</sub> )	45.6 °	99.45	0.13	0.42	1.000	0.911)
$\text{CH}^-$	VDZ	42.8 °	90.16	2.69	7.15	0.983	0.850
	VTZ <sub>b</sub>	47.3 °	90.22	2.57	7.21	0.985	0.854

The compounds  $\text{Cp}_2\text{CeNH}$  and  $\text{Cp}_2\text{CeO}$  reveal a different behavior. Selected results are presented in Table 3.23 for CASSCF(2,2) calculations where  $a_1$ ,  $b_1$  and  $b_2$  symmetric orbitals were involved and an exemplarily full orbital rotation is presented in Figure 3.10. The molecular bonds arising from these orbitals showed comparable energy lowerings at the CASSCF(2,2) level and are therefore all presented. It can be seen that for these complexes no nearly pure cerium f orbital could be created and the Z p character was maximized. As a results nearly pure Z p orbitals were obtained, while the second orbital shows mixed cerium f/d character. However, the orbitals were localized to single atoms

of the Ce-Z unit in each case. Using localized orbitals the leading configuration for these two compounds is open-shell and might be written as Ce-(f/d)<sup>1</sup>Z-p<sup>1</sup>. This configuration can be assigned to a Ce(III) compound and the corresponding contribution ranges from about 53% up to 60%. The Z p<sup>2</sup> configuration also shows high contributions about 25% up to 41% and can be assigned to Ce(IV) compounds. The influence of the p<sup>2</sup> configuration is higher for the oxygen compound, which might results from the increased electronegativity. Except of the CASSCF(2,2) calculation including a<sub>1</sub> symmetric orbitals of Cp<sub>2</sub>CeNH, the (f/d)<sup>2</sup> configuration revealed contributions <10%. According to this Cp<sub>2</sub>CeO and Cp<sub>2</sub>CeNH might be best categorized as mixed valent Ce(III)/Ce(IV) compounds.

For the Cp<sub>2</sub>CeF<sup>+</sup> complex the orbitals could not be well localized. When a nearly pure F 2p orbital is created by orbital rotation the other orbital still showed a mixed character (F:  $\sigma$  46%,  $\pi$  69% and 63%; Ce:  $\sigma$  53%,  $\pi$  29% and 36%). It should be noted that the contributions arising from cerium mainly correspond to d orbitals. Even for the localized orbitals the leading configuration is still closed-shell. Therefore it can be concluded that Cp<sub>2</sub>CeF<sup>+</sup> is definitely a Ce(IV) system.

**Table 3.23:** As Table 3.22 but for the Cp<sub>2</sub>CeZ (Z = NH, O, F<sup>+</sup>) compounds. The rotation angle leading to a maximized Z p character using the VTZ<sub>b</sub> basis are shown.

	Orb. sym.	rotation angle	config. a <sup>1</sup> b <sup>1</sup>	contribution a <sup>2</sup> b <sup>0</sup>	a <sup>0</sup> b <sup>2</sup>	Ce f/d character of orbital a	Z p character of orbital b
NH	a <sub>1</sub>	42.9 °	56.86	17.94	25.19	0.140/0.611	0.719
	b <sub>1</sub>	54.1 °	58.30	5.91	35.78	0.321/0.480	1.013
	b <sub>2</sub>	52.6 °	60.62	7.19	32.19	0.200/0.638	1.015
O	a <sub>1</sub>	52.0 °	58.31	9.10	32.59	0.473/0.468	0.947
	b <sub>1</sub>	56.1 °	52.96	5.16	41.88	0.243/0.448	1.023
	b <sub>2</sub>	55.1 °	54.98	5.79	39.24	0.179/0.554	1.023
F <sup>+</sup>	a <sub>1</sub>	61.0 °	41.58	3.04	55.38	0.130/0.328	0.879
	b <sub>1</sub>	28.9 °	41.44	2.97	55.59	0.113/0.130	1.004
	b <sub>2</sub>	29.0 °	42.02	2.87	55.11	0.084/0.230	1.005

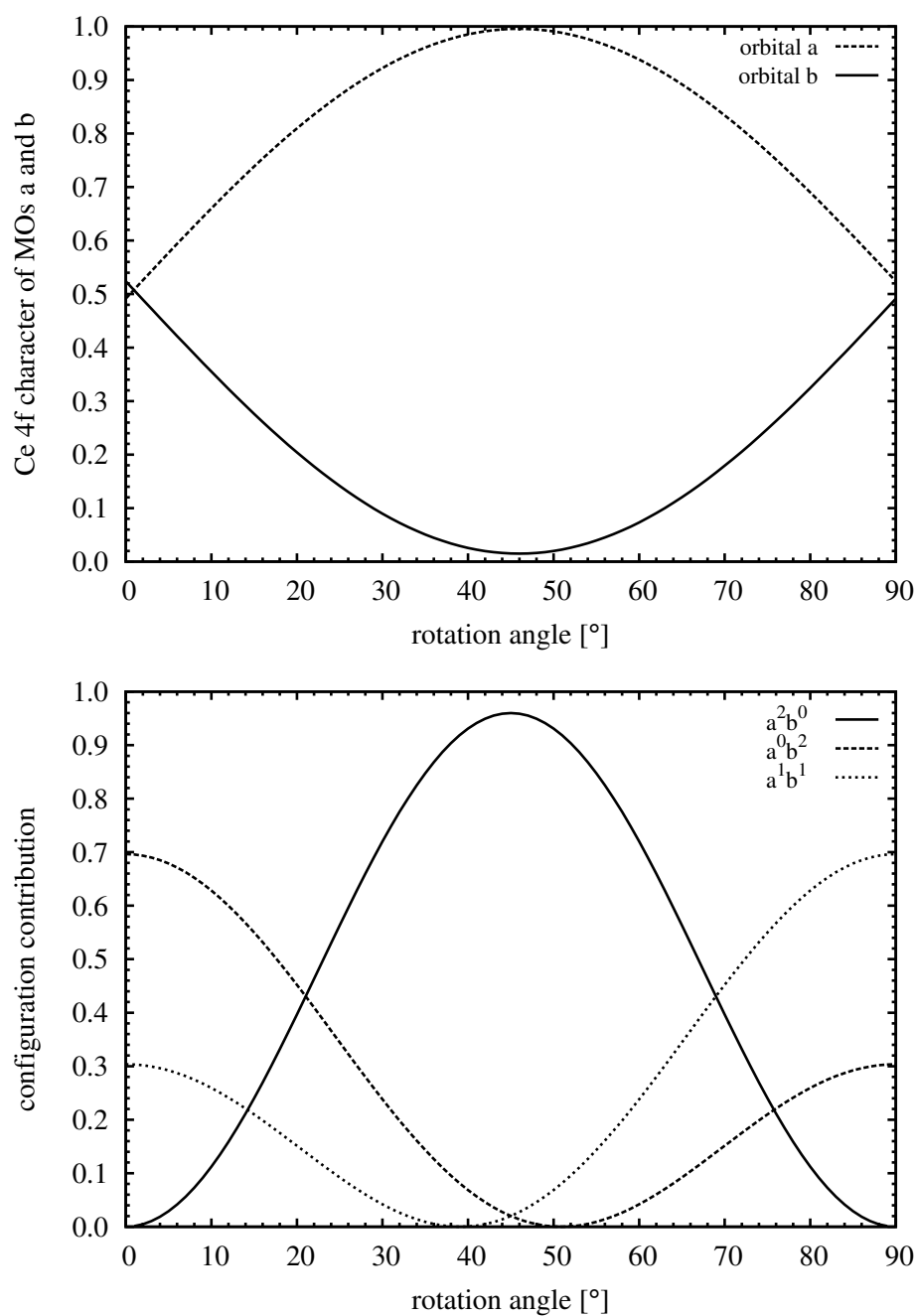


**Figure 3.9:** Orbital characters determined by Mulliken population analysis (top) and configuration contributions to the CASSCF(2,2) wavefunction (bottom) for  $\text{Cp}_2\text{CeCH}_2$  using the VTZ<sub>b</sub> basis sets. The vertical line shows the rotation angle where the f character of orbital a is maximized

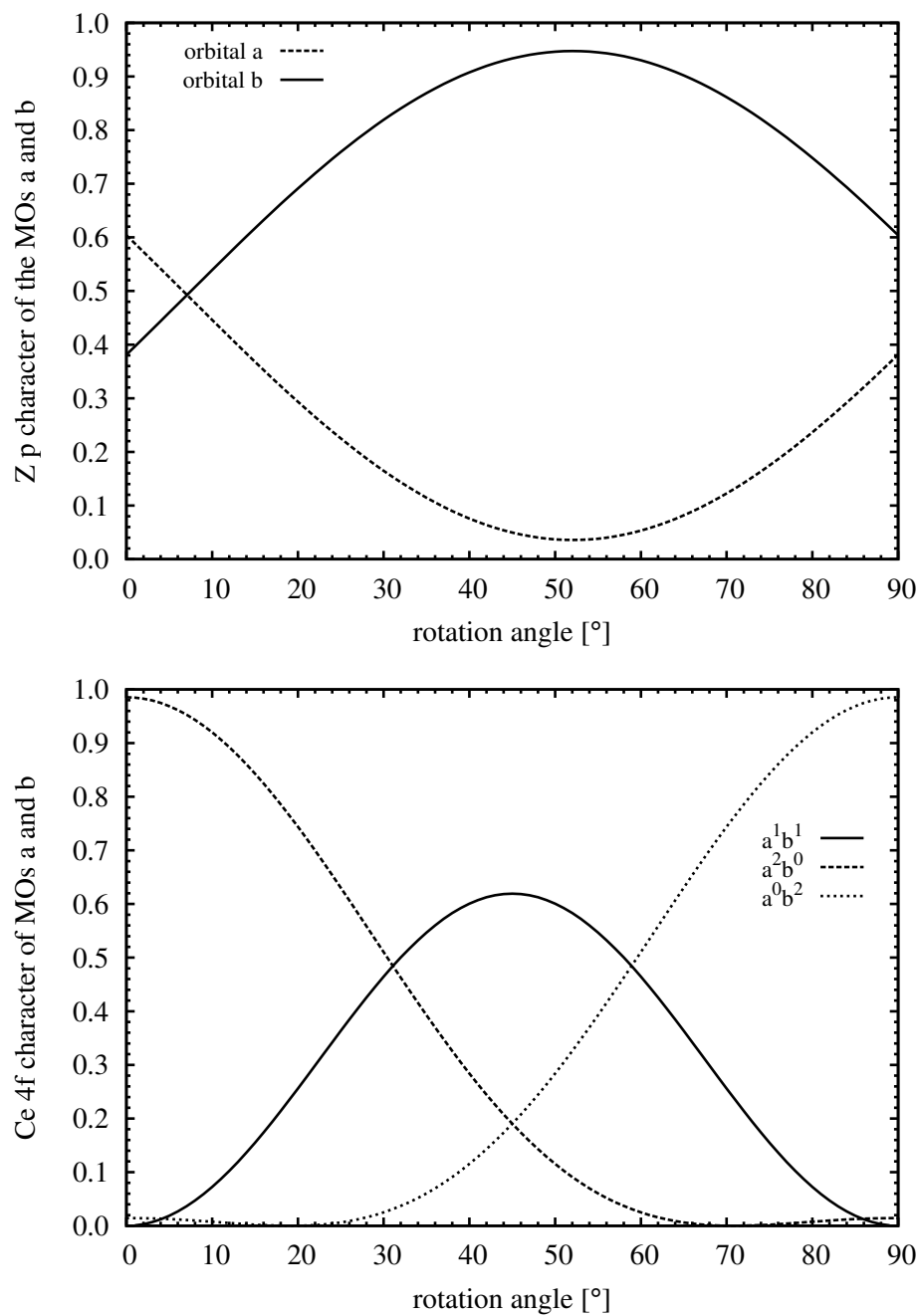


**Figure 3.10:** As Figure 3.9 but for the  $\text{Cp}_2\text{CeO}$  compound using  $a_1$  symmetric orbitals. The p character of orbital b was maximized.



### 3.3.7 Occupation Number Fluctuation Analysis

Finally, the occupation number or charge fluctuation and the local spin were computed and analyzed with respect to one of the two atoms of the Ce-Z unit. This analysis was described by Mödl *et al.* [44, 59]. In the case of an ideal covalent bond including two electrons, these values can be easily calculated. The charge fluctuation on one center is  $3/8$  and the corresponding local spin  $\sqrt{2}/2$ . The corresponding values are  $3/4$  and  $0$  for a dissociated bond. These values were computed for the localized orbitals (maximized f or p character) of the Ce-Z  $\sigma$  and  $\pi$  bonds for all compounds using the active orbitals of the CASSCF(2,2) computation. For comparison the corresponding values of an  $H_2$  dimer were computed for bond distances between  $0.75 \text{ \AA}$  and  $3.0 \text{ \AA}$  in steps of  $0.25 \text{ \AA}$  using the two s orbitals as active space. The resulting curve can be used to detect covalent orbital interactions and to categorize the interaction from weak to strong. The computed results are presented in Figure 3.11.

For  $Cp_2CeCH_2$  and  $Cp_2CeCH^-$  the  $\sigma$  bond of the Ce-C unit as well as one  $\pi$  bond of the  $CH^-$  compound revealed covalent character similar to the hydrogen dimer at its equilibrium geometry. Therefore these orbital interactions can be assigned to be strong covalent. The second  $\pi$  bond of  $Cp_2CeCH^-$  and the  $\pi$  bond of  $Cp_2CeCH_2$  also show covalent character but in contrast to the  $\sigma$  bonds it is similar to the orbital interaction of a stretched  $H_2$  bond. Thus, the orbital interactions can be categorized as weak covalent. It should be noted that for the CASSCF(6,10) optimized structure of  $Cp_2CeCH_2$  the orbital interaction of the  $\pi$  bond corresponds to a nearly dissociated  $H_2$  bond at a distance of  $3 \text{ \AA}$ . The described weak covalent orbital interactions lead to the large MR character of the two complexes.

The orbital interactions for the  $Cp_2CeNH$  and  $Cp_2CeO$  compounds revealed Ce 4f/5d-Z p covalency, but with a slightly increased ionic character. This might result from the increased electronegativity of the nitrogen and oxygen atoms of the Z group. The orbital interactions of the fluorine compound show significantly more ionic character compared to all other compounds, which is in agreement to the conclusion that this compound is a Ce(IV) system.

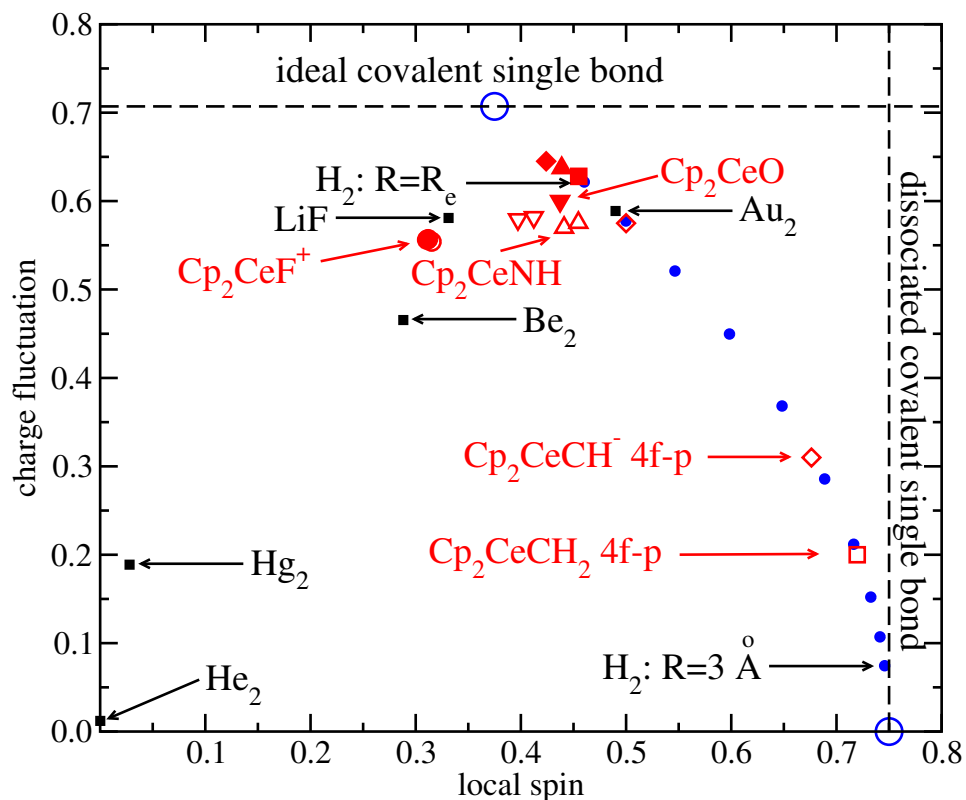


**Figure 3.11:** Charge fluctuation and local spin computed for the Ce-Z bonds of the  $\text{Cp}_2\text{CeZ}$  complexes ( $\text{Z} = \text{CH}_2, \text{CH}^-, \text{NH}, \text{O}, \text{F}^+$ ) at their HF geometries from CASSCF(2,2) calculations in comparison to corresponding results for the  $\text{H}_2$  molecule. Filled symbols are used for  $\sigma$  bonds and empty symbols for  $\pi$  bonds.

### 3.3.8 Conclusions

The bis(cyclopentadienyl)cerium  $\text{Cp}_2\text{CeZ}$  ( $\text{Z} = \text{CH}_2, \text{CH}^-, \text{NH}, \text{O}, \text{F}^+$ ) compounds have been investigated with several computational methods (HF, CASSCF, RSPT2 and DFT) paying special attention to the relevance of the cerium 4f orbitals to the electronic structure. It was shown that the five compounds have a  $^1\text{A}_1$  ground state, but that the influence and the importance of the 4f orbitals are different for these complexes. The CASSCF wavefunction analysis based on localized orbitals revealed that a simple ionic picture ( $2\text{Cp}^-$ ,  $\text{Ce}^{4+}$  and  $\text{Z}^{2-}$  fragments) and a closed-shell description is especially inaccurate for the two compounds  $\text{Cp}_2\text{CeCH}_2$  and  $\text{Cp}_2\text{CeCH}^-$ . The CASSCF(2,2) wavefunction appears to be an appropriate computational level for these complexes and by orbital rotation nearly pure cerium 4f and Z ligand orbitals were obtained. The analysis of the CI coefficients of the corresponding CASSCF wavefunction revealed a leading  $f^1p^1$  configuration and therefore these systems might be best described as open-shell molecular Kondo systems with a Ce(III) oxidation state. For the two complexes  $\text{Cp}_2\text{CeNH}$  and  $\text{Cp}_2\text{CeO}$  significant multi-reference character was obtained from the CASSCF computations, but in contrast to  $\text{Cp}_2\text{CeCH}_2$  and  $\text{Cp}_2\text{CeCH}^-$  the wavefunction analysis revealed that these compounds are best described as mixed valent Ce(III)/Ce(IV) complexes with a leading Ce(III) character. For these compounds no significant multi-reference character arised from the Ce-Cp bonds. The  $\text{Cp}_2\text{CeF}^+$  complex showed no special influence of the cerium 4f orbitals and the CASSCF wavefunction analysis revealed that this compound can be seen as a Ce(IV) complex. According to this, the systematic molecular set  $\text{Cp}_2\text{CeZ}$  ( $\text{Z} = \text{CH}_2, \text{CH}^-, \text{NH}, \text{O}, \text{F}^+$ ) show a clear trend from Ce(III) over mixed Ce(III)/Ce(IV) to a Ce(IV) compound which is in agreement with the chemical structure of the varied Z group. The analysis of the charge fluctuation and the local spin revealed that the orbital interaction of  $\text{Cp}_2\text{CeCH}_2$  and  $\text{Cp}_2\text{CeCH}^-$  can be classified as a weak covalent Ce 4f-C 2p interaction. The mixed valent compounds  $\text{Cp}_2\text{CeNH}$  and  $\text{Cp}_2\text{CeO}$  showed an increased ionic character for the Ce-Z bonds, but the Ce 4f/5d-Z p interaction was still dominant covalent, which is a consistent picture with their electronic structure. As expected from the CASSCF wavefunction analysis, the  $\text{Cp}_2\text{CeF}^+$  compound showed a ionic character of the Ce- $\text{F}^+$  orbital interaction, which also supports the assigned Ce(IV) oxidation state. This systematic trend of the orbital interactions for these five compounds is in a good agreement with the assigned oxidation states.

## 3.4 Cerium Fluorine Compounds

### 3.4.1 Introduction

In two recently published articles Andrews and coworkers investigated the reaction between laser-ablated lanthanide atoms with  $\text{CH}_2\text{F}_2$  and  $\text{OF}_2$  at low temperatures (4 to 6 K) in neon and argon [60, 61]. The infrared (IR) absorption bands were detected and assigned to the resulting products  $\text{CH}_2\text{LnF}_2$  and  $\text{OLnF}_2$ . Additionally, these compounds were studied with quantum chemical methods. The oxidation states of the lanthanide atoms were assigned for the complexes. It was concluded that the  $\text{CH}_2\text{LnF}_2$  compounds are multiradicals and that the Ln-C  $\sigma$  bond is constructed from a single electron in a carbon 2p orbital, which is weakly coupled to the Ln  $4f^n$  ( $n=1$  for Ce, 2 for Pr, ...) shell. For the cerium compound  $\text{CH}_2\text{CeF}_2$  a triplet ground state was computed by unrestricted B3-LYP and CASSCF computations, while the CASPT2 calculations resulted in a singlet ground state for this complex [60]. As discussed in the previous chapter the electronic structures of the bis(cyclopentadienyl)cerium complexes  $\text{Cp}_2\text{CeZ}$  ( $\text{Z} = \text{CH}_2, \text{CH}^-, \text{NH}, \text{O}, \text{F}^+$ ) were investigated at the CASSCF level. For the  $\text{Cp}_2\text{CeCH}_2$  an open-shell singlet ground state was found with a leading  $f^1p^1$  configuration and a weak covalent orbital interaction between the cerium 4f and the carbon 2p orbitals. Therefore it was concluded that  $\text{Cp}_2\text{CeCH}_2$  is best described as a molecular Ce(III)-based Kondo system.

The  $\text{OCeF}_2$  compound was classified as a Ce(IV) system by Andrews and coworkers due to the high experimentally measured cerium-oxygen experimentally stretching frequency [61]. The very similar  $\text{Cp}_2\text{CeO}$  molecule revealed significant multi-reference character and it was shown that this system might be best described as a mixed valent Ce(III)/Ce(IV) compound. Therefore the ground states, their electronic structures, paying special attention to the multi-reference character, and the influence of the cerium 4f orbitals were investigated at the CASSCF level in more detail for  $\text{CH}_2\text{CeF}_2$  and  $\text{OCeF}_2$ . Oxidation states for cerium in the two investigated compounds were assigned based on an analysis of the CASSCF wavefunction using localized orbitals. In order to describe the orbital interactions of the Ce-Z bonds the charge fluctuation and the local spin are computed and analyzed. According to the similarity between these complexes and the corresponding bis(pentadienyl)cerium compounds it was expected that their ( $\text{CH}_2\text{CeF}_2$  and  $\text{OCeF}_2$ ) electron structures should be comparable to  $\text{Cp}_2\text{CeCH}_2$  and  $\text{Cp}_2\text{CeO}$ . The presented results and discussions have already been published in 2016 [62].

### 3.4.2 Computational Details

The cerium compounds  $\text{CH}_2\text{CeF}_2$  and  $\text{OCeF}_2$  are investigated, applying various computational methods. The program package MOLPRO 2012.1 [31] was used for all *ab initio* wavefunction-based computations. The scalar-relativistic small-core pseudopotential ECP28MWB[63] with the corresponding atomic natural orbital (ANO) basis set, including s, p, d, f and g functions[51], was applied for cerium. For all other elements the contracted correlation-consistent polarized triple-zeta basis sets (cc-pVTZ) was used. In case of hydrogen, s, p and d functions and for carbon, oxygen and fluorine, s, p, d and f functions were applied [57]. To investigate the influence of the basis set size double-zeta (cc-pVDZ with sp functions for H and spd functions for C, O and F) and quadruple-zeta (cc-pVQZ with spdf functions for H and spdfig functions for C, O and F) basis sets were also tested. A single h function was also added to cc-pVQZ basis set for cerium. These basis sets are abbreviated as VXZ ( $X = \text{D, T, Q}$ ) and the corresponding augmented basis sets as aVXZ ( $X = \text{D, T, Q}$ ).

All discussed DFT computations were performed with TURBOMOLE version 6.6 [50]. The def-SV(P) and def2-TZVP basis sets were applied for all atoms[52, 64] and in the case of the cerium the ECP28MWB pseudopotential was used. These basis sets are referred to as SVP and TZVP. The BP86[65, 66], B3LYP[67, 68] and M06[69] functionals were applied for closed-shell Kohn-Sham (KS) computations. For open-shell singlet and triplet computations the unrestricted Kohn-Sham (UKS) method was used. Standard Hartree-Fock calculations (HF) as well as unrestricted HF computations were also performed.

Geometry optimizations and vibrational frequencies were computed at various computational levels (DFT, HF, complete active space self-consistent field (CASSCF)[53, 54], coupled cluster including single and double excitations with perturbative triples (CCSD(T))[70, 71], Rayleigh-Schrödinger second-order perturbation theory (RS2C)[43] and multi-reference configuration interaction (MRCI)[55, 56]). Excitations arising from the Ce 4s, 4p, 4d, and the 1s shell for the other elements were not allowed in the CCSD(T), RSC2 and MRCI calculations. Energetical minimum structures were verified by frequency analyses.

To investigate the relevance of the 4f orbitals for the electronic structure and the multi-reference character of the two cerium complexes, CASSCF [53, 54] calculations with several active orbital spaces were executed. Mulliken population analysis [13] was applied to determine the contributions of the atomic orbitals for the active orbitals. The MRCI method[55, 56] was applied to compute and analyze the corresponding CI coefficients.

For these calculations only excitations within the CASSCF active orbital space were used. The occupation number fluctuation and the local spin[44, 59] were analyzed to describe the nature of the interaction of the localized active orbitals for the cerium compounds.

### 3.4.3 Ground State Geometries

As a first step the ground state geometries were investigated for the  $\text{CH}_2\text{CeF}_2$  as well as for the  $\text{OCeF}_2$  complex. Several DFT functionals (BP86, B3-lyp and M06) and basis sets (SVP and TZVP) were applied, as well as a variety of different wavefunction-based methods. The geometry optimizations were performed with and without symmetry constraints and all minima were verified by frequency analyses. The optimized ground state geometries computed by the HF/RS2C method are exemplary shown in the Figure 3.12 for both systems.



**Figure 3.12:** HF/RS2C optimized ground state geometries using the VTZ basis sets for  $\text{CH}_2\text{CeF}_2$  (left) and  $\text{OCeF}_2$  (right).

The ground state geometry of the oxygen complex has definitely  $C_s$  symmetry. This geometry was computed by all applied methods, whether the geometry optimizations were performed imposing  $C_s$  symmetry or not. The fluorine and oxygen ligands are arranged in a pyramidal structure and therefore the symmetry of the previously published ground state geometry for the  $\text{OCeF}_2$  compound can be confirmed [61]. The ground state geometry of the methylene complex appears to be more difficult. The minimum structure of this compound was recently described as a planar molecule showing  $C_{2v}$  for a triplet ground state [60]. No performed calculation resulted in a planar  $C_{2v}$  ground state geometry, even when the optimization was started from the published singlet and triplet geometries. At least one or two imaginary frequencies were obtained for  $C_{2v}$  structures. Improving the used grid and the convergence criteria also did not lead to a  $C_{2v}$  minimum geometry. Even the wavefunction-based geometry optimizations at HF, UHF, MCSCF, CASSCF(2,2), CASSCF(2,8), RS2C and MRCI level using the VTZ

basis set did not converge into a planar structure and minima were only computed in  $C_1$  symmetry. Some converged structures are close to  $C_s$  symmetry and the MRCI optimization, which is the highest applied level approximately converged to a  $C_s$  global minimum structure. Therefore it might be possible that this compound also has  $C_s$  geometry, but in general distorted  $C_1$  structures were obtained by the used methods. *Wang et al.*[60] proposed a triplet ground state and a biradical character of the methylene complex. As it will later be discussed the biradical character of this complex can be confirmed and therefore the molecule should be computed at the unrestricted Kohn-Sham level. Nevertheless, the geometry optimizations at this level also resulted in a distorted minimum structure and the singlet state energies were always lower compared to the triplet state (UHF: 0.42 kcal/mol, BP86: 1.29 kcal/mol, B3-LYP: 0.25 kcal/mol and M06: 0.34 kcal/mol). However, the spin-multiplicity of the ground state, investigated more accurately with multi-reference methods, will be discussed and clarified in the next section. In order to describe both compounds on a comparable level, the following computations were all performed without using symmetry, even for the  $\text{OCeF}_2$  complex.



### 3.4.4 Spin-Multiplicity of the Ground State

For the investigation of the electronic structure of the two cerium complexes, the spin-multiplicity of the ground state was computed for both systems. In principal, singlet or triplet ground states are conceivable for these two molecules and a multi-reference method needs to be applied to compute the ground state spin-multiplicity correctly, as already mentioned in the previous section. Therefore single-point CASSCF/RS2C computations were applied based on the optimized HF/RS2C minimum structures. The active orbital space consists of the seven cerium 4f orbitals and the out-of-plane 2p orbital for carbon ( $\text{CH}_2\text{CeF}_2$ ) or oxygen ( $\text{OCeF}_2$ ). The resulting active space includes eight orbitals and two active electrons (CAS(2,8)). The included 2p orbital was doubly occupied in the HF calculation and corresponds to the highest occupied molecular orbital (HOMO) of the specific molecule, whereby the f orbitals were unoccupied in the closed-shell HF computations. For each compound the lowest singlet and triplet state were optimized separately and the computed results are presented in the following Table 3.24.

**Table 3.24:** Lowest singlet and triplet state energies obtained by CASSCF/RS2C computations using the VTZ basis sets, based on the optimized HF/RS2C structures.

Complex	$^1\text{A}$ state in a.u.	$^3\text{A}$ state in a.u.	$\Delta\text{E}$ in eV
$\text{CH}_2\text{CeF}_2$	-712.636296	-712.614732	0.587
$\text{OCeF}_2$	-748.677834	-748.560183	3.201

The singlet state of the  $\text{OCeF}_2$  molecule is 3.201 eV lower compared to the calculated triplet state. Therefore it can be concluded that the ground state of this molecule is definitely a singlet state and the triplet state corresponds to an excited electronic state. This result agrees with an recently published article by *Mikulas et al.*[61], where the ground state of the  $\text{OCeF}_2$  complex was also assigned to a singlet state. For the methylene compound the energy difference between singlet and triplet state is significantly lower compared to the oxygen complex. This energy difference is computed to be 0.587 eV, revealing that the singlet state is also favored for the  $\text{CH}_2\text{CeF}_2$  complex and the triplet state is an excited state. This result disagrees with the spin-multiplicity reported by *Wang et al.*[60] for this molecule. A triplet ground state was assigned to the methylene compound based on DFT (B3LYP functional), UCCSD(T) and CASSCF(2,2) computations. However, *Wang et al.* also mentioned that CASPT2 results indicate that the singlet state is energetically lower than the triplet state (about 0.04 eV). Nevertheless, the presented results support the singlet ground state for both compounds.

### 3.4.5 Electronic Structure and the Relevance of the 4f Orbitals

For the former discussed cerium complexes, it was shown that the active space in the CASSCF calculation can be reduced, while the influence and the relevance of the Ce 4f orbitals was still described correctly. Therefore the number of active orbitals was decreased to 2 electrons and 2 orbitals (CASSCF(2,2)). In these computations the active space consists of the out-of-plane oxygen or carbon 2p orbital and the lowest Ce 4f orbital, while in the CASSCF(2,8) calculation all seven 4f orbitals were included. The motivation for its reduction was given by the obtained CASSCF(2,8) wavefunction. This wavefunction was dominated by only two configurations for each molecule, which was detected by an analysis of the determined CI coefficients indicating that the CASSCF(2,2) level should deliver a sufficiently accurate description for the two cerium systems. The electronic energies for the different CASSCF computations compared to the HF energies are presented in Table 3.25. These results show that the CASSCF(2,8) energies, including all seven Ce 4f orbitals, are significantly lower compared to the obtained HF energies. For the  $\text{CH}_2\text{CeF}_2$  compound the energy is lowered by 0.824 eV, while the ground state energy for the  $\text{OCeF}_2$  complex is 0.800 eV lower compared to the HF energy.

**Table 3.25:** Electronic energies [a.u.] of the  $^1\text{A}$  ground state for  $\text{CH}_2\text{CeF}_2$  and  $\text{OCeF}_2$  at the HF, CASSCF(2,8) and CASSCF(2,2) level using the VTZ basis set, based on the HF/RS2C optimized geometries. Energy differences to the HF energy are given in eV.

	$\text{CH}_2\text{CeF}_2$	$\text{OCeF}_2$
HF	-711.629470	-747.599643
CASSCF(2,8)	-711.660414	-747.629032
CASSCF(2,2)	-711.658813	-747.621434
$\Delta E_{\text{CASSCF}(2,8)}$	0.842	0.800
$\Delta E_{\text{CASSCF}(2,2)}$	0.798	0.593

The variation principal, which is valid for these methods, states that a better wavefunction results in a lower electronic energy. Therefore it can be concluded that the CASSCF(2,8) wavefunctions deliver a qualitatively improved description of the two cerium compounds in comparison to the HF method. Additionally it can be shown by the results in Table 3.25, that the reduced active space can still describe the influence of the Ce 4f orbitals correctly for both complexes. Applying the CASSCF(2,2) method the electronic energy is also significantly lowered by 0.798 eV for  $\text{CH}_2\text{CeF}_2$  and 0.593 eV

for the oxygen complex. In case of the methylene compound the difference between the two active space CASSCF calculations is with 0.044 eV very small. Therefore it can be concluded that the CASSCF(2,8) and the CASSCF(2,2) wavefunctions have an almost equal quality for the  $\text{CH}_2\text{CeF}_2$  system. For the oxygen complex a slightly different situation is obtained. The electronic energy is lowered by 0.800 eV in the CASSCF(2,8) calculation compared to the HF result, whereby the CASSCF(2,2) ground state energy is only 0.593 eV lowered.

The energy difference of these two CAS computations is 0.207 eV, which is larger compared to the methylene compound. Nevertheless, these result also reveal that the CASSCF(2,2) level is still a good description for the oxygen complex. According to these results, it can be concluded that the CASSCF(2,2) wavefunction is sufficiently accurate for both complexes.

A further insight about the relevance of the Ce 4f orbitals for the electronic structure of the two complexes can be achieved by a Mulliken population analysis. This method allows to detect the occupation of different atomic orbitals in the final wavefunction. In this case the influence of the Ce 4f orbitals in the two cerium complexes was investigated and the computed results for several DFT and wavefunction based methods are presented in Table 3.26.

**Table 3.26:** Mulliken 4f populations for HF, UHF, CASSCF and several DFT methods. For  $\text{CH}_2\text{CeF}_2$  computed values arising from the difference of  $\alpha$  and  $\beta$  spin density matrices are presented in parentheses.

Basis	Method	CH <sub>2</sub> CeF <sub>2</sub> OCeF <sub>2</sub>	
		f populations	
TZVP	BP86	1.29 (0.87)	1.18
	B3-LYP	1.27 (0.99)	1.03
	M06	1.29 (0.98)	0.93
	HF	0.63	
	UHF	1.20 (0.99)	
VTZ	HF		0.64
	UHF	1.19	
	CASSCF(2,8)	1.18	0.66
	CASSCF(2,2)	1.20	0.66

The results of all DFT methods compute high occupations of the Ce f orbital for the two compounds. The range of the f occupation is from about 0.87 up to 1.29.

For the methylene compound the difference arising from the density matrices for  $\alpha$  and

$\beta$  spin reveals f populations, that are very close to one. For the B3-LYP functional the f occupation is 0.99 and the M06 functional delivers a value of 0.98, while the BP86 computations results in a slightly lower occupation of 0.87. The carbon p population for the B3-LYP and M06 computations is 0.92, supporting the biradical character of this molecule, which was also concluded by Wang *et al.*[60] The UHF results are also confirming this conclusion, delivering in this sense the best populations with 0.99 for cerium f and 1.00 for carbon p. For the  $\text{CH}_2\text{CeF}_2$  complex the wavefunction based methods, CASSCF(2,8) and CASSCF(2,2) also reveal an f occupation close to one. The CAS(2,8) determines the f occupation to 1.18, while it is 1.20 for the CAS(2,2) using a smaller active space. This also emphasizes the conclusion that the CAS(2,2) method is an sufficiently accurate description for the relevance of the cerium f orbitals in the molecular electronic structure. The standard DFT computations and the CAS calculations are in agreement, which is different for the oxygen compound. For this system the f population is computed in a range of 0.93 up to 1.18 by the standard DFT methods, indicating a  $f^1$  occupation. The two different CAS methods as well as the HF computation result in a significantly lower f occupation (0.64 – 0.66), which differs from the DFT results. Considering the used methods this discrepancy can be explained. The cerium 4f shell is compact, which leads to a high repulsion of f electrons. The single determinant wavefunction of the HF approach avoids partial f occupations by electrons pairs and therefore the f occupation is low for both complexes. Standard DFT methods can not describe the electron repulsion of f shells well, and therefore tend to result in high f populations. According to this, both systems show a high f occupation for all applied DFT methods. The CASSCF method constructs the wavefunction as a linear combination of determinants (or configuration state functions (CSFs)), which allows an occupancy with unpaired electrons for cerium f orbitals. Therefore this approach can treat the influence and the occupations of the f orbitals more accurately compared to all other methods. According to this the results computed by these methods should be the most reliable ones. The methylene complex show high f occupations close to one for these methods, whereby the f population is significantly lower for the  $\text{OCeF}_2$  molecule. Therefore it can be concluded that the  $\text{CH}_2\text{CeF}_2$  system should be a Ce(III) compound, while the oxygen compound might be best described as a mixed Ce(IV)/Ce(III) complex. The Mulliken population analysis can not distinguish between contributions from unpaired electrons at the cerium and contributions, which arise from partial electron donation to the f shell of the electron density by paired ligand electrons. Therefore the f occupation was investigated by applying orbital rotation of the active orbitals of the CASSCF(2,2) wavefunction for both molecules, which will be discussed in the next section.

### 3.4.6 Active Orbital Rotation

It was shown that for the former discussed cerium complexes, that a rotation of the active orbitals can clarify the relevance of the cerium f orbitals for a molecular electronic structure. As already mentioned, natural orbitals (rotation angle 0 °) provided by MOLPRO for a CASSCF calculation are usually delocalized. An reliable assignment of oxidation states should therefore be based on localized orbitals of individual fragments of the molecule. This can be achieved by a rotation of the active orbitals obtained from a CASSCF computation. For both complexes the rotation angle of the two active orbitals was varied in steps of 1 ° in the range from 0 ° to 90 °. Additionally, the orbital character the the corresponding CI coefficients were evaluated. Afterwards the rotation angle was refined in steps of 0.1 ° to determine the rotation angle which leads to the maximum cerium f character for one of the active orbitals. At this rotation angle the orbitals are as much localized as possible. The results of the full orbital rotations are presented in the Figures 3.13 and 3.14 and explicit values of these computations are given in the following Table 3.27 for the two molecular systems.

**Table 3.27:** Configuration contributions [%] to the  $^1A_1$  ground state of the CASSCF(2,2) wavefunction based on HF/RS2C optimized geometries. In the upper line the rotation angle leading to an orbital with maximized f character is presented, whereby in the lower line the most compact wavefunction in the sense of contributing configurations is shown. The different orbital characters were obtained from a Mulliken poulation analysis.

	rotation angle	config. a <sup>1</sup> b <sup>1</sup>	contribution a <sup>2</sup> b <sup>0</sup>	contribution a <sup>0</sup> b <sup>2</sup>	Z p character of orbital a	Ce f/d character of orbital b
CH <sub>2</sub>	42.6 °	92.7	5.7	1.6	0.883	0.981/0.020
	53.0 °	86.3	0.0	13.7	0.870	0.950/0.035
O	32.0 °	50.4	46.0	3.6	0.951	0.417/0.496
	0.0 °	0.0	98.4	1.6	0.614	0.301/0.259

The results reveal that the influence of the f orbital is differing for the two molecules. For the methylene complex a nearly pure cerium f and carbon p orbitals can be constructed by the orbital rotation at an angle of  $42.6^\circ$ . At this point the f character of orbital b is 0.981 and the p character of orbital a is 0.883. The corresponding CASSCF(2,2) wavefunction can be described as  $92.7\% a^1b^1 + 5.7\% a^2b^0 + 1.6\% a^0b^2$ . According to the nearly pure character of the orbitals the wavefunction can be written as  $92.7\% f^1p^1 + 5.7\% f^0p^2 + 1.6\% f^2p^0$  revealing that the methylene system is dominated ( $\approx 93\%$ ) by a configuration with an  $f^1$  occupation of the cerium. For an optimized geometry at the CASSCF(2,2) level the dominant leading configuration is nearly 100%  $f^1p^1$  (see Figure A.1). According to these insights the oxidation state of cerium in the  $\text{CH}_2\text{CeF}_2$  compound can be assigned to Ce(III) and therefore this complex is the smallest described example for a molecular Ce(III)-based Kondo system. The most compact wavefunction close to this can be obtained at the rotation angles  $37.0^\circ$  and  $53.0^\circ$ , in which one closed-shell configuration vanishes. At these rotation angles the two active orbitals are also quite well localized and the dominant leading configuration is  $f^1p^1$ . The natural orbitals ( $0^\circ$ ) also lead to a compact wavefunction consisting of two configurations, but the active orbitals are nearly 50:50 mixtures of cerium f and carbon p at this angle and the leading configuration is closed-shell. This wavefunction is inappropriate for the assignment of oxidation states.

The molecular electronic structure and the influence of the cerium f orbital of the  $\text{OCeF}_2$  complex differs significantly from the  $\text{CH}_2\text{CeF}_2$  compound. As Figure 3.14 shows, the most compact wavefunction is obtained by the natural orbitals ( $0^\circ$ ). At this rotation angle the orbitals are quite mixed (see Table 3.27), and therefore this wavefunction is also inappropriate to assign the oxidation state of cerium and it can lead to the conclusion that this complex is Ce(IV), which was proposed by Mikulas *et al.*[61]. After, applying the orbital rotation the f character was maximized for one orbital ( $32.0^\circ$ ). It can be seen that in contrast to the methylene compound no nearly pure f orbitals were obtained, but the active orbitals were separated to one nearly pure oxygen p orbital and a mixed cerium f/d orbital. Therefore the oxidation state of cerium can be also assigned, due to the fact that the two orbitals correspond to different atoms. The resulting CASSCF(2,2) wavefunction can be written as  $50.4\% (d/f)^1p^1 + 46.0\% (d/f)^0p^2 + 3.6\% (d/f)^2p^0$ . The wavefunction shows nearly 50% Ce(IV) and 50% Ce(III) contribution, with a slightly increased Ce(III) character. According to this results the  $\text{OCeF}_2$  complex might be best described as a mixed valent Ce(III)/Ce(IV) compound.

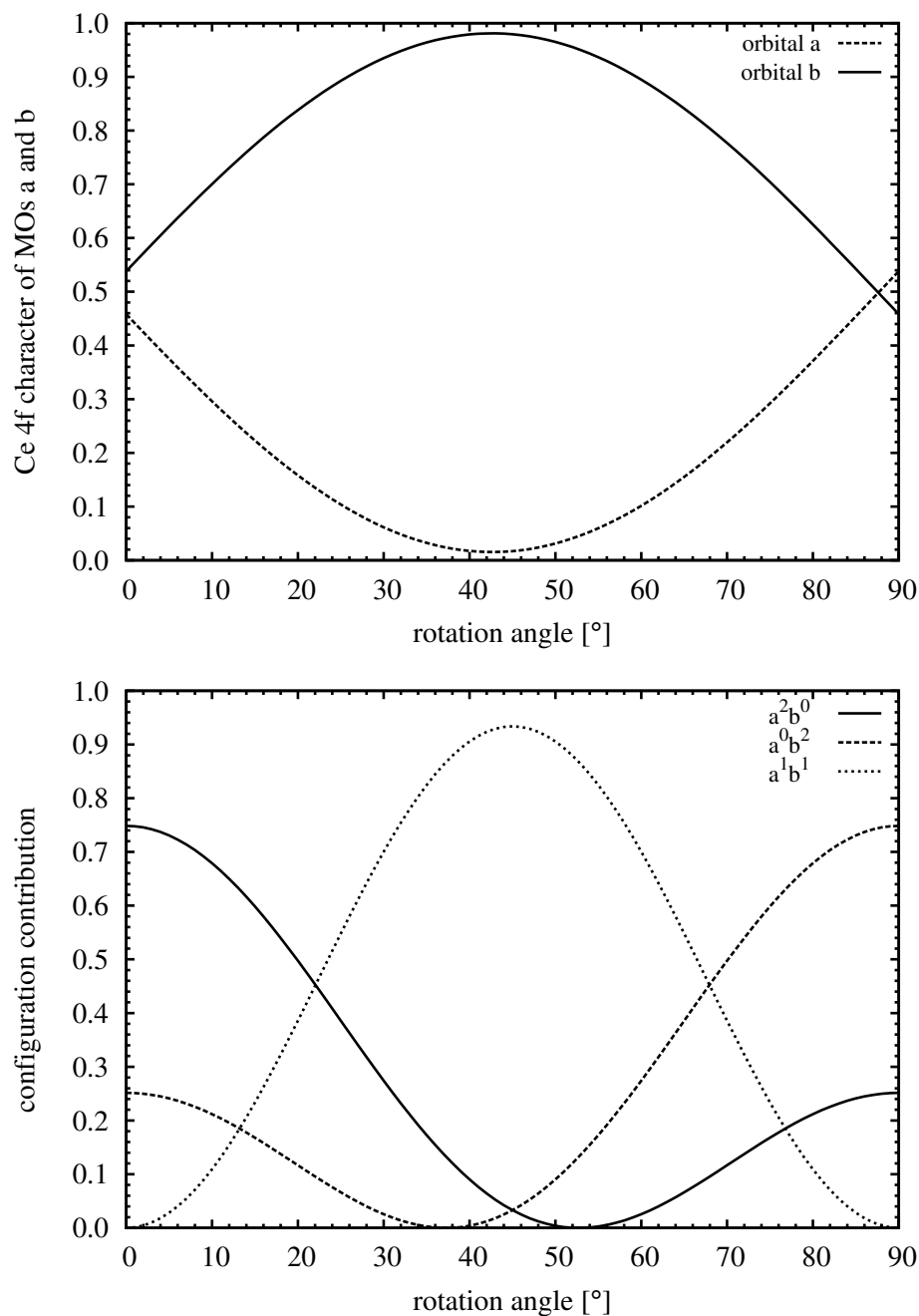


**Figure 3.13:** Orbital characters determined by Mulliken population analysis (top) and configuration contributions to the CASSCF(2,2) wavefunction (bottom) for  $\text{CH}_2\text{CeF}_2$  using the VTZ basis sets. The vertical line shows the rotation angle where the f character of orbital b is maximized

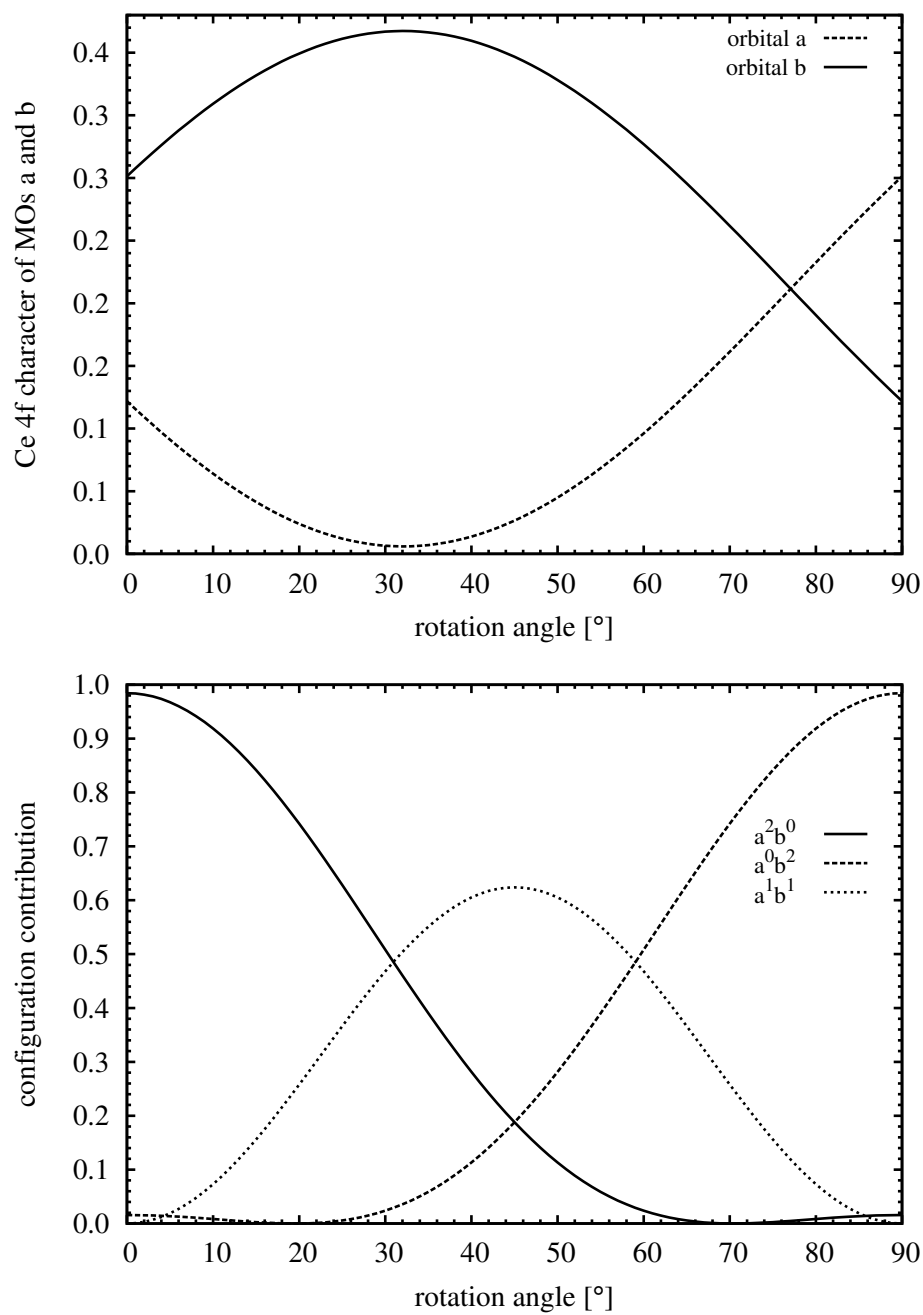


**Figure 3.14:** As Figure 3.13, but for the  $\text{OCeF}_2$  complex.



### 3.4.7 Occupation Number Fluctuation Analysis

The analysis of the occupation number fluctuation and the local spin for the localized active orbitals[44, 59] can be used to categorize the nature of the orbital interaction. Therefore the occupation number fluctuation and the local spin were analyzed for the CASSCF(2,2) wavefunctions of the two compounds. The results are presented in Figure 3.15. As it can be seen the character of the orbital interaction differs for the complexes. The methylene compound reveals a covalent character of the interacting cerium 4f and carbon 2p orbitals. The interaction is similar to the orbital interaction of a stretched hydrogen dimer at a bond distance of approximately 2 Å, which leads to the conclusion that the orbital interaction can be classified as weak covalent. The local spin of the OCeF<sub>2</sub> complex is shifted to the left of the dissociating single bond of the hydrogen dimer and the charge fluctuation reveals a lower value compared to a covalent bond. These results agree with the derived mixed valent character of this compound and show an increased ionic character of the orbital interaction, which is also in line with the results for the molecular electronic structure of this complex.

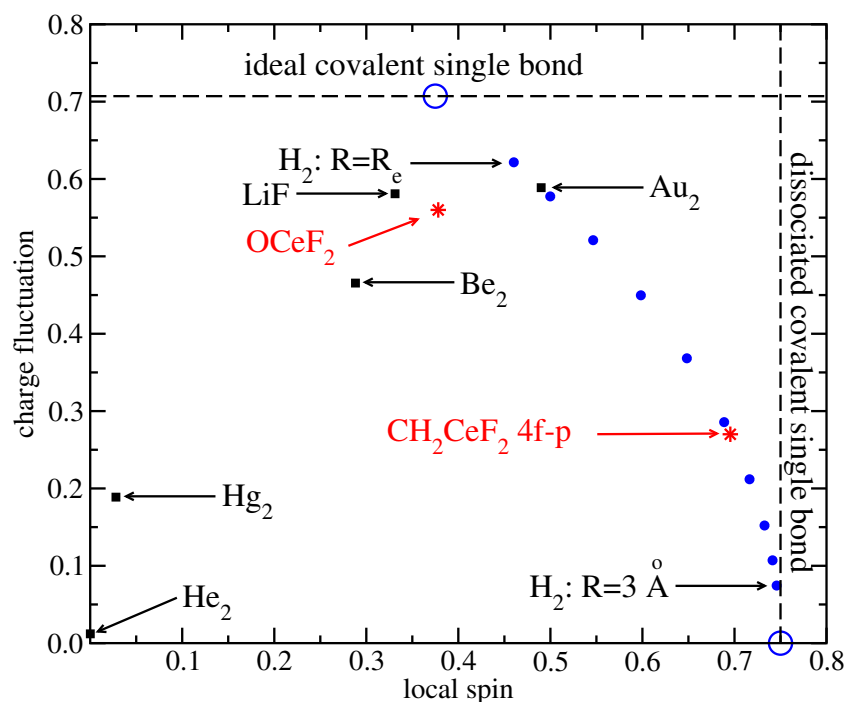


**Figure 3.15:** Occupation number fluctuations and local spin from CASSCF(2,2) calculations of OCeF<sub>2</sub> and CH<sub>2</sub>CeF<sub>2</sub> using the VTZ basis set in comparison to corresponding results for the H<sub>2</sub> molecule (the dots correspond to H<sub>2</sub> bond distances from 0.75 to 3.0 Å in steps of 0.25 Å).

### 3.4.8 Vibrational Frequencies

It was emphasized that the Ce-C and Ce-O bond are important for the multi-reference character of the wavefunction for the two complexes. Experimentally these compounds were investigated via IR spectroscopy [60, 61]. Therefore the computed frequencies for these molecules will be discussed paying special attention to the Ce-C and Ce-O stretching modes. All results are presented in Table 3.28. The calculated Ce-C stretching frequencies of the methylene complex, singlet state  $436\text{ cm}^{-1}$  and triplet state  $437\text{ cm}^{-1}$ , published by *Wang et al.*[60] can be confirmed by the results given in Table 3.28. In case of the BP86 computation, rocking modes were strongly mixed to the stretching frequency and therefore this result is not included in Table 3.28.

**Table 3.28:** Ce-C and Ce-O stretching frequencies in  $\text{cm}^{-1}$  (singlet ground states) computed by various DFT and wavefunction-based methods compared to experimental frequencies measured in a solid argon (neon) matrix ( $\text{CH}_2\text{CeF}_2$ : *Wang et al.*[60] and  $\text{OCeF}_2$ : *Mikulas et al.*[61]). The reported computed (B3LYP/DZVP2) frequency for the methylene complex is given in square brackets.

Method	Basis	$\text{CH}_2\text{CeF}_2$	$\text{OCeF}_2$
		Frequency	
Lit.:		[436]	793.9 (808.4)
BP86	SVP/TZVP		800.5/783.4
B3LYP	TZVP	427.7	835.8
M06	TZVP	427.5	874.1
HF	VTZ/TZVP		937.0/940.7
UHF	VTZ/TZVP	431.4/434.7	
HF/RS2C	VTZ	437.8	844.0
CAS(2,8)	VTZ	429.3	918.2
CAS(2,2)	VTZ	429.2	914.0
CAS(2,2)/RS2C	VTZ	432.0	883.8
CAS(2,2)/MRCI	VTZ/aVTZ	435.9/435.4	920.3/945.8
CCSD(T)	VDZ/aVDZ		844.5/838.3
	VTZ/aVTZ		836.4/849.5
	VQZ/aVQZ		861.7/855.9

In principle all computed frequencies of the Ce-C stretching mode of the methylene compound are in good agreement to the reported values of *Wang et al.*[60] The performed DFT computations as well as the CASSCF(2,2) and CASSCF(2,8) calculation underemphasize this frequency. If a triplet state in  $C_{2v}$  symmetry is enforced the B3-LYP/TZVP calculation determines the frequency to  $432\text{ cm}^{-1}$ , which nearly reproduces the reported frequency. The highest applied theoretical level, CASSCF(2,2)/MRCI, resulted in frequencies very close to the reported ones using a singlet ground state. For the VTZ basis set the frequency was computed to  $435.9\text{ cm}^{-1}$  and  $435.4\text{ cm}^{-1}$  for the aVTZ basis. However, the experimental frequency of this compound is unknown and therefore a linear extrapolation of the experimentally obtained frequencies for the Ln-C ( $\text{Ln} = \text{Sm} - \text{Lu}$ ) stretching mode was performed. This extrapolation resulted in a Ce-C frequency of  $439\text{ cm}^{-1}$ , which agrees with the computed CASSCF(2,2)/MRCI values. The symmetric and antisymmetric  $\text{CeF}_2$  stretching frequencies were computed at the CASSCF(2,2)/MRCI level (aVTZ basis) to  $530.6$  and  $516.7\text{ cm}^{-1}$ . The corresponding experimental values are  $504.8$  and  $491.0\text{ cm}^{-1}$  measured in a solid argon matrix. The computed results are about  $15\text{ cm}^{-1}$  higher compared to the experiments, but the difference of these two stretching modes is computed accurately. The experiments are also emphasizing that the matrix has a significant effect on the frequencies, i.e. the antisymmetric frequency in neon is  $509.7\text{ cm}^{-1}$ , which is in good agreement with the calculated value. The difference of this experiment and the gas phase calculation is only  $7\text{ cm}^{-1}$ .

The computed results for the Ce-O stretching frequency are spreading for the applied computational methods. Experimentally this frequency was  $808.4\text{ cm}^{-1}$  in an argon matrix and  $793.9\text{ cm}^{-1}$  in neon. The BP86/SVP result is the closest computation compared to the experiments, determining the frequency to  $800.5\text{ cm}^{-1}$ . The error is therefore only about  $8\text{ cm}^{-1}$  measured in argon and  $6\text{ cm}^{-1}$  for neon. The B3-LYP and the M06 functionals determine this frequency to  $835.8\text{ cm}^{-1}$  and  $874.1\text{ cm}^{-1}$ , which show a larger deviation compared to the experiment. The multi-reference methods, which were expected to describe the molecule more accurately resulted in frequencies  $900\text{ cm}^{-1}$ , except of the CASSCF(2,2)/RS2C method with a computed frequency of  $883.8\text{ cm}^{-1}$ . Therefore these methods can not describe the frequency more accurate. The orbital rotation and the analysis of the CI coefficients revealed that for the natural orbital (rotation angle  $0^\circ$ ) the wavefunction of the  $\text{OCeF}_2$  complex was clearly dominated by a single configuration (98.4%  $a^2b^0$ ). Therefore the frequency was computed at the CCSD(T) level using several basis sets VXZ and aVXZ ( $X = \text{D, T, Q}$ ). The calculated frequencies of these methods range from  $836.4\text{ cm}^{-1}$  to  $861.7\text{ cm}^{-1}$  showing that the experimental frequency can not be well computed. Increasing the basis set size results in increased vibrational

frequencies. This is also obtained for the  $\text{CeF}_2$  stretching modes. The computed values at the CCSD(T) level are  $537.2\text{ cm}^{-1}$  (aVDZ) and  $552.5\text{ cm}^{-1}$  (aVQZ) for the symmetric stretch,  $509.0\text{ cm}^{-1}$  (aVDZ) and  $525.3\text{ cm}^{-1}$  (aVQZ), respectively. The corresponding experimental values in argon (neon) are  $516.6$  ( $533.0$ ) and  $487.9$  ( $504.1$ )  $\text{cm}^{-1}$ . The comparison, additionally reveals that the computed frequency show a better agreement to the neon measured frequencies as to the argon measured ones, which was also obtained for the methylene compound. There it can be concluded that the argon matrix has larger effect on the molecules than the neon matrix.

The Ce-O frequency shows the highest experimental value for the Ln-O series and this frequency does not deliver a regular trend in the Ln series. The frequency of the direct neighbor element praseodymium is  $100(80)\text{ cm}^{-1}$  lower compared to the cerium compound [61]. *Mikulas et al.* assigned this behavior to a change of the oxidation state of the f-element, IV for Ce, III/IV for Pr and Tb as well as III for the other elements. An extrapolation for the known  $\text{OLn(III)F}_2$  complexes lead to a stretching frequency of  $475\text{ cm}^{-1}$  for the corresponding cerium compound. Therefore it appears to be reasonable that the high value for the Ce-O is caused by a Ce(IV) oxidation state in this compound or at least by a mixing of the Ce(III)/Ce(IV) oxidation state, that was indicated by the already presented electronic structure analysis. The Ce-C stretching frequency is in agreement to the Ln-C series and therefore the oxidation state of III for cerium in the  $\text{CH}_2\text{CeF}_2$  is implied by the experiments as well as by the previously discussed CASSCF computations.

### 3.4.9 Conclusions

The two cerium compounds  $\text{CH}_2\text{CeF}_2$  and  $\text{OCeF}_2$  were investigated at several computational levels. The CASSCF computations revealed that both compounds have a singlet ground state. As expected, the electronic structure investigation as well as the charge fluctuation analysis of these two systems were in excellent agreement with the corresponding bis(cyclopentadienyl)cerium compounds. A dominant  $\text{Ce } 4f^1 \text{ C } 2p^1$  configuration is obtained for  $\text{CH}_2\text{CeF}_2$  if nearly pure cerium 4f and carbon 2p orbitals were used, which is consistent with the computed results for  $\text{CH}_2\text{CeCp}_2$ . The fluorine and the cyclopentadienyl ligands show no significant influence on the multi-configurational character of these compounds, which means that no MR contributions arise from the Ce-Cp and Ce-F bonds. The oxidation state of cerium can be assigned to Ce(III) in  $\text{CH}_2\text{CeF}_2$  based on these results and therefore it can be concluded that the  $\text{CH}_2\text{CeF}_2$  compound is the smallest Ce(III)-based molecular Kondo system. The charge fluctuation analysis revealed that the orbital interaction of the Ce-CH<sub>2</sub> bond in  $\text{CH}_2\text{CeF}_2$  can be classified as weak covalent, which is also in agreement with the corresponding bis(cyclopentadienyl)cerium compound.

The  $\text{OCeF}_2$  complex revealed a different influence of the cerium 4f orbital to the electronic structure. The CASSCF computations emphasized that this complex is best described as a mixed valent Ce(III)/Ce(IV) compound, which is in agreement with the computed results for  $\text{OCeCp}_2$ . The analysis of the charge fluctuation and the local spin showed an increased ionic character for the interaction of the active orbitals (Ce 4f/5d-O 2p) compared to the methylene complex. The influence of the Ce 4f orbitals for the electronic structure as well as the contribution of the Ce(III) character to the CASSCF ground state wavefunction is smaller for the fluorine complex compared to the bis(cyclopentadienyl)cerium compound. Furthermore the ionic character of the orbital interaction is higher for  $\text{OCeF}_2$  compared to  $\text{OCeCp}_2$ . This behavior might be explained by the higher electronegativity of the fluorine ligands. Therefore the electron density at the cerium center decreases stronger for the fluorine ligands compared to the cyclopentadienyl ligands.

## 3.5 Density Functional Theory Investigations

### 3.5.1 Introduction

Density functional theory (DFT) calculations are the most performed computations in the field of chemistry. Especially in the organic chemical community, DFT calculations are performed to investigate reaction mechanisms or experimental trends. Most of the DFT computations are performed after the experimental results are available and predictive DFT computations are rare. The enormous pool of functionals, basis sets, thermal corrections, solvent models and other additional corrections provide an almost infinite variety to construct theoretical explanations of trends or experimental outcomes. The applicability of DFT methods and the reliability of the computed results compared to experiments is an interesting field of research. Therefore an analysis of systematically performed calculations and systematical syntheses of similar molecular systems will be given in the following chapter to point out the strenghts and weaknesses of several DFT methods.

### 3.5.2 Computational Details

The density functional theory (DFT) calculations presented in this part, were performed using TURBOMOLE version 6.6 [50]. In these calculations the basis sets, def2-SVP, def2-SVPD, def2-TZVP and def2-QZVP[52, 73], with the corresponding pseudopotential for iodine were used [51]. We made use of different density functionals (BP86, B3-LYP, BH-LYP, PBE, PBE0, TPSS, TPSSH, M06) [65–69, 74–78]. All geometry optimizations were performed using the TPSSH functional and the def2-TZVP basis set. All minima and transition states were verified by analyzing the eigenvalues of the Hessian matrix. COSMO [79] was used to include solvent effects and the D3 method [80] to include dispersion. The quasiharmonic approximation was not applied [81].

### 3.5.3 Iodine Catalysis

To emphasize the problems with DFT calculations and investigations, we analyzed a specific theoretical article in the field of organic chemistry, which is an excellent representative for usual DFT studies [72]. The former mentioned article deals with the theoretical investigation of iodine catalysis and proclaims that the published calculations confirm the catalytic mechanism and gives an explanation for the reason of the catalytic behavior of iodine. In this article many inconsistencies can be found, some are listed up in the following. The nomenclature of the reactions follows the mentioned article and the investigated reactions are shown in Figure 3.16.

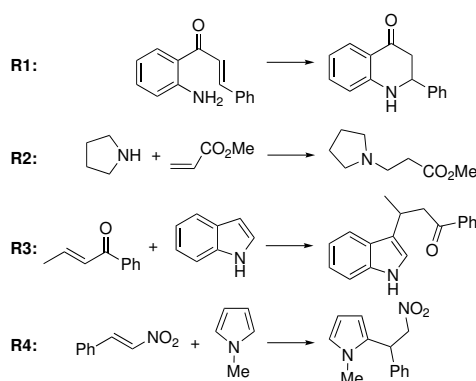


**Figure 3.16:** The four former investigated iodine catalyzed reactions [72].

- (i) All computations for the four reactions were performed including a solvent model for dichlormethane, although not all syntheses were executed using dichlormethane. The intramolecular cyclization of the amino chalcone (first reaction in the article) was synthesized in absence of any solvent.
- (ii) All calculations were performed at 25°C whereas the first investigated reaction was synthesized at 100°C. Apparently, the underlying conditions of the calculations do not cover the experimental ones. Since chemical reactions are highly complex physical systems this procedure is questionable and theoretically problematic. The solvent and the temperature can have a significant effect on the performance of reactions.
- (iii) Transition states between intermediates themselves and between intermediates and products are missing, resulting in an incomplete free-energy profile for all reactions. For instance, the transformation of **24-I<sub>2</sub>** (9.4 kcal/mol) into the intermediate **25** (13.3 kcal/mol) would require a transition state, which has to be energetically

higher than 13.3 kcal/mol. It is possible that this transition state would have a higher energy than **TS2-I<sub>2</sub>** (15.9 kcal/mol) and eventually even higher than **TS2** (18.3 kcal/mol), which would be problematic for the given explanation of the iodine catalysis.

- (iv) The published free-energy profile of the Friedel-Crafts reaction of indole (**17**) and *trans*-crotonophenone (**16**) shows a transition state **TS3** (34.7 kcal/mol) which connects the starting materials and the Wheland intermediate **26** (35.8 kcal/mol). This is suspect, because the transition state should have a higher energy than the energy of the intermediate.
- (v) The catalyzed transition states **TS1-I<sub>2</sub>** (26.6 kcal/mol), **TS3-I<sub>2</sub>** (27.1 kcal/mol) and **TS4-I<sub>2</sub>** (24.7 kcal/mol) are significantly higher compared to transition state **TS2** (18.3 kcal/mol) of the uncatalyzed free-energy profile of the intermolecular Michael reaction. Especially the comparison of **TS3-I<sub>2</sub>** and **TS4-I<sub>2</sub>** to **TS2** is interesting because the syntheses were performed at the same temperature. These calculations indicate that the investigated intermolecular Michael reaction should work properly (short reaction time and high yield) without using molecular iodine as a catalyst, or vice versa.

These aspects support the conclusion that the published calculations focused solely on generating results where products have a lower energy than the starting materials and where the calculated iodine-catalyzed transition state is lower than the uncatalyzed one. These information can already be taken out of the experimental results. Formation of a product gives the information that under specific reaction conditions the product has a negative  $\Delta G$  value compared to the starting materials. The fact, that a reaction only works properly in presence of a catalyst already reveals a transition state which is lowered by the catalyst. These information can be used to find a DFT approach explaining any already experimentally performed reaction.



### 3.5.4 Unbenchmarked iodine catalysis

In many DFT articles a certain computational procedure emerges, which can be shown through the following scheme:

$$F2/B2/C2//F1/B1/C1 \quad (3.1)$$

*F1*: Functional used for the geometry optimization

*B1*: Basis set used for the geometry optimization

*C1*: Additional corrections used for the geometry optimization

*F2*: Functional used for the electronic energies of the results

*B2*: Basis set used for the electronic energies of the results

*C2*: Additional corrections used for the electronic energies of the results

The computational method for optimizing the geometries and the one, which is afterwards performed to compute the electronic energies, differs. In general, the additional computation, which is performed after the geometry optimization, is not necessary. All results, that are needed to compute the reaction energies (thermal correction and electronic energy) are already obtained from the geometry optimization. This procedure indicates that the presented results are created to support a specific point of view or an experimental outcome.

The mentioned article on the iodine catalysis has also used this computation technique and the presented results were calculated with the B2-PLYP-D3/aug-cc-pVTZ/-IEFPCM//M06-2X-D3/6-311+G(d,p)/IEFPCM, aug-cc-pVTZ-PP for iodine, combined DFT method. Additionally further corrections were taken into account, e.g. standard state correction and the quasiharmonic approximation.

To analyze the computational procedure and to emphasize the variety of performable DFT calculations in absence of reliable data (kinetic experiments, high quality computations or benchmarks), further single-point computations were performed additionally, which resulted in electronic energies differing from the former calculations[72] by varying the functional, the basis set and the additional corrections. For these calculations the published geometries and thermal corrections of every structure were used [72]. It was reinsured that the products have a lower energy compared to the starting materials and that the iodine-catalyzed transition state is energetically lower than the uncatalyzed transition state.

A short overview of some DFT methods is given in Table 3.29 and 3.30 (all applied combinations are attached in the *Appendix*). In principal, it can be shown, that it is possible to support the iodine catalysis or not, by changing the single-point energies,

based on the same geometries and thermal corrections. It can further be shown that it is possible to support the four reactions with an extensive amount of different calculations. To give an example the catalytic effect of iodine on the four reactions can be supported with or without using standard state correction just as applying the quasiharmonic approximation for the thermal corrections.

The results given in Table 3.29 encourage the iodine catalysis for most of the methods, but the basis set trend and a different functional (in this case the BH-LYP functional) can be used to not support the iodine catalysis.

Applying a different method changes this picture significantly. In Table 3.30 the results for similar calculations are presented, whereas the dispersion (D3) correction was not applied. These results also vary between confirming all experiments or not. In contrast to Table 3.29 most of the calculations do not confirm the experiments. The PBE/def2-SVP/COSMO(CH<sub>2</sub>Cl<sub>2</sub>) computation also approves all experiments and the given mechanism. Due to the fact that this is an old functional combined with a small basis set a publication of this investigation would be rejected. In principal it was shown that exchanging the single-point electronic energies is the fastest way to compute the desired trend or result.

The comparison of these two tables shows quite different results for almost unchanged calculations and is therefore of special interest. For this reason the effect of the dispersion correction will be briefly discussed in the next section.

**Table 3.29:** Results of the iodine catalysis for the investigated reactions 1-4 using COSMO(CH<sub>2</sub>Cl<sub>2</sub>), dispersion (D3), quasiharmonic and standard state correction (+: calculation confirms the experiment, -: calculation does not confirm the experiment).

	def2-SVP	def2-SVPD	def2-TZVP	def2-QZVP
BP86	++ ++	++ ++	++ ++	
B3-LYP	++ ++	++ +-	+ - +-	
BH-LYP	++ ++	+ - +-	- - +-	- - - -
PBE	++ ++	++ ++	++ +-	
PBE0	++ ++	++ ++	+ - +-	
TPSS	++ ++	++ ++	++ ++	
TPSSH	++ ++	++ ++	++ +-	

**Table 3.30:** Results of the iodine catalysis for the investigated reactions 1-4 using COSMO(CH<sub>2</sub>Cl<sub>2</sub>), quasiharmonic and standard state correction (+: calculation confirms the experiment, -: calculation does not confirm the experiment).

	def2-SVP	def2-SVPD	def2-TZVP
BP86	+ - - -	+ - - -	+ - - -
B3-LYP	+ - - -	+ - - -	- - - -
BH-LYP	+ - - -	- - - -	- - - -
PBE	++ ++	+ - +-	+ - - -
PBE0	+ - +-	+ - +-	+ - - -
TPSS	+ - - -	+ - - -	+ - - -
TPSSH	+ - - -	+ - - -	+ - - -

### 3.5.5 The Effect of the Dispersion Correction

The dispersion correction showed the most significant influence on the computations and the capability to support the catalytic effect of iodine. The reason for this tendency is the mathematical structure of this correction. Dispersion correction systematically lowers the energy for big molecules more than for small ones. This effect is presented in Table 3.31 for an intermolecular Aza-Michael reaction. Calculating the starting materials separately results in well separated intramolecular dispersion corrected energies, e.g.  $\Delta E_{\text{Disp}}(\text{I}_2)$ ,  $\Delta E_{\text{Disp}}(\mathbf{13})$  and  $\Delta E_{\text{Disp}}(\mathbf{14})$ . In the calculation of the transition state **TS2**, an intermolecular dispersion of **13** with **14** is computed. Comparing **TS2** and **TS2-I<sub>2</sub>** the additional intermolecular dispersion of **13** and **14** with iodine is obtained. This results in a relative lowering of **TS2-I<sub>2</sub>** compared to **TS2**. This trend depends on the used geometry and the applied functional. The quality of the dispersion correction is unquantified for this specific reaction, but in general this correction can be used to lower the energy for bigger systems more than for small ones, which could be problematic for the computation of decomposition reactions, where one molecule results in two products.

**Table 3.31:** Electronic energy differences ( $\Delta E_{\text{Disp}} = E_{\text{COSMO+D3}} - E_{\text{COSMO}}$ ) of  $\text{I}_2$  in kcal/mol. The def2-TZVP basis set was used.

	$\text{I}_2$	13	14	TS2	TS2-I <sub>2</sub>	(TS2-I <sub>2</sub> )-TS2
BP86	-0.07	-4.57	-5.63	-16.31	-22.92	-6.54
B3-LYP	-0.06	-4.05	-4.77	-14.10	-19.96	-5.79
BH-LYP	-0.05	-3.29	-3.78	-11.29	-16.02	-4.68
PBE	-0.03	-2.20	-2.70	-8.19	-11.68	-3.46
PBE0	-0.03	-2.42	-2.85	-8.69	-12.40	-3.68
TPSS	-0.04	-3.22	-4.00	-11.77	-16.63	-4.81
TPSSH	-0.05	-3.19	-3.84	-11.42	-16.19	-4.73

### 3.5.6 Barrierless Decomposition

The former published free-energy profiles for the iodine-catalyzed Friedel-Crafts reaction of indole and *trans*-crotophenone revealed a rather wrong description of the transition state (**TS3**) and the following Wheland intermediate (**26**). As already mentioned in the introduction the transition state was calculated with an energy of 34.7 kcal/mol and the intermediate has a higher energy with 35.8 kcal/mol. In the article it is mentioned that on the M06-2X potential energy surface this inconsistency did not occur and the energy of the transition state was higher than the energy of the intermediate. According to this behavior it was concluded that this result indicates that the decomposition of the intermediate is barrierless. The electronic energies of the M06-2X method, that was used for the geometry optimizations, were not published and can not be verified. These aspects of the presented computations were analyzed for the following methods:

- (a) PBE-D3/def2-SVPD/COSMO//M06-2X/6-311+G(d,p)/IEFPCM, aug-cc-pVTZ-PP for iodine in kcal/mol using the quasiharmonic approximation and the standard state correction.
- (b) BP86-D3/def2-SVPD/COSMO//M06-2X/6-311+G(d,p)/IEFPCM, aug-cc-pVTZ-PP for iodine in kcal/mol using the quasiharmonic approximation.
- (c) PBE-D3/def2-TZVP/COSMO//M06-2X/6-311+G(d,p)/IEFPCM, aug-cc-pVTZ-PP for iodine in kcal/mol using the free-energy correction.

that were able to support the iodine catalysis for the four reactions. In Table 3.32 the results for this reaction and the Michael reaction of *N*-methylpyrrole and nitrostyrene (reaction 4) are presented.

**Table 3.32:** Free-energies  $\Delta G$  for the transition states and the following intermediates in kcal/mol for reaction 3 and 4.

Method	<b>TS3</b>	<b>26</b>	<b>TS4</b>	<b>27</b>
article	34.7	35.8	26.6	26.2
(a)	26.5	25.9	18.3	18.9
(b)	27.1	26.8	17.8	18.8
(c)	32.0	31.9	26.2	28.0

It can be seen that the Wheland intermediate can be computed lower than the corresponding transition state, but the results also show that an additional disagreement for the Michael reaction is obtained for the used method. The results of the Friedel-Crafts

reaction are in agreement with the chemical understanding of a transition state and the following intermediate, but the energy differences are very small ( $<1$  kcal/mol), which is in line with the discussed results for the M06-2X potential energy surface. The transition state (**TS4**) is higher than the corresponding intermediate (**27**) for the Michael reaction for the three calculations presented in Table 3.32, which was not obtained by the former published results. Analogue to the Friedel-Crafts reaction it could be concluded that this behavior indicates a barrierless decomposition of the intermediate. Considering the general performance of DFT calculations it could also be concluded that this aspect of the computation reveals that DFT can not deal with this question properly for these two reactions using the same method. The intermediates have to be energetically lower than the transition states and the real energy differences can deviate from these computations. Trends and the energetical ordering of different molecules and geometries can change if the computational method is also changed. A barrierless decomposition is possible but would be out of the ordinary. This special aspect of these systems might only be investigated and described correctly by experiments and emphasizes the limitation of the nowadays available computational methods.

### 3.5.7 Computational Validation

The question, which should be answered in a DFT study is: Why is the applied computational level usable for the specific chemical problem? In the former published article two answers were given: (1) A benchmark study[82] has shown that the applied method is suitable for the description of halogen bonding. (2) A benchmark on experimental  $\Delta G$  values (Table 3.33) for iodine bonding of several carbonyl compounds is presented [72]. Within the scope of the mentioned benchmark article the used method was not tested.

**Table 3.33:**  $\Delta G$  values in kcal/mol for several carbonyl compounds with iodine, recently published[72].

	Carb-1	Carb-2	Carb-3	Carb-4	Carb-5	SD	Max. Err.
Exp.[83]	0.1	0.1	0.2	0.3	0.4		
Calc. (Table[72])	1.0	2.1	1.2	2.1	1.7	0.48	2.0

Every functional was tested for itself and not in a combined way whereby both functionals were not tested including the dispersion correction. As highlighted before, the dispersion correction has a significant influence on the energies and the relative ordering of the energy levels. According to this, the used method should be tested including this correction. The B97, PBE, TPSS, B3-LYP, PBE0, TPSSH,  $\omega$ B97X and the DSD-PBE-P86 functionals were tested including the D2 dispersion correction and the article concludes that dispersion correction tend to be detrimental for halogen bonds. Following this benchmark article the dispersion correction should not have been applied. In the statistical analysis of this benchmark the M06-2X functional performs better than the B2PLYP functional. Changing the electronic energies from M06-2X to B2PLYP appears to be illogical, but was done in the computational study of the iodine catalysis.

The benchmark article presents energy benchmarks for two different chemical test sets. The first set is named XB18, where 18 different systems were analyzed. This set consists of nine halogen complexes with formaldehyde and nine halogen complexes with hydrogen cyanide. The nine halogen compounds are HBr, HI, Br<sub>2</sub>, I<sub>2</sub>, ClBr, BrI, ClI, FBr and FI. In this ordering the second atom of the two atomic systems is coordinated to the oxygen of the formaldehyde or to the nitrogen of the hydrogen cyanide. The bond distances between the halogen and the organic compound were analyzed. The M06-2X performs quite well for this bond distance and showed a root mean square deviation (RMSD) of 0.028 Å and a mean signed error (MSE) of -0.009 Å. The  $\omega$ B97X and the BMK functionals revealed a better performance on the bond distances, but the M06-2X method seems to be an understandable choice too. The size of the test systems appears to be small and

at least only one carbonyl compound was tested. Therefore the derived statistic might not be representative for general applications to other carbonyl compounds. Energies of this test set were not benchmarked.

In the benchmark article, dissociation energies were analyzed using the XB51 test set, consisting of 51 test systems. This set does not include I<sub>2</sub> compounds. Nevertheless the analysis of the energies reveals that the M06-2X functional shows an RMSD of 0.43 kcal/mol, a MSE of 0.01 kcal/mol and a maximum error of 1.58 kcal/mol. The B2-PLYP functional showed an RMSD of 0.82 kcal/mol, a MSE of -0.53 kcal/mol and a maximum error of -2.57 kcal/mol. According to these results the M06-2X functional should be preferred for energy applications and changing the functional to the B2-PLYP functional is due to the benchmark article illogical and the statement (1) in the beginning of this section is invalid. Nevertheless the benchmark article seems to be inappropriate for the investigation of iodine catalyzed reactions, because the test sets are small, there is only one I<sub>2</sub>-carbonyl compound in the whole benchmark and the energy analysis corresponds to the dissociation energy and not to the free-energy of coordinated iodine on carbonyl compounds. Therefore the small benchmark, mentioned in statement (2), should be more relevant for the computation of iodine catalyzed reactions.

The experimental data presented in Table 3.33 are more suitable to benchmark DFT methods and afterwards to analyze the effect of iodine on the free-energy surface of the reactions. The performance of the used method on the experimental data given in the Table 3.33 is not very good. The computed  $\Delta G$  values for the different iodine-carbonyl interactions are systematically too large, while the standard deviation (SD), which can be calculated from the published data, is also not good. The maximum error is 2.0 kcal/mol, which is also quite large and according to these five experimental outcomes and the corresponding performance of the used method, the choice of the functional also seems to be illogical.



### 3.5.8 Experimental Benchmarking

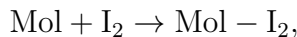
The logical procedure to perform DFT calculations is minimizing the error for a specific chemical problem, based on reliable data (experimental data or high wavefunction based methods) of similar systems and to afterwards apply this method. Therefore, the same benchmark set for the  $\Delta G$  values of the iodine binding was used and the occurring errors for a set of DFT methods were analyzed. All geometries were optimized using the TPSSH functional and the def2-TZVP basis set. The obtained free-energy correction combined with single-point energies of different methods were used to derive the final  $\Delta G$  values. The COSMO model and the D3 correction were applied to take care of solvent effects and long-range interactions. The results are presented in the following Tables 3.34 and 3.35 for calculations including and not including the standard state correction. The three lowest maximum errors are highlighted in bold.

In general it can be seen that the basis set trend (increasing basis set size) results in a systematic increasing  $\Delta G$  value for the five test systems. The best result without using the standard state correction is obtained by the TPSSH functional with the smallest tested basis set, the def2-SVP basis set, with a maximum error of -0.60 kcal/mol (see Table 3.34). This emphasizes the error cancellation of DFT methods. A small basis set combined with a functional can lead to accurate results for specific cases.

**Table 3.34:** Maximum signed error compared to the experimental  $\Delta G$  values in kcal/mol of the five test systems calculated with COSMO( $\text{CCl}_4$ ) including dispersion correction, free-energy correction without standard state correction. The def2-X basis sets were used.

	SVP	SVPD	TZVP	TZVPP	TZVPD	QZVP
BP86	-1.89	-1.13	1.91	1.91	2.13	2.22
B3-LYP	0.71	1.86	3.08	3.09	3.34	3.44
BH-LYP	1.98	2.76	4.08	4.09	4.29	4.42
PBE	-1.91	0.99	1.92	1.92	2.22	2.29
PBE0	0.67	1.39	2.80	2.80	3.02	3.11
TPSS	-1.42	1.23	2.21	2.21	2.48	2.54
TPSSH	<b>-0.60</b>	1.43	2.46	2.46	2.70	2.77
M06	0.83	1.46	3.44	3.43	3.59	3.69

The standard state correction adds 1.89 kcal/mol to every calculated electronic energy. For the given reaction scheme of the benchmark



this correction leads to a relative lowering of the free-energy of 1.89 kcal/mol for the iodine coordination. The performance of the computational method is not affected by this correction, but as it can be seen in Table 3.35, larger basis sets can be used to obtain results, which are very close to the experiment.

Table 3.35 reveals that the TPSSH-D3/def2-TZVP/COSMO//TPSSH/def2-TZVP calculation gives the lowest error for the specific benchmark reactions. The maximum signed error is 0.57 kcal/mol which is lower than the often mentioned chemical accuracy of 1 kcal/mol. In the sense of statistical evidence this calculation should be preferred for the application, but it should also be mentioned that the TPSSH-D3/def2-SVP/COSMO//TPSSH/def2-TZVP method without using standard state correction would also be a good choice, according to the statistical analysis.

**Table 3.35:** Maximum signed error compared to the experimental  $\Delta G$  values in kcal/mol of the five test systems calculated with COSMO( $\text{CCl}_4$ ) including dispersion correction, free-energy correction and standard state correction. The def2-X basis sets were used.

	SVP	SVPD	TZVP	TZVPP	TZVPD	QZVP
BP86	-3.78	-3.02	-1.41	-1.41	-1.28	-1.10
B3-LYP	-1.77	-1.00	1.19	1.20	1.45	1.55
BH-LYP	-0.95	0.87	2.19	2.20	2.40	2.53
PBE	-3.80	-2.43	-1.05	-1.07	-0.69	-0.61
PBE0	-1.87	-1.13	0.91	0.91	1.13	1.22
TPSS	-3.31	-2.46	-0.84	-0.84	-0.65	0.65
TPSSH	-2.49	-1.84	<b>0.57</b>	<b>0.57</b>	0.81	0.88
M06	-2.14	-1.61	1.55	1.54	1.70	1.80

### 3.5.9 Iodine Catalysis in CH<sub>2</sub>Cl<sub>2</sub> at 25°C

The TPSSH-D3/def2-TZVP/COSMO//TPSSH/def2-TZVP method (including standard state correction) performed well for the chosen benchmark and the computed results were very close to the experimental ones. Therefore we investigated 18 iodine catalyzed reactions with this method. All analyzed iodine catalyzed reactions are shown in Figure 3.17 and the following discussion uses the nomenclature, which is given in this scheme.

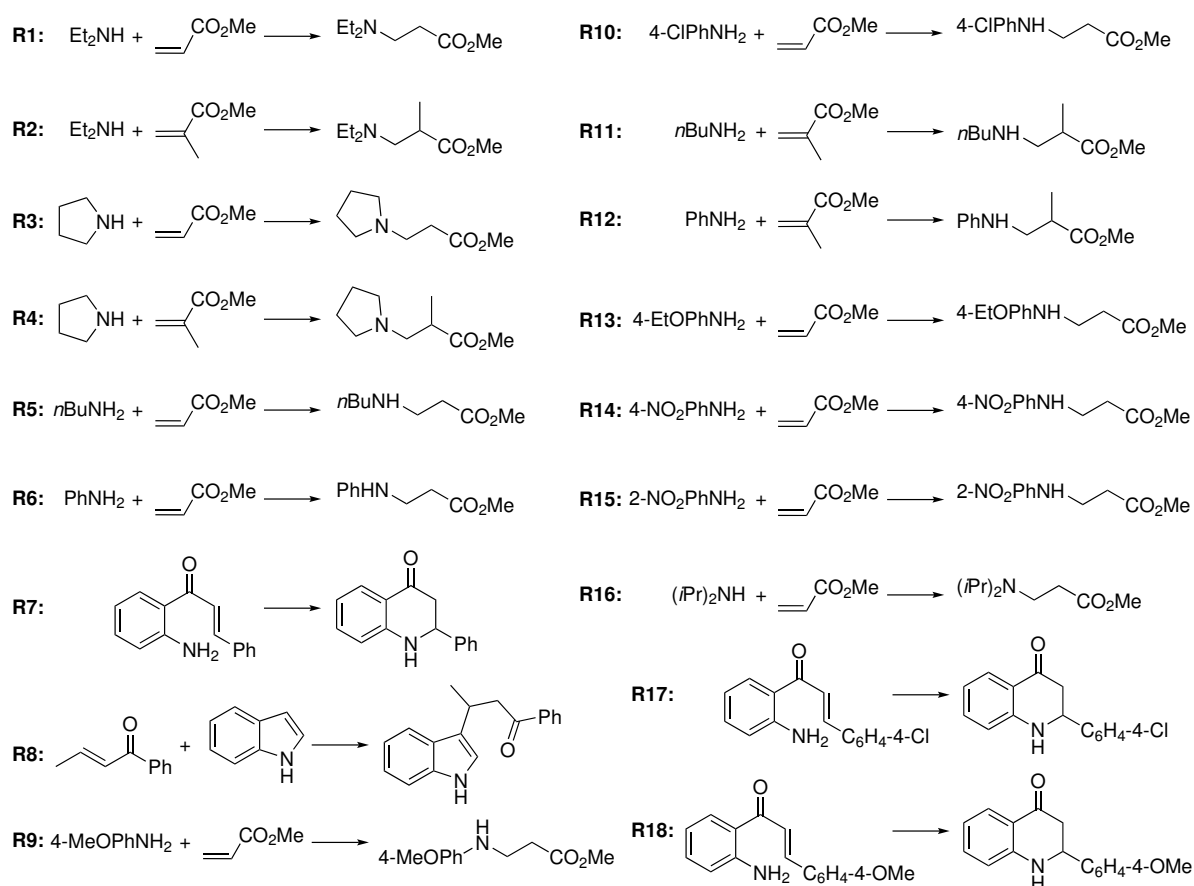


**Figure 3.17:** Investigated iodine catalyzed reactions.

First of all the reactions, that were experimentally synthesized in dichlormethane at room temperature (R1-R6, R8 and R16) will be discussed. All calculations were performed using the COSMO model for dichlormethane and the thermal corrections were computed at room temperature, covering the experimental conditions and avoiding contradictions, mentioned in the introduction under the statements (i) and (ii) for the former published article on the iodine catalysis. Additionally, only systems are considered where iodine coordinates to the carbonyl group. This is in line with the chemical situation of the chosen experimental benchmark. The results of these systems and the corresponding computations are provided in Table 3.36 for the uncatalyzed and catalyzed transition states as well as for the resulting products. The reported experimental results, product yields and reaction times, are also included.

**Table 3.36:**  $\Delta G$  in kcal/mol computed for  $\text{CH}_2\text{Cl}_2$  at 298.15 K computed by TPSSH-D3/def2-TZVP/COSMO//TPSSH/def2-TZVP using standard state correction. (Experiments for R8[84], R1-R5 and R16[85])

	Prod	TS	(TS-I <sub>2</sub> )-TS	TS-I <sub>2</sub>	yield	reaction time
R1	-3.28	20.48	-5.65	14.83	93 %	15 min
R2	-0.71	23.36	-5.97	17.40	89 %	25 min
R3	-8.14	17.20	-5.17	12.03	89 %	15 min
R4	-4.90	21.13	-5.82	15.31	91 %	25 min
R5	-4.04	21.39	-6.32	15.07	86 %	3 h
R6	-3.67	27.81	-4.10	23.71	NR	-
R8	-5.97	34.03	-4.75	29.28	76 %	3 min
R16	0.10	21.98	-5.08	16.90	82 %	40 min

The results confirm the iodine catalysis for all reactions, in a sense of lowering the transition state. But the free-energy of the product of reaction 16 is positiv (0.10 kcal/mol) and therefore a wrong reaction outcome is computed by the used method. In the case of reaction 2 the free-energy of the product is also discussable. The  $\Delta G$  value is determined to be -0.71 kcal/mol, which is in agreement with the experiment. Considering the standard state correction, all product energies of the shown systems are shifted by 1.89 kcal/mol compared to the starting materials. The computed energies without this shift are 1.99 kcal/mol for the product of reaction 16 and 1.18 kcal/mol for the product of reaction 2, which shows that the computation is not stable for the product energies. The method was chosen due to the benchmark of the iodine coordination and therefore only this aspect of the reactions might be computed reliably. The determined lowering of the

transition by iodine is stable for the used method. It should be mentioned that this trend is also obtained without using the relative shift resulting from the standard state correction. This aspect of the computation is not obtained by the former published results for the iodine catalysis. For the Michael reaction of *N*-methylpyrrole with nitrostyrene the catalytic effect of iodine is not obtained without using the standard state correction. The computation itself delivers a positive energy,  $\Delta G((\text{TS-I}_2)\text{-TS}) = 0.05$  kcal/mol, for the catalyzed transition state without applying the relative shift. This indicates that the former applied method is not well chosen for the coordination of iodine.

The results in Table 3.36 additionally show that the heights of the catalyzed transition states are spreading. Comparing these results with the experimental outcome and the reaction time reveals consistencies and inconsistencies, e.g. the experimental outcome for reaction 6 is in agreement with reactions 1-5 and 16, but disagrees with reaction 8. Reaction 5 has the longest reaction time, which implies that the transition state is comparative the highest one of the working systems. The DFT results are not supporting this point of view. The catalyzed transition states of the reaction 2, 8 and 16 are higher than the transition state for reaction 5, which is inconsistent. Reaction 1 and 4 show nearly the same energy for the catalyzed transition states, compared to TS5-I<sub>2</sub>, but the reaction times are much lower. The height inconsistencies will be discussed later in more detail. Reactions 5 and 6 are of special interest, due to the bad performance of these systems in the experiments and will be discussed in the following.

### 3.5.10 R-NH and R-NH<sub>2</sub> Compounds

The published experiments of the iodine catalysis show a significantly lower performance for R-NH<sub>2</sub> compounds compared to the R-NH compounds. For instance reaction 5 using *n*-BuNH<sub>2</sub> as a starting material shows a long reaction time, which was already presented in Table 3.36. For this system two different types of the catalyzed transition state (R5 and R5\*) were computed. Each imaginary frequency corresponds to the logical reaction path. In Figure 3.18 the geometries of the uncatalyzed and catalyzed transition states are presented,

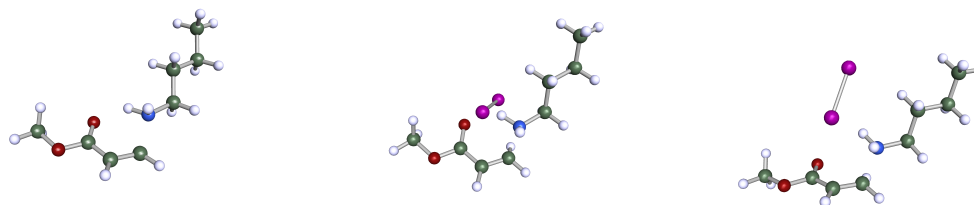


**Figure 3.18:** Transition states for reaction 5 (TS, TS-I<sub>2</sub> for R5\*, TS-I<sub>2</sub> for R5).

whereby in Table 3.37 the corresponding computed  $\Delta G$  values can be found. The uncatalyzed transition state shows a coordination of the NH<sub>2</sub> group to the oxygen of the carbonyl group. This type of transition state was found for all R-NH<sub>2</sub> systems but was not obtained for the NH compounds. The catalyzed transition state TS5-I<sub>2</sub>\* shows the same coordination. The transition state is therefore not lowered as much as for the R-NH compounds, which could be a possible explanation for the experimental trend of the R-NH<sub>2</sub> systems. The transition state R5 does not have such a coordination and is in line with the transition states for all R-NH systems and the lowest computed one for reaction 5. This result can not deliver an explanation for significantly higher reaction times of these systems. The transition state TS5-I<sub>2</sub>\* is energetically not the lowest computed one but could give an explanation for the experimental performance of this system. These results reveal that it is possible to confirm experiments without computing the correct transition states and how insights for special questions arising from an experiment can be obtained.

**Table 3.37:**  $\Delta G$  in kcal/mol computed for  $\text{CH}_2\text{Cl}_2$  at 298.15 K computed by TPSSH-D3/def2-TZVP/COSMO//TPSSH/def2-TZVP using standard state correction. (Experiments for R8[84], all other[85])

	TS	(TS-I <sub>2</sub> )-TS	TS-I <sub>2</sub>	yield	reaction time
R1	20.48	-5.65	14.83	93 %	15 min
R2	23.36	-5.97	17.39	89 %	15 min
R3	17.20	-5.17	12.03	89 %	15 min
R4	21.13	-5.82	15.31	91 %	25 min
R5	21.39	-6.32	15.07	86 %	3 h
R5*	21.39	-3.79	17.60	86 %	3 h
R6	27.81	-4.10	23.71	NR	-
R8	34.03	-4.75	29.28	76 %	3 min
R16	21.98	-5.08	16.90	82 %	40 min

In principal the explanation of the poor performance for the  $\text{NH}_2$  systems is logical, but as it is shown in Table 3.37, the energy corresponding to the transition state TS5-I<sub>2</sub><sup>\*</sup> does not agree with all experimental results and the corresponding calculations. The computed energy matches the trend compared to the reactions 1, 3 and 4 but is not consistent with the derived energies for the reactions 2, 8 and 16. According to the general performance of DFT computations and the shown unreliability of the used DFT method in view of the determined transition state energies, this aspect of the experimental study can not be definitely answered. It can not be ruled out that TS5-I<sub>2</sub> is the correct transition state, but the calculated free-energy is wrong. It is also conceivable that the TS-I<sub>2</sub><sup>\*</sup> transition state is correct and that the energetical ordering of TS5-I<sub>2</sub> and TS5-I<sub>2</sub><sup>\*</sup> is computed wrong. This emphasizes that computed insights and underlying reasons for experimental results or trends should be treated with caution.

### 3.5.11 Reaction of Aniline and Methyl Acrylate

The reaction between aniline and methyl acrylate is a mentionable system, because no reaction occurs in  $\text{CH}_2\text{Cl}_2$  at room temperature. Including such a reaction is a special task. There are three physical reasons for this outcome. (1) The  $\Delta G$  value is positive for the product under the specific reaction conditions. (2) The catalyst does not lower the transition state. (3) The catalyst lowers the transition state but it remains too high. And in addition there can be an error in the experiment. Without detailed experimental studies, it is not possible to decide which of these four statements is correct for the investigated system.

The  $\Delta G$  value of TS6-I<sub>2</sub> is the highest calculated one, comparing the reactions 1-6 and 16. In the sense of statement (3) this would be a consistent picture. However, after including reaction 8 this point of view is contradictory, according to the experimental outcome and the high calculated energy of the transition state TS8-I<sub>2</sub>. The statements (1) and (2) are also possible for the reaction 6 and therefore these two statements will be discussed in the following part of this section. All computations using the def2-TZVP basis set were analyzed with regard to the experimental outcome and the former mentioned possible reasons (1) and (2).

The results of this analysis are given in the Tables 3.38 and 3.39. In Table 3.38 all computations are presented including standard state correction. The obtained results reveal that several functionals can not compute the reaction outcome correctly for the set of eight reactions. The B3-LYP, BH-LYP, PBE, TPSS and the TPSSH functional are already failing for at least one experimental working reaction. This indicates that these functionals are not very reliable for computing the catalytic effect of iodine or the free-energy of the resulting products. The BP86, PBE0 and the modern M06 functional can compute the experimental outcome for every working reaction and appear to be robust. Every calculation using the standard state correction can not describe the experimental outcome of the reaction between aniline and methyl acrylate correctly. Considering statement (3), the heights of the catalyzed transition states need to be analyzed, which will be done in the next section for all methods.

The results given in Table 3.39 were computed without using the standard state correction, which is an additional shift for all free-energies compared to the starting materials, as already mentioned. Without this shift the M06 and the BP86 functional can also not compute the experimental outcome for all working reactions correctly and the only calculation which is stable onto all reaction outcomes, without using shifts, is the PBE0-D3/def2-TZVP/COSMO method based on the TPSSH/def2-TZVP geometry optimization. Therefore it can be concluded that this method delivers the most stable



**Table 3.38:** DFT performance on similar reactions in  $\text{CH}_2\text{Cl}_2$  at 298.15 K. (+: calculation confirms the experiment, -: calculation does not confirm the experiment). Geometry optimizations and free-energy corrections were computed using TPSSH/def2-TZVP. Electronic energies were computed by the given functionals including D3 correction and a COSMO correction for  $\text{CH}_2\text{Cl}_2$ . Standard state correction was used.

	BP86	B3-LYP	BH-LYP	PBE	PBE0	TPSS	TPSSH	M06
R1	+	+	+	+	+	+	+	+
R2	+	-	+	+	+	-	+	+
R3	+	+	+	+	+	+	+	+
R4	+	+	+	+	+	+	+	+
R5	+	+	+	+	+	+	+	+
R6	-	-	-	-	-	-	-	-
R8	+	+	+	+	+	+	+	+
R16	+	-	-	-	+	-	-	+

**Table 3.39:** DFT performance on the prediction of reactions in  $\text{CH}_2\text{Cl}_2$  at 298.15 K. (+: calculation confirms the experiment, -: calculation does not confirm the experiment). Geometry optimizations and free-energy corrections were computed using TPSSH/def2-TZVP. Electronic energies were computed by the given functionals including D3 correction and a COSMO correction for  $\text{CH}_2\text{Cl}_2$ . Standard state correction was not used.

	BP86	B3-LYP	BH-LYP	PBE	PBE0	TPSS	TPSSH	M06
R1	+	-	-	+	+	+	+	+
R2	-	-	-	-	+	-	-	+
R3	+	+	-	+	+	+	+	-
R4	+	+	-	+	+	+	+	+
R5	+	-	+	+	+	+	+	+
R6	-	+	+	-	+	-	-	+
R8	+	+	+	+	+	+	+	+
R16	-	-	-	-	+	-	-	+

computations for reactions that are similar to the test set.

### 3.5.12 Height Consistency for the Iodine Catalysis in $\text{CH}_2\text{Cl}_2$ at 25 °C

Considering the reaction of aniline and methyl acrylate, it is possible that the catalyzed transition state is still too high and therefore the reaction can not happen. In Table 3.40 all catalyzed transition states are presented, whereby the reaction of aniline is highlighted in bold. This system should have the highest transition state. The results reveal that all functionals can not compute the heights of this test set correctly. In all computations the catalyzed transition state of reaction 8 is higher compared to reaction 6. Reaction 8 has a good performance at room temperature in dichlormethane, whereas for reaction 6 no product was obtained. Therefore it can be concluded that the performed computations are not able to compute the reaction outcomes correctly for the whole set of reactions. In case of reaction 8 a new carbon-carbon bond is synthesized, whereas a nitrogen-carbon bond is established in all other cases. The inconsistency of the computed transition states might show that the DFT methods can not compute this different situation at the same quality.

Furthermore, it can be seen that the heights of all systems are spreading, but from the B3-LYP and the M06 functional more or less the same values are obtained for all reactions. Therefore it can be concluded that these two functionals have the same quality concerning the transition states and that the modern M06 functional does not lead to better results compared to the old B3-LYP functional for this specific reaction type. Additionally the results reveal, that the former mentioned inconsistencies between the reactions can not be generally overcome by any method and these systems can not be computed in agreement to the published reaction times and product yields (see Table 3.36) using one computational method.

**Table 3.40:**  $\Delta G$  for the catalyzed transition states TS-I<sub>2</sub> using dispersion (D3) and standard state correction in CH<sub>2</sub>Cl<sub>2</sub> at 298.15 K.

	BP86	B3-LYP	BH-LYP	PBE	PBE0	TPSS	TPSSH	M06
R1	9.82	19.61	24.78	11.69	16.11	12.79	14.83	19.21
R2	11.93	22.56	28.39	14.24	19.14	15.10	17.40	22.00
R3	7.31	16.41	21.15	8.68	12.96	10.13	12.03	17.53
R4	10.19	20.07	25.56	11.89	16.79	13.11	15.31	21.24
R5	11.13	19.82	24.37	11.87	16.19	13.16	15.07	21.04
<b>R6</b>	<b>20.03</b>	<b>28.26</b>	<b>31.81</b>	<b>21.08</b>	<b>24.38</b>	<b>22.16</b>	<b>23.71</b>	<b>28.77</b>
R8	23.21	34.61	40.66	25.71	30.81	27.00	29.28	34.12
R16	11.44	21.90	26.97	14.41	18.40	14.92	16.90	20.40

**Table 3.41:** As Table 3.38 including height consistency for reaction 6.

	BP86	B3-LYP	BH-LYP	PBE	PBE0	TPSS	TPSSH	M06
R1	+	+	+	+	+	+	+	+
R2	+	-	+	+	+	-	+	+
R3	+	+	+	+	+	+	+	+
R4	+	+	+	+	+	+	+	+
R5	+	+	+	+	+	+	+	+
R6	+	+	+	+	+	+	+	+
R8	-	-	-	-	-	-	-	-
R16	+	-	-	-	+	-	-	+

### 3.5.13 Iodine Catalysis in Toluene at 70°C

The PBE0-D3/def2-TZVP/COSMO//TPSSH/def2-TZVP method seemed to be the most appropriate method for iodine catalyzed reactions in dichloromethane at room temperature. Therefore this procedure was extended to 5 additional systems, which were synthesized in refluxing toluene. According to the experimental conditions all calculations were performed using the COSMO model for toluene and the thermal corrections were determined at 343.15 K, which intends to cover the published experiments [85]. Reaction 6 was published to be malfunctioning in  $\text{CH}_2\text{Cl}_2$  at room temperature, but it is working in refluxing toluene. By combining Table 3.39 and Table 3.42 it can be shown that there is no calculation which can cover these two experiments of the same starting materials and catalyst, without using shifts. The results also reveal that for the five used reactions it is not possible to find a calculation which covers all experimental outcomes. Especially the bad performance of the PBE0 functional indicates that it is not possible to compute reliable energies and trends for a set of reactions and for different experimental conditions and additional shifts have to be included.

**Table 3.42:** As Table 3.39 but for toluene at 343.15 K

	BP86	B3-LYP	BH-LYP	PBE	PBE0	TPSS	TPSSH	M06
R6	+	-	-	+	-	-	+	-
R9	+	-	-	+	-	-	+	-
R10	+	-	-	+	-	-	+	-
R14	+	+	+	+	+	+	+	+
R15	-	+	+	+	+	-	-	+

According to this insight the standard state correction was applied and all reaction energies reanalyzed. Including the standard state correction (2.18 kcal/mol at 343.15 K) for all reactions results in an improved picture for the whole set of reactions. In Table 3.43 the reactions were analyzed due to the experimental outcome and the statements (1) and (2). In this set all reactions that were synthesized in refluxing toluene were included, but additionally further reactions, where the experimental outcome is implicitly given by the experiments were also used. The reactions 1-5, 8 and 16 are already synthesized in dichlormethane at room temperature and according to this, the reaction should also work properly in toluene applying a higher temperature. Additionally, reaction 7 can also be added in this set, because this system was synthesized at 70 °C, but in absence of any solvent. Including these reactions for the analysis improves the statistics for every DFT method and the reliability can be better assessed and checked.

**Table 3.43:** DFT performance on the prediction of reactions in toluene at 343.15 K. (+: calculation confirms the experiment, -: calculation does not confirm the experiment). Geometry optimizations and free-energy corrections were computed using TPSSH/def2-TZVP. Electronic energies were computed by the given functionals including D3 correction and a COSMO correction for toluene. Standard state correction was used. †: Reaction outcome is implicitly given.

	BP86	B3-LYP	BH-LYP	PBE	PBE0	TPSS	TPSSH	M06
R1 <sup>†</sup>	+	+	+	+	+	+	+	+
R2 <sup>†</sup>	+	-	+	+	+	-	+	+
R3 <sup>†</sup>	+	+	+	+	+	+	+	+
R4 <sup>†</sup>	+	+	+	+	+	+	+	+
R5 <sup>†</sup>	+	+	+	+	+	+	+	+
R6	+	+	+	+	+	+	+	+
R7 <sup>†</sup>	+	+	+	+	+	+	+	+
R8 <sup>†</sup>	+	+	+	+	+	+	+	+
R9	+	+	+	+	+	+	+	+
R10	+	+	+	+	+	+	+	+
R14	+	+	+	+	+	+	+	+
R15	-	-	-	-	-	-	-	-
R16 <sup>†</sup>	-	-	-	-	+	-	-	+

**Table 3.44:** As Table 3.43 including height consistency.

	BP86	B3-LYP	BH-LYP	PBE	PBE0	TPSS	TPSSH	M06
R1 <sup>†</sup>	+	+	+	+	+	+	+	+
R2 <sup>†</sup>	+	-	+	+	+	-	+	+
R3 <sup>†</sup>	+	+	+	+	+	+	+	+
R4 <sup>†</sup>	+	+	+	+	+	+	+	+
R5 <sup>†</sup>	+	+	+	+	+	+	+	+
R6	+	+	+	+	+	+	+	+
R7 <sup>†</sup>	+	+	+	+	+	+	+	+
R8 <sup>†</sup>	+	+	-	+	-	+	+	+
R9	+	+	+	+	+	+	+	+
R10	+	+	+	+	+	+	+	+
R14	+	+	+	+	+	+	+	+
R15	+	+	+	+	+	+	+	+
R16 <sup>†</sup>	-	-	-	-	+	-	-	+

The Table 3.43 shows quite a good performance for all working systems. Especially the PBE0 and the M06 functionals are in agreement with all experimental outcomes, except the not working reaction 15. Reaction 14 showed a positive  $\Delta G$  value for all functionals and therefore the correct reaction trend can be computed by all tested DFT methods. As previously done for the reactions in dichlormethane, the height consistency for all reactions was additionally investigated for the whole reaction set. The determined results presented in Table 3.44 revealed that all 13 reactions can be computed consistent to the experimental outcome by the M06 functional. This method was also reliable for the dichlormethane test set, except reaction 8. Reaction 8 does not lead to a height inconsistency compared to the not working reactions 14 and 15. Therefore reaction 8 in dichlormethane at room temperature seems to be the only reaction, which could not be computed consistent to all other reactions and the M06 methods shows a robust reliability compared to the experimental outcome. The PBE0 functional determines nearly all transition state heights consistent, but the catalyzed transition state of reaction 8 (TS8-I<sub>2</sub>= 32.19 kcal/mol) is computed higher compared to the not working reaction 14 (TS14-I<sub>2</sub>= 31.85 kcal/mol). However, the computations in dichlormethane already emphasized that a consistency between reaction 8 and all other systems can not be expected. Therefore the PBE0 functional shows a good performance on systems, where a new nitrogen-carbon bond is established.

Nevertheless the heights are spreading for all reactions and the energy differences be-

tween working and not working systems are small. The reaction time and product yield trends can not be computed reliably for the whole set. Especially, reaction 8 shows a similar, or even higher transition state compared to the reactions 6, 9 or 10 (see Table A.41). These three reactions have reaction times of 7-8 h resulting in a product yield of 60-85%, but reaction 8 already showed better performance (3 min and 76%) at room temperature.

This emphasizes that a proper testing of the available computational methods requires as many reactions as possible including systems which showed a low performance or even systems, in which reaction occurred. Experimental results for the same reaction varying the solvent and the temperature are also needed. Finding such systems is often a problem due to the publishing habits in the experimental organic chemical community. Especially the systems, where no reaction occurs, need to be published and included in DFT studies to verify the reliability of these methods in the view of reaction prediction. Without these experimental information the height consistency can not be investigated and predictive application of DFT computations can not be performed controllably. The PBE0 and the M06 method showed a good quality on the reaction prediction for many systems in toluene and dichloromethane for temperatures between 25 and 70 °C. According to that all DFT methods were also tested for three reactions that were synthesized at 100 °C and will be discussed in the next section.

### 3.5.14 Iodine Catalysis at 100 °C

The syntheses of the reactions 7, 17 and 18 were executed at 100 °C isolating high product yields. To test the stability of the DFT methods the reaction energies were computed for this temperature including standard state correction (2.53 kcal/mol at 100 °C). All further analyzed working reactions synthesized at lower temperatures were also included to verify the reliability of the applied method. As it is shown in Table 3.45 all reaction outcomes are predicted correctly, but according to the fact that for this temperature no not working reaction was published, height consistency could not be analyzed. The PBE0 and M06 functionals determine all reaction outcomes correctly. Therefore it can be concluded that the PBE0-D3/def2-TZVP/COSMO and the M06-D3/def2-TZVP/COSMO method based on TPSSH/def2-TZVP optimized geometries using standard state correction appear to be good choices for further investigations of iodine catalyzed reactions.

**Table 3.45:** As Table 3.43 for toluene at 373.15 K.

	BP86	B3-LYP	BH-LYP	PBE	PBE0	TPSS	TPSSH	M06
R1 <sup>†</sup>	+	-	+	+	+	+	+	+
R2 <sup>†</sup>	-	-	-	-	+	-	-	+
R3 <sup>†</sup>	+	+	+	+	+	+	+	+
R4 <sup>†</sup>	+	+	+	+	+	+	+	+
R5 <sup>†</sup>	+	+	+	+	+	+	+	+
R6 <sup>†</sup>	+	-	+	+	+	+	+	+
R7 <sup>†</sup>	+	+	+	+	+	+	+	+
R8 <sup>†</sup>	+	+	+	+	+	+	+	+
R9 <sup>†</sup>	+	-	+	+	+	+	+	+
R10 <sup>†</sup>	+	-	-	+	+	+	+	+
R16 <sup>†</sup>	-	-	-	-	+	-	-	+
R17 <sup>†</sup>	+	+	+	+	+	+	+	+
R18 <sup>†</sup>	+	+	+	+	+	+	+	+



### 3.5.15 Experimentally Undescribed Iodine Catalyzed Systems

It was shown that the PBE0-D3/COSMO/def2-TZVP//TPSSH/def2-TZVP method a stable calculation regarding the reaction outcome. Therefore it might be the best choice to investigate experimentally undescribed systems for the iodine catalysis. Especially the results for reaction 8 and reaction 5 are emphasizing that DFT computation might lead to wrong trends and inconsistent results compared to the experiments, if the systems are chemically too different. According to this, three additional systems of unknown experimental outcome (R11-R13) were computed and will be analyzed in the following. The experiments in dichlormethane at room temperature and the corresponding computations (see Table 3.46) reveal that the reactions using methyl methacrylate (highlighted in bold) perform worse compared to the reactions using methyl acrylate as a starting material. This trend is stable over all computations. Therefore two reactions were computed exchanging the methyl acrylate with methyl methacrylate. These systems are not experimentally described.

**Table 3.46:** Computed  $\Delta G$  values using the PBE0-D3/COSMO/def2-TZVP method based TPSSH/def2-TZVP optimized structures using the standard state correction in dichlormethane at 25 °C.

	Prod	TS	TS-I <sub>2</sub>	yield	reaction time
R1	-6.67	19.66	16.11	93 %	15 min
<b>R2</b>	-3.62	22.90	19.14	89 %	25 min
R3	-11.79	16.04	12.96	89 %	15 min
<b>R4</b>	-8.16	20.51	16.90	91 %	25 min
R5	-7.62	20.49	16.19	86 %	3 h
<b>R11</b>	-4.17	22.11	18.68		
R6	-7.05	26.17	24.38	NR	
<b>R12</b>	-3.99	29.86	26.76		

As the results in Table 3.46 show, the trend of a lower experimental performance for this starting material should also appear for the reactions 11 and 12. According to the experimental outcome of reaction 6, the corresponding system using methyl methacrylate should not be applicable in dichlormethane at room temperature. Combining the starting materials *n*-BuNH<sub>2</sub> and methyl methacrylate should also increase the reaction time for this case. Transition state TS11-I<sub>2</sub> compared to TS5-I<sub>2</sub> shows more or less the same difference as reaction 1 compared to reaction 2 and reaction 3 compared to reaction 4. Therefore it can be concluded that this reaction time might be slightly increased.

For the test set corresponding to experimental outcomes for iodine catalyzed reactions in refluxing toluene, an additional undescribed reaction (R13) was computed. For system 13 the methoxy group of reaction 9 is replaced by an ethoxy group. As Table 3.47 reveals the catalyzed transition state heights of all systems are consistent with the reaction time and the isolated yield. These results and the chemical similarity of reaction 13 indicates that the computed results can be seen as reliable, but this indicates that computations which are in agreement to the experimental performance might just be possible for extremely similar systems. The correct trend of these reactions (R6, R9-10 and R14-15) can be computed by any tested computational method (see Table A.41 in the *Appendix*).

System 13 reveals a higher thermodynamic stability of the resulting product and the catalyzed transition state is computed comparable to the corresponding methoxy compound. Therefore it can be concluded that the performance of this reaction should be as good as it is for reaction 9. In general the used DFT method seems to lead to reliable trends for this test system set and as it was emphasized by the results presented in Table 3.45, the computations for the whole test set were stable. Reaction 12 was also included in the Table 3.47, to emphasize that the trend of a lower experimental performance by using methyl methacrylate as a starting material is also obtained for the reactions in refluxing toluene, but according to the computed results this reaction should also work under these reaction conditions. According to these results the computational method can be used to investigate further iodine catalyzed systems in refluxing toluene for more similar systems, for example the halogene series for reaction 10.

**Table 3.47:** Computed  $\Delta G$  values using the PBE0-D3/COSMO/def2-TZVP method based TPSSH/def2-TZVP optimized structures using the standard state correction in toluene at 70 °C.

	Prod	TS	TS-I <sub>2</sub>	yield	reaction time
R6	-6.52	28.33	26.70	70%	7 h
R9	-6.67	26.92	24.76	85%	7 h
R10	-6.54	29.06	27.76	60%	9 h
R12	-3.45	31.69	29.06		
R13	-11.20	26.71	24.75		
R14	0.02	32.56	31.85	NR	
R15	-6.59	33.51	32.88	NR	

### 3.5.16 Catalyzed and Uncatalyzed Transition States

In the introduction a special problem of the former published computations of the iodine catalysis was mentioned (statement (v)). The catalyzed and uncatalyzed transition states were not in agreement, which means that catalyzed transition states had a higher energy than uncatalyzed ones for other reactions. Therefore this point of the computation was additionally analyzed for all reactions, which were synthesized in dichloromethane at room temperature. All results are presented in Table 3.48.

**Table 3.48:** Free-energy  $\Delta G$  of catalyzed and uncatalyzed transition states using COSMO, D3 and standard state correction for dichloromethane at 25 °C in kcal/mol.

uncatalyzed transition states TS								
	BP86	B3-LYP	BH-LYP	PBE	PBE0	TPSS	TPSSH	M06
R1	17.45	24.12	26.34	18.16	19.66	19.83	20.48	22.74
R2	20.20	27.12	29.77	21.15	22.90	22.58	23.36	25.28
R3	14.18	20.30	22.16	14.77	16.04	16.69	17.20	19.35
R4	17.98	24.63	27.15	18.61	20.40	20.39	21.13	23.46
R5	19.26	24.82	26.51	19.09	20.49	20.86	21.39	24.32
R8	29.64	38.52	43.07	30.90	34.34	32.57	34.03	37.00
R16	18.69	25.72	27.78	20.27	21.29	21.43	21.98	23.14
catalyzed transition states TS-I <sub>2</sub>								
	BP86	B3-LYP	BH-LYP	PBE	PBE0	TPSS	TPSSH	M06
R1	9.82	19.61	24.78	11.69	16.11	12.79	14.83	19.21
R2	<i>11.93</i>	<i>22.56</i>	<i>28.39</i>	14.24	<i>19.14</i>	<i>15.10</i>	<i>17.40</i>	<i>22.00</i>
R3	7.31	16.41	21.15	8.68	12.96	10.13	12.03	17.53
R4	10.19	20.07	25.56	11.89	16.79	13.11	15.31	21.24
R5	11.13	19.82	24.37	11.87	16.19	13.16	15.07	21.04
<b>R8</b>	<b>23.21</b>	<b>34.61</b>	<b>40.66</b>	<b>25.71</b>	<b>30.81</b>	<b>27.00</b>	<b>29.28</b>	<b>34.12</b>
R16	11.44	21.90	26.97	<i>14.41</i>	18.40	14.92	16.90	20.40

The highest catalyzed transition states were determined for reaction 8 and are highlighted in bold. The synthesis of this system results after 3 minutes in a product yield of 76% revealing a good performance of the catalyst. The uncatalyzed transition states of all other iodine catalyzed reactions should show a higher energy compared to the catalyzed transition states. This trend was not obtained for the whole set of reactions for every method. The catalyzed transition state of reaction 8 is always higher compared

to the uncatalyzed transition states of all other systems, which would indicate that all these reactions should have a good performance without using any catalyst. It can be concluded that DFT methods do not have a reliable quality considering a whole mechanism of different molecules or reaction types.

Reaction 8 is the only system where a carbon-carbon bond is established and therefore the height consistency for the catalyzed and uncatalyzed transition state were analyzed without including this reaction. The highest catalyzed transition state is highlighted in *italic* for all systems, where a new nitrogen-carbon bond is synthesized. The highest catalyzed transition state is obtained for reaction 2 for all methods except the PBE functional. This method determines the TS16-I<sub>2</sub> as the highest one for these reactions. Experimentally both systems showed a good performance using iodine as a catalyst. Reaction 2 results in 89% product yield after 25 minutes and 82% in 40 minutes for reaction 16. Dividing the computed reactions chemically reduces the height inconsistencies between catalyzed and uncatalyzed reaction paths significantly. For the BP86 and the TPSS functionals all transition states are in agreement. The PBE functional is in principal also consistent, but the TS16-I<sub>2</sub> free-energy is very close to the uncatalyzed transition state of reaction 3. For the B3-LYP, PBE0, TPSSH and the M06 functionals at least one inconsistency is obtained. All these methods are not in an agreement compared to reaction 3 and in the case of the PBE0 and M06 computations the uncatalyzed transition state TS1 is very close to the highest catalyzed one. Following these results it can be concluded that DFT based computations are only able to determine consistent free-energies for very similar reactions and applications and that the actual determined free-energy heights do not necessarily correspond to the experimental results and insights, especially for different chemical systems. Therefore DFT computations are not an appropriate instrument, which can be applied to unsimilar chemical systems. This also indicates that computed transition state heights and free-energies of intermediates or products should not be compared and interpreted for systems which are chemically too different, based on the same DFT method.

### 3.5.17 Statistically Derived Shifts Based on Experimental Data

Statistical shifts can be derived by a comparison of computational results and experimental data. Therefore the calculations of the benchmark systems were reanalyzed according to the standard deviation (SD) and the determined averaged error of the tested DFT methods. It was shown in the last sections that the PBE0 and the M06 functionals deliver reliable results for all systems compared to the experimental outcomes. In Table 3.49 the standard deviations of all used methods compared to the experimental data of the benchmark set are presented.

The analysis of the standard deviations reveals that the PBE0 functional has the lowest SD and should therefore be able to compute trends with a better quality than the other functionals. The PBE0 functional combined with the def2-TZVP basis set seems to be the best compromise between quality and computation time with a standard deviation of 0.17 kcal/mol. The QZVP basis set delivers a slightly better SD of 0.16 kcal/mol, but using the def2-QZVP basis set increases the computation time for all systems significantly. The M06 functional, which also showed a good performance on all reactions and experimental outcomes, delivers a higher SD and therefore the trends on the effect of the iodine might be less reliable compared to the PBE0 functional. It also emphasizes that the used method of the former published analysis of the iodine catalysis has quite a bad performance with a standard deviation of 0.48 kcal/mol (see Table 3.33) and the trends of the iodine on different systems might be of low quality.

**Table 3.49:** Standard Deviation using COSMO(CCl<sub>4</sub>) and D3 at 25 °C.

Basis	BP86	B3-LYP	BH-LYP	PBE	PBE0	TPSS	TPSSH	M06
SVP	0.69	0.23	0.41	0.63	0.26	0.61	0.42	0.39
SVPD	0.76	0.37	0.44	0.63	0.31	0.68	0.51	0.44
TZVP	0.56	0.29	0.56	0.43	0.17	0.45	0.28	0.42
TZVPP	0.56	0.29	0.56	0.43	0.18	0.45	0.28	0.41
TZVPD	0.58	0.32	0.57	0.43	0.18	0.46	0.30	0.43
QZVP	0.55	0.29	0.56	0.41	0.16	0.44	0.28	0.41

Nevertheless, the more interesting values are the determined averaged errors of all methods, which are shown in the Tables 3.50 and 3.51. The averaged error reveals, if the method over- or underestimates the effect of the iodine in the view of the computed  $\Delta G$  value. In a statistical sense it might be allowed to subtract the averaged error of these methods to derive a good absolute value for the specific application, in this case the  $\Delta\Delta G$  value for all TS-I<sub>2</sub> and TS differences. It can be seen that all functionals result in

higher averaged errors, if larger basis sets are used. Especially the BH-LYP functional shows the highest averaged errors of all methods. According to this, it can be understood why the BH-LYP/QZVP calculation could be used to compute all iodine catalyzed transition states higher than the uncatalyzed ones in Table 3.29. Not using these systematical errors for the application might also be an explanation for the exchange of the electronic energies from the M06-2X functional to the B2-PLYP functional in the former published article. The Table 3.50 also reveals the reason for the good performance of the TPSSH-D3/def2-TZVP/COSMO//TPSSH/def2-TZVP method including standard state correction for the small set of experimental data. The standard state correction was coincidentally very close to the averaged error of this method for the small benchmark set. Therefore in the following section the  $\Delta\Delta G$  values of the catalyzed and uncatalyzed transition states will be analyzed by including the systematical shifts derived from the averaged error of the benchmark set (see Table 3.51).

**Table 3.50:** Averaged error to the experimental results without using standard state correction in kcal/mol.

Basis	BP86	B3-LYP	BH-LYP	PBE	PBE0	TPSS	TPSSH	M06
SVP	-1.19	0.42	1.57	-1.17	0.47	-0.83	-0.12	0.29
SVPD	-0.28	1.52	2.31	-0.10	1.29	0.12	0.68	0.76
TZVP	1.11	2.75	3.64	1.18	2.56	1.46	2.07	2.82
TZVPP	1.11	2.75	3.63	1.18	2.55	1.46	2.07	2.81
TZVPD	1.32	3.01	3.84	1.48	2.77	1.72	2.30	2.95
QZVP	1.43	3.13	3.99	1.57	2.88	1.80	2.39	3.08

**Table 3.51:** Averaged error to the experimental results using standard state correction kcal/mol.

Basis	BP86	B3-LYP	BH-LYP	PBE	PBE0	TPSS	TPSSH	M06
SVP	-3.08	-1.47	-0.32	-3.06	-1.42	-2.72	-2.01	-1.60
SVPD	-2.17	-0.37	0.42	-1.99	-0.60	-1.77	-1.21	-1.13
TZVP	-0.78	0.86	1.75	-0.71	0.67	-0.43	0.18	0.93
TZVPP	-0.78	0.86	1.74	-0.71	0.66	-0.43	0.18	0.92
TZVPD	-0.57	1.12	1.95	-0.41	0.88	-0.17	0.41	1.06
QZVP	-0.46	1.24	2.10	-0.32	0.99	-0.09	0.50	1.19

### 3.5.18 Iodine Catalyzed Transition States including Shifts

For completely unshifted catalyzed transition states the BH-LYP functional is in most of the cases not able to confirm the iodine catalysis. The PBE0 and M06 functionals seemed to be the most robust functionals for all systems under all investigated reaction conditions. Therefore the effect of the experimentally derived shifts is analyzed for these three functionals and presented in Table 3.52. The results show that by including the experimental shift the BH-LYP functional could also be used to confirm the catalytic effect of the iodine for all reactions. According to these results it can be concluded that an experimental benchmark can be used to derive empirical shifts, which can be applied for a specific question. Therefore the exchange of electronic energies by additional single-point calculations seems to be superfluous for the catalytic effect of the iodine on the transition states. The applied standard state correction already includes this kind of shifting. It was shown that shift is necessary for lowering the iodine catalyzed transition states, but in principal the quality of this correction considering all other free-energies can not be analyzed without experimental data. This can be emphasized by the results shown in Table 3.48 and the fact that the determined heights of the PBE0 functional will be comparable to the B3-LYP or the M06 computation, without applying this correction. This can also be shown in the literature by combining two articles[72, 86] from the one author. The same Friedel-Crafts reaction is calculated in both articles and for the uncatalyzed reaction path different  $\Delta G$  values for the TS (34.7 or 37.7 kcal/mol), an intermediate (35.8 or 38.7 kcal/mol) and the resulting product (-9.5 or -8.0 kcal/mol) were published, emphasizing the unsystematic usage of DFT methods and the meaning of the absolute values.

**Table 3.52:** Catalyzed transition states including the experimentally derived shift compared to unshifted values for all reactions in  $\text{CH}_2\text{Cl}_2$  at 25 °C in kcal/mol.

	Unshifted			Shifted		
	BH-LYP	PBE0	M06	BH-LYP	PBE0	M06
R1	0.32	-1.65	-1.65	-3.32	-4.21	-4.47
R2	0.51	-1.87	-1.39	-3.13	-4.43	-4.21
R3	0.88	-1.19	0.07	-2.76	-3.75	-2.75
R4	0.30	-1.72	-0.32	-3.34	-4.28	-3.14
R5	-0.26	-2.41	-1.39	-3.90	-4.97	-4.21
R6	1.32	0.10	0.23	-2.32	-2.46	-2.59
R8	-0.53	-1.63	-0.99	-4.17	-4.19	-3.81
R16	1.08	-1.01	-0.85	-2.56	-3.57	-3.67

### 3.5.19 Conclusions

It was shown how DFT methods can be used to support or confirm organic reaction outcomes, but that the used DFT methods are not able to create a consistent picture for a larger set of synthesized reactions, including opposite experimental outcomes and analyzing the transition state energies in all cases. Computing unsimilar systems with the same functional lead to incorrect results compared to the experiments. Dividing the reactions according to their chemical structure improved the quality of the computed reaction trends and the consistency of all transition state heights. The chemical similarity should be very high in order to derive reliable reaction trends with DFT methods.

The huge variety of available DFT methods resulted in published investigations that can not be combined. According to this the controllability and consistencies between different chemical reactions or systems can not be detected. Therefore more systematic quantum chemical articles and benchmarks (exactly same geometry optimizations, functionals, basis sets, additional corrections) based on reliable experiments, e.g. reactions with 0%-100% yield (same solvent, temperature, reaction time) and experimental data from kinetic studies are needed to investigate the controllability and reliability of these methods, especially for the same research field.



# A Appendix

## A.1 Electronic Structure of 4f Element Compounds

**Table A.1:** CASSCF(6,10) for  $\text{Cp}_2\text{CeCH}_2$  in  $C_{2v}$  symmetry. CI coefficients of leading determinants for NO basis.

$a_1$	$b_1$	$b_2$	$a_2$	coeff
200	200	200	0	0.7514869
200	200	020	0	-0.6396642
020	200	200	0	-0.0680978
020	200	020	0	0.0604783

**Table A.2:** CASSCF(6,10) for  $\text{Cp}_2\text{CeCH}_2$  in  $C_{2v}$  symmetry. NO occupation numbers (orbital.irrep).

	$a_1$		$b_1$		$b_2$		$a_2$
20.1	1.97135	15.2	1.98716	11.3	1.15408	9.4	0.00317
21.1	0.02740	16.2	0.00342	12.3	0.83844		
22.1	0.00531	17.2	0.00124	13.3	0.00843		

**Table A.3:** CASSCF(6,10) for  $\text{Cp}_2\text{CeCH}^-$  in  $C_{2v}$  symmetry. CI coefficients of leading determinants for NO basis.

a <sub>1</sub>	b <sub>1</sub>	b <sub>2</sub>	a <sub>2</sub>	coeff
200	200	200	0	0.7862187
200	020	200	0	-0.5517574
200	200	020	0	-0.1245526
200	020	020	0	0.0949267
200	aa0	bb0	0	0.0514140
200	bb0	aa0	0	0.0514140

**Table A.4:** CASSCF(6,10) for  $\text{Cp}_2\text{CeCH}^-$  in  $C_{2v}$  symmetry. NO occupation numbers (orbital.irrep).

	a <sub>1</sub>		b <sub>1</sub>		b <sub>2</sub>		a <sub>2</sub>
20.1	1.95995	15.2	1.32126	11.3	1.91055	9.4	0.00180
21.1	0.02907	16.2	0.66771	12.3	0.08164		
22.1	0.00870	17.2	0.01322	13.3	0.00611		

**Table A.5:** CASSCF(6,10) for  $\text{Cp}_2\text{CeNH}$  in  $C_{2v}$  symmetry. CI coefficients of leading determinants for NO basis.

a <sub>1</sub>	b <sub>1</sub>	b <sub>2</sub>	a <sub>2</sub>	coeff
200	200	200	0	0.9523693
200	020	200	0	-0.1227568
200	200	020	0	-0.1102006
200	ba0	ab0	0	-0.0864004
200	ab0	ba0	0	-0.0864004
200	ba0	ba0	0	0.0680148
200	ab0	ab0	0	0.0680148
ba0	ab0	200	0	-0.0525487
ab0	ba0	200	0	-0.0525487
ab0	200	ba0	0	0.0502159
ba0	200	ab0	0	0.0502159

**Table A.6:** CASSCF(6,10) for  $\text{Cp}_2\text{CeNH}$  in  $C_{2v}$  symmetry. NO occupation numbers (orbital.irrep).

	a <sub>1</sub>		b <sub>1</sub>		b <sub>2</sub>		a <sub>2</sub>
20.1	1.96435	15.2	1.91562	11.3	1.92384	9.4	0.00050
21.1	0.02719	16.2	0.07556	12.3	0.06765		
22.1	0.00920	17.2	0.00814	13.3	0.00794		

**Table A.7:** CASSCF(6,10) for  $\text{Cp}_2\text{CeO}$  in  $C_{2v}$  symmetry. CI coefficients of leading determinants for NO basis.

	a <sub>1</sub>	b <sub>1</sub>	b <sub>2</sub>	a <sub>2</sub>	coeff
200	200	200	0	0	0.9550371
020	200	200	0	0	-0.0966726
200	200	020	0	0	-0.0895051
200	020	200	0	0	-0.0890121
ba0	ab0	200	0	0	-0.0686933
ab0	ba0	200	0	0	-0.0686933
ab0	200	ba0	0	0	0.0674860
ba0	200	ab0	0	0	0.0674860
200	ba0	ab0	0	0	-0.0641647
200	ab0	ba0	0	0	-0.0641647
ab0	ab0	200	0	0	0.0572398
ba0	ba0	200	0	0	0.0572398
ab0	200	ab0	0	0	-0.0559458
ba0	200	ba0	0	0	-0.0559458

**Table A.8:** CASSCF(6,10) for  $\text{Cp}_2\text{CeO}$  in  $C_{2v}$  symmetry. NO occupation numbers (orbital.irrep).

	a <sub>1</sub>		b <sub>1</sub>		b <sub>2</sub>		a <sub>2</sub>
20.1	1.93385	15.2	1.93953	11.3	1.94062	9.4	0.00028
21.1	0.06083	16.2	0.05443	12.3	0.05370		
22.1	0.00513	17.2	0.00597	13.3	0.00566		

**Table A.9:** CASSCF(6,10) for  $\text{Cp}_2\text{CeF}^+$  in  $\text{C}_{2v}$  symmetry. CI coefficients of leading determinants for NO basis.

a <sub>1</sub>	b <sub>1</sub>	b <sub>2</sub>	a <sub>2</sub>	coeff
200	200	200	0	0.9645844
000	200	200	2	-0.0651703
200	000	200	2	-0.0633498
b00	a00	2a0	b	0.0624602
a00	b00	2b0	a	0.0624602
000	200	220	0	-0.0584396
b00	a00	2b0	a	-0.0582289
a00	b00	2a0	b	-0.0582289
200	020	200	0	-0.0564037
200	000	220	0	-0.0527667
200	200	002	0	-0.0510344

**Table A.10:** CASSCF(6,10) for  $\text{Cp}_2\text{CeF}^+$  in  $\text{C}_{2v}$  symmetry. NO occupation numbers (orbital.irrep).

a <sub>1</sub>		b <sub>1</sub>		b <sub>2</sub>		a <sub>2</sub>	
20.1	1.94844	15.2	1.94323	11.3	1.96512	9.4	0.04140
21.1	0.01296	16.2	0.02555	12.3	0.03859		
22.1	0.00624	17.2	0.00556	13.3	0.01292		

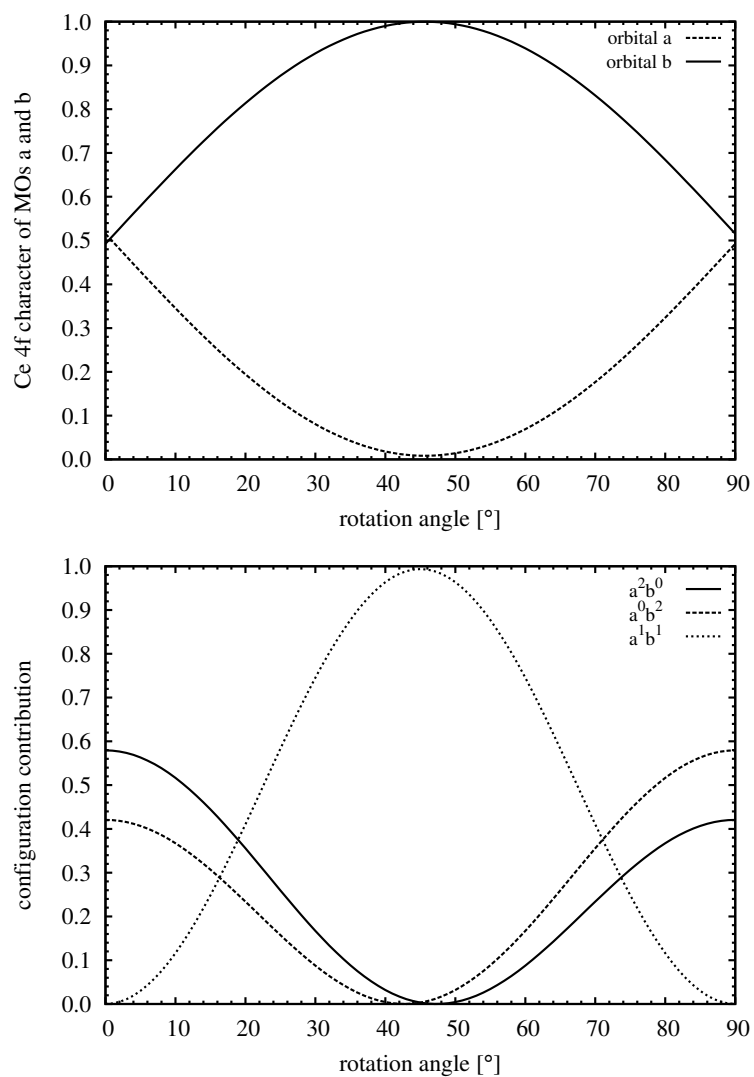


**Figure A.1:** As Figure 3.13 but for a CASSCF(2,2) optimized geometry.

## A.2 Experimental Benchmark

**Table A.11:** Error compared to the experimental results in kcal/mol. SVP basis set was applied without using standard state correction.

	BP86	B3-LYP	BH-LYP	PBE	PBE0	TPSS	TPSSH	M06
Acetone	-3.78	-1.77	-0.44	-3.80	-1.87	-3.31	-2.49	-2.14
Acetophenone	-3.32	-1.39	-0.01	-3.33	-1.38	-2.95	-2.12	-1.49
Benzophenone	-3.44	-1.64	-0.30	-2.98	-1.34	-2.89	-2.14	-1.63
Benzaldehyde	-2.84	-1.18	0.09	-3.12	-1.22	-2.77	-1.95	-1.06
Methyl Acrylate	-2.00	-1.37	-0.95	-2.08	-1.28	-1.69	-1.34	-1.66

**Table A.12:** Error compared to the experimental results in kcal/mol. SVPD basis set was applied without using standard state correction.

	BP86	B3-LYP	BH-LYP	PBE	PBE0	TPSS	TPSSH	M06
Acetone	-2.43	-0.28	0.63	-2.27	-0.82	-1.94	-1.30	-1.31
Acetophenone	-2.51	-0.35	0.68	-2.33	-0.78	-2.08	-1.40	-1.05
Benzophenone	-3.02	-1.00	0.03	-2.43	-1.13	-2.46	-1.84	-1.61
Benzaldehyde	-1.86	-0.03	0.87	-1.99	-0.50	-1.73	-1.07	-0.43
Methyl Acrylate	-1.03	-0.22	-0.14	-0.90	-0.51	-0.66	-0.46	-1.23

**Table A.13:** Error compared to the experimental results in kcal/mol. TZVP basis set was applied without using standard state correction.

	BP86	B3-LYP	BH-LYP	PBE	PBE0	TPSS	TPSSH	M06
Acetone	0.81	2.80	3.83	0.84	2.45	1.22	1.92	2.68
Acetophenone	0.96	2.94	4.07	1.01	2.69	1.31	2.05	3.00
Benzophenone	0.48	2.35	3.48	0.99	2.42	1.05	1.72	2.61
Benzaldehyde	1.40	3.08	4.08	1.16	2.80	1.49	2.21	3.44
Methyl Acrylate	1.91	2.59	2.74	1.92	2.43	2.21	2.46	2.35

**Table A.14:** Error compared to the experimental results in kcal/mol. TZVPP basis set was applied without using standard state correction.

	BP86	B3-LYP	BH-LYP	PBE	PBE0	TPSS	TPSSH	M06
Acetone	0.80	2.78	3.81	0.82	2.44	1.21	1.91	2.66
Acetophenone	0.94	2.93	4.05	0.99	2.67	1.29	2.03	2.99
Benzophenone	0.48	2.35	3.47	0.99	2.42	1.05	1.72	2.60
Benzaldehyde	1.41	3.09	4.09	1.17	2.80	1.51	2.22	3.43
Methyl Acrylate	1.91	2.59	2.74	1.92	2.43	2.21	2.46	2.36

**Table A.15:** Error compared to the experimental results in kcal/mol. TZVPD basis set was applied without using standard state correction.

	BP86	B3-LYP	BH-LYP	PBE	PBE0	TPSS	TPSSH	M06
Acetone	1.10	3.14	4.10	1.22	2.74	1.57	2.24	2.86
Acetophenone	1.14	3.19	4.26	1.28	2.89	1.56	2.26	3.14
Benzophenone	0.61	2.54	3.63	1.20	2.57	1.24	1.88	2.67
Benzaldehyde	1.62	3.34	4.29	1.45	3.02	1.76	2.44	3.59
Methyl Acrylate	2.13	2.85	2.94	2.22	2.64	2.48	2.70	2.49

**Table A.16:** Error compared to the experimental results in kcal/mol. QZVP basis set was applied without using standard state correction.

	BP86	B3-LYP	BH-LYP	PBE	PBE0	TPSS	TPSSH	M06
Acetone	1.18	3.22	4.21	1.28	2.82	1.62	2.29	2.95
Acetophenone	1.26	3.31	4.41	1.38	3.00	1.64	2.35	3.29
Benzophenone	0.79	2.72	3.83	1.36	2.74	1.37	2.02	2.88
Benzaldehyde	1.70	3.44	4.42	1.53	3.11	1.82	2.51	3.69
Methyl Acrylate	2.22	2.95	3.08	2.29	2.75	2.54	2.77	2.62

**Table A.17:** Maximal signed error to the experimental results without using standard state correction.

Basis	BP86	B3-LYP	BH-LYP	PBE	PBE0	TPSS	TPSSH	M06
TZVP	0.48	3.08	4.08	0.84	2.80	1.05	2.46	3.44
TZVPP	0.48	3.09	4.09	0.99	2.80	1.05	2.46	3.43
TZVPD	0.61	3.34	4.29	1.20	3.02	1.24	2.70	3.59
QZVP	0.79	3.44	4.42	1.28	3.11	2.54	2.77	3.69

**Table A.18:** Averaged error to the experimental results without using standard state correction.

Basis	BP86	B3-LYP	BH-LYP	PBE	PBE0	TPSS	TPSSH	M06
TZVP	1.11	2.75	3.64	1.18	2.56	1.46	2.07	2.82
TZVPP	1.11	2.75	3.63	1.18	2.55	1.46	2.07	2.81
TZVPD	1.32	3.01	3.84	1.48	2.77	1.72	2.30	2.95
QZVP	1.43	3.13	3.99	1.57	2.88	1.80	2.39	3.08

**Table A.19:** Error compared to the experimental results in kcal/mol. SVP basis set was applied without using standard state correction.

	BP86	B3-LYP	BH-LYP	PBE	PBE0	TPSS	TPSSH	M06
Acetone	-1.89	0.12	1.45	-1.91	0.02	-1.42	-0.60	-0.25
Acetophenone	-1.43	0.50	1.88	-1.44	0.51	-1.06	-0.23	0.40
Benzophenone	-1.55	0.25	1.59	-1.09	0.55	-1.00	-0.25	0.26
Benzaldehyde	-0.95	0.71	1.98	-1.23	0.67	-0.88	-0.06	0.83
Methyl Acrylate	-0.11	0.52	0.94	-0.19	0.61	0.20	0.55	0.23

**Table A.20:** Error compared to the experimental results in kcal/mol. SVPD basis set was applied without using standard state correction.

	BP86	B3-LYP	BH-LYP	PBE	PBE0	TPSS	TPSSH	M06
Acetone	-0.54	1.61	2.52	-0.38	1.07	-0.05	0.59	0.58
Acetophenone	-0.62	1.54	2.57	-0.44	1.11	-0.19	0.49	0.84
Benzophenone	-1.13	0.89	1.92	-0.54	0.76	-0.57	0.05	0.28
Benzaldehyde	0.03	1.86	2.76	-0.10	1.39	0.16	0.82	1.46
Methyl Acrylate	0.86	1.67	1.75	0.99	1.38	1.23	1.43	0.66

**Table A.21:** Error compared to the experimental results in kcal/mol. TZVP basis set was applied with using standard state correction.

	BP86	B3-LYP	BH-LYP	PBE	PBE0	TPSS	TPSSH	M06
Acetone	-1.08	0.91	1.94	-1.05	0.56	-0.67	0.03	0.79
Acetophenone	-0.93	1.05	2.18	-0.88	0.80	-0.58	0.16	1.11
Benzophenone	-1.41	0.46	1.59	-0.90	0.53	-0.84	-0.17	0.72
Benzaldehyde	-0.49	1.19	2.19	-0.73	0.91	-0.40	0.32	1.55
Methyl Acrylate	0.02	0.70	0.85	0.03	0.54	0.32	0.57	0.46



**Table A.22:** Error compared to the experimental results in kcal/mol. TZVPP basis set was applied with using standard state correction.

	BP86	B3-LYP	BH-LYP	PBE	PBE0	TPSS	TPSSH	M06
Acetone	-1.09	0.89	1.92	-1.07	0.55	-0.68	0.02	0.77
Acetophenone	-0.95	1.04	2.16	-0.90	0.78	-0.60	0.14	1.10
Benzophenone	-1.41	0.46	1.58	-0.90	0.53	-0.84	-0.17	0.71
Benzaldehyde	-0.48	1.20	2.20	-0.72	0.91	-0.38	0.33	1.54
Methyl Acrylate	0.02	0.70	0.85	0.03	0.54	0.32	0.57	0.47

**Table A.23:** Error compared to the experimental results in kcal/mol. TZVPD basis set was applied with using standard state correction.

	BP86	B3-LYP	BH-LYP	PBE	PBE0	TPSS	TPSSH	M06
Acetone	-0.79	1.25	2.21	-0.67	0.85	-0.32	0.35	0.97
Acetophenone	-0.75	1.30	2.37	-0.61	1.00	-0.33	0.37	1.25
Benzophenone	-1.28	0.65	1.74	-0.69	0.68	-0.65	-0.01	0.78
Benzaldehyde	-0.27	1.45	2.40	-0.44	1.13	-0.13	0.55	1.70
Methyl Acrylate	0.24	0.96	1.05	0.33	0.75	0.59	0.81	0.60

**Table A.24:** Error compared to the experimental results in kcal/mol. QZVP basis set was applied with using standard state correction.

	BP86	B3-LYP	BH-LYP	PBE	PBE0	TPSS	TPSSH	M06
Acetone	-0.71	1.33	2.32	-0.61	0.93	-0.27	0.40	1.06
Acetophenone	-0.63	1.42	2.52	-0.51	1.11	-0.25	0.46	1.40
Benzophenone	-1.10	0.83	1.94	-0.53	0.85	-0.52	0.13	0.99
Benzaldehyde	-0.19	1.55	2.53	-0.36	1.22	-0.07	0.62	1.80
Methyl Acrylate	0.33	1.06	1.19	0.40	0.86	0.65	0.88	0.73

**Table A.25:** Averaged error compared to the experimental results with using standard state correction in kcal/mol.

Basis	BP86	B3-LYP	BH-LYP	PBE	PBE0	TPSS	TPSSH	M06
TZVP	-0.78	0.86	1.75	-0.71	0.67	-0.43	0.18	0.93
TZVPP	-0.78	4.28	8.71	-3.57	3.31	-2.17	0.89	4.58
TZVPD	-0.57	1.12	1.95	-0.41	0.88	-0.17	0.41	1.06
QZVP	-0.46	1.24	2.10	-0.32	0.99	-0.09	0.50	1.19

## A.3 Reaction Energies of the Iodine Catalysis

### A.3.1 Dichlormethane at 25 °C

**Table A.26:**  $\Delta G$  (TS-I<sub>2</sub>)-TS without standard state shift in CH<sub>2</sub>Cl<sub>2</sub> at 298.15 K in kcal/mol. \*: Optimized using the m5 grid.

	BP86	B3-LYP	BH-LYP	PBE	PBE0	TPSS	TPSSH	M06
R1*	-5.74	-2.63	0.32	-4.59	-1.65	-5.15	-3.76	-1.65
R2	-6.38	-2.66	0.51	-5.02	-1.87	-5.59	-4.08	-1.39
R3	-4.99	-2.00	0.88	-4.19	-1.19	-4.67	-3.28	0.07
R4	-5.90	-2.67	0.30	-4.84	-1.72	-5.39	-3.93	-0.32
R5	-6.24	-3.12	-0.26	-5.34	-2.41	-5.80	-4.43	-1.39
R6	-3.71	-1.29	1.32	-2.69	0.10	-3.56	-2.21	0.23
R7	-6.26	-2.37	1.23	-6.02	-2.10	-6.47	-4.76	-0.46
R8	-4.54	-2.03	-0.53	-3.30	-1.63	-3.68	-2.86	-0.99
R9	-4.05	-1.46	1.27	-3.06	-0.12	-3.85	-2.44	0.25
R10	-3.39	-1.01	1.44	-2.32	0.31	-3.15	-1.87	0.48
R11	-5.91	-2.41	0.76	-4.74	-1.54	-5.30	-3.79	-0.28
R12	-5.40	-2.67	0.15	-4.22	-1.21	-5.18	-3.72	-0.86
R13	-3.94	-1.39	1.29	-2.92	-0.04	-3.71	-2.33	0.33
R14	-2.47	-0.81	0.70	-1.34	0.18	-2.40	-1.58	-0.32
R15	-2.38	-0.63	1.09	-1.21	0.60	-2.42	-1.48	-0.18
R16	-5.37	-1.93	1.08	-3.97	-1.01	-4.62	-3.19	-0.85
R17	-5.98	-2.06	1.56	-5.75	-1.81	-6.18	-4.46	-0.33
R18	-7.16	-3.16	0.48	-6.92	-2.95	-7.37	-5.64	-1.14

**Table A.27:**  $\Delta G$  TS-I<sub>2</sub> without standard state shift in CH<sub>2</sub>Cl<sub>2</sub> at 298.15 K in kcal/mol.

	BP86	B3-LYP	BH-LYP	PBE	PBE0	TPSS	TPSSH	M06
R1	13.60	23.39	28.56	15.47	19.89	16.57	18.61	22.99
R2	15.71	26.34	32.17	18.02	22.92	18.88	21.18	25.78
R3	11.09	20.19	24.93	12.46	16.74	13.91	15.81	21.31
R4	13.97	23.85	29.34	15.67	20.57	16.89	19.09	25.02
R5	14.91	23.60	28.15	15.65	19.97	16.94	18.85	24.82
R6	23.81	32.04	35.59	24.86	28.16	25.94	27.49	32.55
R7	24.34	31.84	35.34	25.02	28.05	25.39	26.78	33.04
R8	26.99	38.39	44.44	29.49	24.59	30.78	33.06	37.90
R9	21.74	30.16	34.08	22.76	26.51	23.87	25.60	31.00
R10	24.84	33.23	36.75	25.94	29.21	27.20	28.72	33.82
R11	16.59	26.09	31.40	17.53	22.46	18.68	20.87	27.55
R12	25.21	34.33	38.82	26.42	30.54	27.38	29.29	35.17
R13	21.66	30.03	33.91	22.72	26.42	23.81	25.52	30.95
R14	30.02	38.23	40.71	31.10	33.26	32.47	33.54	38.12
R15	31.14	39.80	42.45	32.40	34.79	33.74	34.93	39.95
R16	15.22	25.68	30.75	18.19	22.18	18.70	20.68	24.18
R17	24.57	32.02	35.40	25.23	28.13	25.64	26.98	33.02
R18	23.70	31.03	34.31	24.36	27.16	24.73	26.02	32.15

**Table A.28:**  $\Delta G$  TS without standard state shift in  $\text{CH}_2\text{Cl}_2$  at 298.15 K in kcal/mol.

	BP86	B3-LYP	BH-LYP	PBE	PBE0	TPSS	TPSSH	M06
R1	19.34	26.01	28.23	20.05	21.55	21.72	22.37	24.63
R2	22.09	29.01	31.66	23.04	24.79	24.47	25.25	27.17
R3	16.07	22.19	24.05	16.66	17.93	18.58	19.09	21.24
R4	19.87	26.52	29.04	20.50	22.29	22.28	23.02	25.35
R5	21.15	26.71	28.40	20.98	22.38	22.75	23.28	26.21
R6	27.52	33.33	34.27	27.56	28.06	29.50	29.70	32.32
R7	30.60	34.21	34.11	31.04	30.15	31.85	31.54	33.50
R8	31.53	40.41	44.96	32.79	36.23	34.46	35.92	38.89
R9	25.79	31.62	32.81	25.83	26.63	27.73	28.04	30.75
R10	28.24	34.24	35.31	28.25	28.90	30.36	30.60	33.33
R11	22.50	28.50	30.63	22.28	24.00	23.99	24.66	27.83
R12	30.61	37.00	38.67	30.64	31.75	32.56	33.01	36.03
R13	25.60	31.42	32.62	25.64	26.45	27.53	27.85	30.61
R14	32.49	39.04	40.01	32.44	33.09	34.86	35.12	38.44
R15	33.53	40.43	41.35	33.60	34.19	36.16	36.41	40.12
R16	20.58	27.61	29.67	22.16	23.18	23.32	23.87	25.03
R17	30.55	34.07	33.83	30.98	29.94	31.82	31.45	33.34
R18	30.85	34.19	33.83	31.28	30.11	32.10	31.67	33.30

**Table A.29:**  $\Delta G$  products without standard state shift in  $\text{CH}_2\text{Cl}_2$  at 298.15 K in kcal/mol.

	BP86	B3-LYP	BH-LYP	PBE	PBE0	TPSS	TPSSH	M06
R1	-1.54	1.31	-1.58	-1.91	-4.78	-0.21	-1.39	-4.07
R2	0.85	3.88	1.39	0.91	-1.73	2.22	1.18	-1.52
R3	-6.59	-4.16	-7.23	-6.83	-9.90	-4.98	-6.25	-9.20
R4	-3.41	-1.10	-4.12	-3.31	-6.39	-1.78	-3.01	-5.72
R5	-1.89	0.21	-3.04	-2.64	-5.73	-0.85	-2.15	-4.55
R6	-1.60	0.68	-2.41	-2.15	-5.16	-0.54	-1.78	-3.31
R7	-5.37	-4.54	-8.74	-5.43	-9.87	-4.64	-6.38	-8.00
R8	-5.76	-2.68	-5.31	-5.16	-8.41	-2.74	-4.08	-7.67
R9	-1.69	0.57	-2.55	-2.24	-5.28	-0.62	-1.86	-3.52
R10	-1.61	0.65	-2.43	-2.16	-5.17	-0.56	-1.79	-3.29
R11	1.22	3.23	0.07	0.77	-2.28	2.13	0.90	-1.04
R12	0.96	3.24	0.37	0.81	-2.10	2.00	0.86	-0.52
R13	-1.56	0.72	-2.39	-2.12	-5.14	-0.50	-1.74	-3.32
R14	-2.04	0.28	-2.69	-2.57	-5.47	-1.00	-2.18	-3.50
R15	-1.75	0.82	-1.90	-2.20	-4.93	-0.68	-1.79	-2.71
R16	1.60	4.87	2.07	1.98	-1.09	3.14	1.99	-1.08
R17	-5.25	-4.56	-8.88	-5.29	-9.86	-4.56	-6.35	-7.99
R18	-4.25	-3.72	-8.11	-4.31	-8.99	-3.54	-5.39	-7.22

**Table A.30:**  $\Delta G$  (TS-I<sub>2</sub>)-TS with standard state shift in CH<sub>2</sub>Cl<sub>2</sub> at 298.15 K in kcal/mol. \*: Optimized using the m5 grid.

	BP86	B3-LYP	BH-LYP	PBE	PBE0	TPSS	TPSSH	M06
R1*	-7.63	-4.52	-1.57	-6.48	-3.54	-7.04	-5.65	-3.54
R2	-8.27	-4.55	-1.38	-6.91	-3.76	-7.48	-5.97	-3.28
R3	-6.88	-3.89	-1.01	-6.08	-3.08	-6.56	-5.17	-1.82
R4	-7.79	-4.56	-1.59	-6.73	-3.61	-7.28	-5.82	-2.21
R5	-8.13	-5.01	-2.15	-7.23	-4.30	-7.69	-6.32	-3.28
R6	-5.60	-3.18	-0.57	-4.58	-1.79	-5.45	-4.10	-1.66
R7	-8.15	-4.26	-0.66	-7.91	-3.99	-8.36	-6.65	-2.35
R8	-6.43	-3.92	-2.42	-5.19	-3.52	-5.57	-4.75	-2.88
R9	-5.94	-3.35	-0.62	-4.95	-2.01	-5.74	-4.33	-1.64
R10	-5.28	-2.90	-0.45	-4.21	-1.58	-5.04	-3.76	-1.41
R11	-7.80	-4.30	-1.13	-6.63	-3.43	-7.19	-5.68	-2.17
R12	-7.29	-4.56	-1.74	-6.11	-3.10	-7.07	-5.61	-2.75
R13	-5.83	-3.28	-0.60	-4.81	-1.93	-5.60	-4.22	-1.56
R14	-4.36	-2.70	-1.19	-3.23	-1.71	-4.29	-3.47	-2.21
R15	-4.27	-2.52	-0.80	-3.10	-1.29	-4.31	-3.37	-2.07
R16	-7.26	-3.82	-0.81	-5.86	-2.90	-6.51	-5.08	-2.74
R17	-7.87	-3.95	-0.33	-7.64	-3.70	-8.07	-6.35	-2.22
R18	-9.05	-5.05	-1.41	-8.81	-4.84	-9.26	-7.53	-3.03

**Table A.31:**  $\Delta G$  TS-I<sub>2</sub> with standard state shift in CH<sub>2</sub>Cl<sub>2</sub> at 298.15 K in kcal/mol.

	BP86	B3-LYP	BH-LYP	PBE	PBE0	TPSS	TPSSH	M06
R1	9.82	19.61	24.78	11.69	16.11	12.79	14.83	19.21
R2	11.93	22.56	28.39	14.24	19.14	15.10	17.40	22.00
R3	7.31	16.41	21.15	8.68	12.96	10.13	12.03	17.53
R4	10.19	20.07	25.56	11.89	16.79	13.11	15.31	21.24
R5	11.13	19.82	24.37	11.87	16.19	13.16	15.07	21.04
R6	20.03	28.26	31.81	21.08	24.38	22.16	23.71	28.77
R7	22.45	29.95	33.45	23.13	26.16	23.50	24.89	31.15
R8	23.21	34.61	40.66	25.71	30.81	27.00	29.28	34.12
R9	17.96	26.38	30.30	18.98	22.73	20.09	21.82	27.22
R10	21.06	29.45	32.97	22.16	25.43	23.42	24.94	30.04
R11	12.81	22.31	27.62	13.75	18.68	14.90	17.09	23.77
R12	21.43	30.55	35.04	22.64	26.76	23.60	25.51	31.39
R13	17.88	26.25	30.13	18.94	22.64	20.03	21.74	27.17
R14	26.24	34.45	36.93	27.32	29.48	28.69	29.76	34.34
R15	27.36	36.02	38.67	28.62	31.01	29.96	31.15	36.17
R16	11.44	21.90	26.97	14.41	18.40	14.92	16.90	20.40
R17	22.68	30.13	33.51	23.34	26.24	23.75	25.09	31.13
R18	21.81	29.14	32.42	22.47	25.27	22.84	24.13	30.26

**Table A.32:**  $\Delta G$  TS with standard state shift in  $\text{CH}_2\text{Cl}_2$  at 298.15 K in kcal/mol.

	BP86	B3-LYP	BH-LYP	PBE	PBE0	TPSS	TPSSH	M06
R1	17.45	24.12	26.34	18.16	19.66	19.83	20.48	22.74
R2	20.20	27.12	29.77	21.15	22.90	22.58	23.36	25.28
R3	14.18	20.30	22.16	14.77	16.04	16.69	17.20	19.35
R4	17.98	24.63	27.15	18.61	20.40	20.39	21.13	23.46
R5	19.26	24.82	26.51	19.09	20.49	20.86	21.39	24.32
R6	25.63	31.44	32.38	25.67	26.17	27.61	27.81	30.43
R7	30.60	34.21	34.11	31.04	30.15	31.85	31.54	33.50
R8	29.64	38.52	43.07	30.90	34.34	32.57	34.03	37.00
R9	23.90	29.73	30.92	23.94	24.74	25.84	26.15	28.86
R10	26.35	32.35	33.42	26.36	27.01	28.47	28.71	31.44
R11	20.61	26.61	28.74	20.39	22.11	22.10	22.77	25.94
R12	28.72	35.11	36.78	28.75	29.86	30.67	31.12	34.14
R13	23.71	29.53	30.73	23.75	24.56	25.64	25.96	28.72
R14	30.60	37.15	38.12	30.55	31.20	32.97	33.23	36.55
R15	31.64	38.54	39.46	31.71	32.30	34.27	34.52	38.23
R16	18.69	25.72	27.78	20.27	21.29	21.43	21.98	23.14
R17	30.55	34.07	33.83	30.98	29.94	31.82	31.45	33.34
R18	30.85	34.19	33.83	31.28	30.11	32.10	31.67	33.30



**Table A.33:**  $\Delta G$  products with standard state shift in  $\text{CH}_2\text{Cl}_2$  at 298.15 K in kcal/mol.

	BP86	B3-LYP	BH-LYP	PBE	PBE0	TPSS	TPSSH	M06
R1	-3.43	-0.58	-3.47	-3.80	-6.67	-2.10	-3.28	-5.96
R2	-1.04	1.99	-0.50	-0.98	-3.62	0.33	-0.71	-3.41
R3	-8.48	-6.05	-9.12	-8.72	-11.79	-6.87	-8.14	-11.09
R4	-5.30	-2.99	-6.01	-5.20	-8.28	-3.67	-4.90	-7.61
R5	-3.78	-1.68	-4.93	-4.53	-7.62	-2.74	-4.04	-6.44
R6	-3.49	-1.21	-4.30	-4.04	-7.05	-2.43	-3.67	-5.20
R7	-5.37	-4.54	-8.74	-5.43	-9.87	-4.64	-6.38	-8.00
R8	-7.65	-4.57	-7.20	-7.05	-10.30	-4.63	-5.97	-9.56
R9	-3.58	-1.32	-4.44	-4.13	-7.17	-2.51	-3.75	-5.41
R10	-3.50	-1.24	-4.32	-4.05	-7.06	-2.45	-3.68	-5.18
R11	-0.67	1.34	-1.82	-1.12	-4.17	0.24	-0.99	-2.93
R12	-0.93	1.35	-1.52	-1.08	-3.99	0.11	-1.03	-2.41
R13	-3.45	-1.17	-4.28	-4.01	-7.03	-2.39	-3.63	-5.21
R14	-3.93	-1.61	-4.58	-4.46	-7.36	-2.89	-4.07	-5.39
R15	-3.64	-1.07	-3.79	-4.09	-6.82	-2.57	-3.68	-4.60
R16	-0.29	2.98	0.18	0.09	-2.98	1.25	0.10	-2.97
R1	-5.25	-4.56	-8.88	-5.29	-9.86	-4.56	-6.35	-7.99
R1	-4.25	-3.72	-8.11	-4.31	-8.99	-3.54	-5.39	-7.22

**A.3.2 Toluene at 70 °C****Table A.34:**  $\Delta G$  (TS-I<sub>2</sub>)-TS without standard state shift in toluene at 343.15 K in kcal/mol. \*: Optimized using the m5 grid.

	BP86	B3-LYP	BH-LYP	PBE	PBE0	TPSS	TPSSH	M06
R1*	-5.34	-2.39	0.39	-4.20	-1.46	-4.75	-3.45	-1.57
R2	-5.49	-2.01	1.09	-4.14	-1.11	-4.73	-3.28	-0.83
R3	-5.01	-2.21	0.48	-4.23	-1.43	-4.70	-3.40	-0.27
R4	-5.34	-2.37	0.37	-4.29	-1.46	-4.85	-3.52	-0.21
R5	-5.95	-2.98	-0.29	-5.06	-2.32	-5.51	-4.22	-1.43
R6	-2.85	-0.80	1.50	-1.84	0.55	-2.71	-1.54	0.54
R7	-5.63	-2.25	0.84	-5.37	-1.97	-5.83	-4.35	-0.53
R8	-3.57	-1.25	0.01	-2.35	-0.91	-2.68	-1.97	-0.43
R9	-3.49	-1.29	1.13	-2.52	0.02	-3.31	-2.09	0.27
R10	-2.42	-0.40	1.76	-1.36	0.88	-2.19	-1.09	0.91
R11	-4.92	-1.64	1.31	-3.77	-0.83	-4.31	-2.92	0.24
R12	-4.12	-1.86	5.86	-2.96	-0.44	-3.92	-2.69	4.43
R13	-3.28	-1.11	1.27	-2.27	0.22	-3.08	-1.87	0.46
R14	-0.81	0.53	1.75	0.30	1.47	-0.73	-0.08	0.83
R15	-1.07	0.37	1.84	0.09	1.54	-1.11	-0.34	0.66
R16	-4.87	-1.60	1.24	-3.48	-0.72	-4.12	-2.79	-0.66
R17	-5.29	-1.87	1.24	-5.04	-1.61	-5.47	-3.98	-0.33
R18	-6.57	-3.07	0.06	-6.31	-2.84	-6.78	-5.26	-1.25

**Table A.35:**  $\Delta G$  TS without standard state shift in toluene at 343.15 K in kcal/mol.

	BP86	B3-LYP	BH-LYP	PBE	PBE0	TPSS	TPSSH	M06
R1	22.07	28.84	31.15	22.79	24.38	24.50	25.19	27.42
R2	24.69	31.72	34.32	25.63	27.35	27.14	27.91	29.72
R3	19.19	25.43	27.39	19.78	21.17	21.76	22.31	24.41
R4	22.71	29.48	32.11	23.35	25.25	25.18	25.97	28.24
R5	24.13	29.77	31.55	23.96	25.48	25.77	26.35	29.29
R6	29.79	35.82	36.88	29.82	30.51	31.86	32.13	34.88
R7	36.54	40.64	40.99	36.92	36.55	37.86	37.76	39.91
R8	32.67	41.64	46.30	33.92	37.45	35.64	37.14	40.25
R9	28.14	34.13	35.40	28.16	29.10	30.14	30.51	33.32
R10	30.39	36.63	37.83	30.39	31.24	32.59	32.91	35.78
R11	25.01	31.11	33.34	24.79	26.64	26.55	27.27	30.45
R12	32.56	39.17	35.66	32.56	33.87	34.59	35.12	33.52
R13	27.91	33.90	35.18	27.93	28.89	29.91	30.28	33.15
R14	33.78	40.71	41.96	33.73	34.74	36.25	36.66	40.21
R15	34.68	41.95	43.08	34.75	35.69	37.41	37.81	41.75
R16	23.61	30.73	32.87	25.19	26.31	26.39	26.98	28.10
R17	36.64	40.66	40.88	37.00	36.49	37.98	37.81	39.89
R18	36.71	40.56	40.67	37.08	36.44	38.03	37.81	39.66

**Table A.36:**  $\Delta G$  products without standard state shift in toluene at 343.15 K.

	BP86	B3-LYP	BH-LYP	PBE	PBE0	TPSS	TPSSH	M06
R1	-0.72	2.12	-0.85	-1.08	-4.02	0.61	-0.60	-3.25
R2	1.63	4.66	2.09	1.69	-1.02	3.01	1.94	-0.75
R3	-5.80	-3.40	-6.53	-6.04	-9.16	-4.19	-5.48	-8.40
R4	-2.67	-0.37	-3.45	-2.56	-5.71	-1.03	-2.28	-4.98
R5	-1.16	0.92	-2.40	-1.90	-5.05	-0.12	-1.44	-3.80
R6	-0.72	1.55	-1.61	-1.27	-4.34	0.34	-0.92	-2.44
R7	-4.58	-3.71	-7.97	-4.66	-9.15	-3.87	-5.62	-7.17
R8	-4.85	-1.79	-4.53	-4.26	-7.59	-1.81	-3.19	-6.72
R9	-0.84	1.41	-1.78	-1.39	-4.49	0.23	-1.03	-2.67
R10	-0.75	1.51	-1.64	-1.30	-4.36	0.30	-0.95	-2.44
R11	1.95	3.94	0.73	1.51	-1.60	2.87	1.62	-0.28
R12	1.85	4.13	1.20	1.70	-1.27	2.90	1.74	0.37
R13	-0.71	-2.93	-6.48	-1.27	-9.02	0.36	-5.35	-6.80
R14	5.46	8.01	5.35	4.88	2.20	6.49	5.38	3.93
R15	-1.15	1.42	-1.39	-1.60	-4.41	-0.08	-1.23	-2.13
R16	2.56	5.82	2.93	2.96	-0.19	4.11	2.93	-0.12
R17	-4.34	-3.60	-7.97	-4.40	-9.01	-3.65	-5.46	-7.05
R18	-3.66	-3.04	-7.46	-3.73	-8.42	-2.94	-4.79	-6.53

**Table A.37:**  $\Delta G$  TS-I<sub>2</sub> without standard state shift in toluene at 343.15 K.

	BP86	B3-LYP	BH-LYP	PBE	PBE0	TPSS	TPSSH	M06
R1	16.74	26.46	31.54	18.59	22.92	19.75	21.74	25.85
R2	19.19	29.72	35.42	21.49	26.24	22.41	24.62	28.89
R3	14.19	23.21	27.87	15.55	19.74	17.06	18.90	24.14
R4	17.37	27.12	32.48	19.06	23.79	20.34	22.45	28.03
R5	18.18	26.79	31.26	18.90	23.16	20.26	22.13	27.86
R6	26.95	35.02	38.37	27.98	31.06	29.15	30.59	35.42
R7	30.91	38.39	41.82	31.56	34.58	32.03	33.41	39.38
R8	29.10	40.39	46.32	31.57	36.55	32.96	35.17	39.83
R9	24.64	32.85	36.53	25.64	29.12	26.82	28.42	33.59
R10	27.97	36.23	39.59	29.03	32.12	30.40	31.82	36.69
R11	20.10	29.46	34.65	21.02	25.81	22.24	24.35	30.69
R12	28.44	37.31	41.53	29.60	33.42	30.67	32.43	37.95
R13	24.63	32.80	36.45	25.66	29.11	26.84	28.42	33.61
R14	32.98	41.24	43.72	34.02	36.21	35.53	36.58	41.04
R15	33.61	42.32	44.93	34.84	37.24	36.30	37.47	42.41
R16	18.75	29.13	34.11	21.71	25.59	22.27	24.19	27.44
R17	31.35	38.78	42.12	31.96	34.88	32.50	33.83	39.56
R18	30.14	37.49	40.73	30.76	33.60	31.25	32.55	38.41

**Table A.38:**  $\Delta G$  (TS-I<sub>2</sub>)-TS with standard state shift in toluene at 343.15 K in kcal/mol.

\*: Optimized using the m5 grid.

	BP86	B3-LYP	BH-LYP	PBE	PBE0	TPSS	TPSSH	M06
R1*	-7.52	-4.57	-1.79	-6.38	-3.64	-6.93	-5.63	-3.75
R2	-7.67	-4.19	-1.09	-6.32	-3.29	-6.91	-5.46	-3.01
R3	-7.19	-4.39	-1.70	-6.41	-3.61	-6.88	-5.58	-2.45
R4	-7.52	-4.55	-1.81	-6.47	-3.64	-7.03	-5.70	-2.39
R5	-8.13	-5.16	-2.47	-7.24	-4.50	-7.69	-6.40	-3.61
R6	-5.03	-2.98	-0.68	-4.02	-1.63	-4.89	-3.72	-1.64
R7	-7.81	-4.43	-1.34	-7.55	-4.15	-8.01	-6.53	-2.71
R8	-5.75	-3.43	-2.17	-4.53	-3.09	-4.86	-4.15	-2.61
R9	-5.67	-3.47	-1.05	-4.70	-2.16	-5.49	-4.27	-1.91
R10	-4.60	-2.58	-0.42	-3.54	-1.30	-4.37	-3.27	-1.27
R11	-7.10	-3.82	-0.87	-5.95	-3.01	-6.49	-5.10	-1.94
R12	-6.30	-4.04	3.68	-5.14	-2.62	-6.10	-4.87	2.25
R13	-5.46	-3.29	-0.91	-4.45	-1.96	-5.26	-4.05	-1.72
R14	-2.99	-1.65	-0.43	-1.88	-0.71	-2.91	-2.26	-1.35
R15	-3.25	-1.81	-0.34	-2.09	-0.64	-3.29	-2.52	-1.52
R16	-7.05	-3.78	-0.94	-5.66	-2.90	-6.30	-4.97	-2.84
R17	-7.47	-4.05	-0.94	-7.22	-3.79	-7.65	-6.16	-2.51
R18	-8.75	-5.25	-2.12	-8.49	-5.02	-8.96	-7.44	-3.43

**Table A.39:**  $\Delta G$  TS with standard state shift in toluene at 343.15 K in kcal/mol.

	BP86	B3-LYP	BH-LYP	PBE	PBE0	TPSS	TPSSH	M06
R1	19.89	26.66	28.97	20.61	22.20	22.32	23.01	25.24
R2	22.51	29.54	32.14	23.45	25.17	24.96	25.73	27.54
R3	17.01	23.25	25.21	17.60	18.99	19.58	20.13	22.23
R4	20.53	27.30	29.93	21.17	23.07	23.00	23.79	26.06
R5	21.95	27.59	29.37	21.78	23.30	23.59	24.17	27.11
R6	27.61	33.64	34.70	27.64	28.33	29.68	29.95	32.70
R7	36.54	40.64	40.99	36.92	36.55	37.86	37.76	39.91
R8	30.49	39.46	44.12	31.74	35.27	33.46	34.96	38.07
R9	25.96	31.95	33.22	25.98	26.92	27.96	28.33	31.14
R10	28.21	34.45	35.65	28.21	29.06	30.41	30.73	33.60
R11	22.83	28.93	31.16	22.61	24.46	24.37	25.09	28.27
R12	30.38	36.99	33.48	30.38	31.69	32.41	32.94	31.34
R13	25.73	31.72	33.00	25.75	26.71	27.73	28.10	30.97
R14	31.60	38.53	39.78	31.55	32.56	34.07	34.48	38.03
R15	32.50	39.77	40.90	32.57	33.51	35.23	35.63	39.57
R16	21.43	28.55	30.69	23.01	24.13	24.21	24.80	25.92
R17	36.64	40.66	40.88	37.00	36.49	37.98	37.81	39.89
R18	36.71	40.56	40.67	37.08	36.44	38.03	37.81	39.66

**Table A.40:**  $\Delta G$  products with standard state shift in toluene at 343.15 K in kcal/mol.

	BP86	B3-LYP	BH-LYP	PBE	PBE0	TPSS	TPSSH	M06
R1	-2.90	-0.06	-3.03	-3.26	-6.20	-1.57	-2.78	-5.43
R2	-0.55	2.48	-0.09	-0.49	-3.20	0.83	-0.24	-2.93
R3	-7.98	-5.58	-8.71	-8.22	-11.34	-6.37	-7.66	-10.58
R4	-4.85	-2.55	-5.63	-4.74	-7.89	-3.21	-4.46	-7.16
R5	-3.34	-1.26	-4.58	-4.08	-7.23	-2.30	-3.62	-5.98
R6	-2.90	-0.63	-3.79	-3.45	-6.52	-1.84	-3.10	-4.62
R7	-4.58	-3.71	-7.97	-4.66	-9.15	-3.87	-5.62	-7.17
R8	-7.03	-3.97	-6.71	-6.44	-9.77	-3.99	-5.37	-8.90
R9	-3.02	-0.77	-3.96	-3.57	-6.67	-1.95	-3.21	-4.85
R10	-2.93	-0.67	-3.82	-3.48	-6.54	-1.88	-3.13	-4.62
R11	-0.23	1.76	-1.45	-0.67	-3.78	0.69	-0.56	-2.46
R12	-0.33	1.95	-0.98	-0.48	-3.45	0.72	-0.44	-1.81
R13	-2.89	-5.11	-8.66	-3.45	-11.20	-1.82	-7.53	-8.98
R14	3.28	5.83	3.17	2.70	0.02	4.31	3.20	1.75
R15	-3.33	-0.76	-3.57	-3.78	-6.59	-2.26	-3.41	-4.31
R16	0.38	3.64	0.75	0.78	-2.37	1.93	0.75	-2.30
R17	-4.34	-3.60	-7.97	-4.40	-9.01	-3.65	-5.46	-7.05
R18	-3.66	-3.04	-7.46	-3.73	-8.42	-2.94	-4.79	-6.53



**Table A.41:**  $\Delta G$  TS-I<sub>2</sub> with standard state shift in toluene at 343.15 K in kcal/mol.

	BP86	B3-LYP	BH-LYP	PBE	PBE0	TPSS	TPSSH	M06
R1	12.38	22.10	27.18	14.23	18.56	15.39	17.38	21.49
R2	14.83	25.36	31.06	17.13	21.88	18.05	20.26	24.53
R3	9.83	18.85	23.51	11.19	15.38	12.70	14.54	19.78
R4	13.01	22.76	28.12	14.70	19.43	15.98	18.09	23.67
R5	13.82	22.43	26.90	14.54	18.80	15.90	17.77	23.50
R6	22.59	30.66	34.01	23.62	26.70	24.79	26.23	31.06
R7	28.73	36.21	39.64	29.38	32.40	29.85	31.23	27.20
R8	24.74	36.03	41.96	27.21	32.19	28.60	30.81	35.47
R9	20.28	28.49	32.17	21.28	24.76	22.46	24.06	29.23
R10	23.61	31.87	35.23	24.67	27.76	26.04	27.46	32.33
R11	15.74	25.10	30.29	16.66	21.45	17.88	19.99	26.33
R12	24.08	32.95	37.17	25.24	29.06	26.31	28.07	33.59
R13	20.27	28.44	32.09	21.30	24.75	22.48	24.06	29.25
R14	28.62	36.88	39.36	29.66	31.85	31.17	32.22	36.68
R15	29.25	37.96	40.57	30.48	32.88	31.94	33.11	38.05
R16	14.39	24.77	29.75	17.35	21.23	17.91	19.83	23.08
R17	29.17	36.60	39.94	29.78	32.70	30.32	31.65	37.38
R18	27.96	35.31	38.55	28.58	31.42	29.07	30.37	36.23

**A.3.3 Toluene at 100 °C****Table A.42:**  $\Delta G$  (TS-I<sub>2</sub>)-TS without standard state shift in toluene at 373.15 K in kcal/mol. \*: Optimized using the m5 grid.

	BP86	B3-LYP	BH-LYP	PBE	PBE0	TPSS	TPSSH	M06
R1*	-4.47	-1.52	1.25	-3.34	-0.60	-3.89	-2.59	-0.70
R2	-4.52	-1.04	2.06	-3.17	-0.14	-3.76	-2.31	0.14
R3	-4.22	-1.42	1.28	-3.43	-0.64	-3.91	-2.61	0.52
R4	-4.47	-1.49	1.24	-3.42	-0.59	-3.97	-2.64	0.67
R5	-5.12	-2.15	0.54	-4.23	-1.49	-4.68	-3.39	-0.60
R6	-2.03	0.02	2.31	-1.03	1.37	-1.89	-0.73	1.36
R7	-4.71	-1.33	1.76	-4.44	-1.04	-4.91	-3.42	0.39
R8	-2.63	-0.31	0.96	-1.41	0.04	-1.74	-1.03	0.51
R9	-2.69	-0.48	1.93	-1.72	0.82	-2.51	-1.29	1.07
R10	-1.58	0.44	2.59	-0.52	1.72	-1.35	-0.25	1.75
R11	-3.85	-0.58	2.38	-2.71	0.23	-3.24	-1.86	1.30
R12	-3.32	-1.05	6.67	-2.15	0.36	-3.11	-1.89	5.24
R13	-2.46	-0.28	2.09	-1.45	1.04	-2.25	-1.04	1.29
R14	0.07	1.41	2.63	1.17	2.34	0.15	0.80	1.70
R15	-0.17	1.27	2.74	0.98	2.44	-0.22	0.56	1.56
R16	-3.96	-0.69	2.15	-2.57	0.19	-3.21	-1.87	0.25
R17	-4.36	-0.95	2.17	-4.12	-0.68	-4.55	-3.05	0.60
R18	-5.67	-2.17	0.96	-5.41	-1.94	-5.87	-4.36	-0.34

**Table A.43:**  $\Delta G$  TS without standard state shift in toluene at 373.15 K in kcal/mol.

	BP86	B3-LYP	BH-LYP	PBE	PBE0	TPSS	TPSSH	M06
R1	23.40	30.17	32.47	24.11	25.71	25.82	26.52	28.74
R2	25.96	33.00	35.60	26.90	28.62	28.42	29.18	31.00
R3	20.52	26.76	28.72	21.11	22.50	23.08	23.64	25.73
R4	24.04	30.81	33.43	24.68	26.58	26.51	27.29	29.57
R5	25.41	31.05	32.82	25.24	26.75	27.05	27.63	30.57
R6	31.15	37.18	38.24	31.18	31.87	33.22	33.49	36.24
R7	36.90	40.99	41.34	37.28	36.90	38.22	38.11	40.26
R8	34.10	43.07	47.73	35.35	38.88	37.07	38.56	41.68
R9	29.50	35.49	36.77	29.52	30.47	31.50	31.87	34.68
R10	31.75	37.99	39.19	31.75	32.60	33.95	34.27	37.14
R11	26.06	32.15	34.39	25.84	27.69	27.60	28.32	31.50
R12	33.87	40.48	36.97	33.87	35.18	35.90	36.43	34.83
R13	29.27	35.26	36.54	29.29	30.24	31.27	31.64	34.50
R14	35.16	42.08	43.34	35.10	36.11	37.63	38.04	41.58
R15	36.10	43.36	44.50	36.17	37.11	38.83	39.23	43.17
R16	25.05	32.17	34.31	26.63	27.75	27.83	28.41	29.54
R17	36.97	40.99	41.22	37.34	36.83	38.31	38.15	40.22
R18	37.05	40.91	41.01	37.42	36.78	38.37	38.15	40.00

**Table A.44:**  $\Delta G$  products without standard state shift in toluene at 373.15 K in kcal/mol.

	BP86	B3-LYP	BH-LYP	PBE	PBE0	TPSS	TPSSH	M06
R1	0.44	3.28	0.31	0.08	-2.86	1.77	0.57	-2.08
R2	2.84	5.87	3.30	2.90	0.18	4.22	3.15	0.46
R3	-4.67	-2.27	-5.40	-4.91	-8.03	-3.06	-4.35	-7.27
R4	-1.46	0.84	-2.25	-1.36	-4.50	0.18	-1.07	-3.77
R5	-0.02	2.06	-1.26	-0.76	-3.91	1.02	-0.30	-2.66
R6	0.43	2.70	-0.45	-0.12	-3.19	1.49	0.23	-1.28
R7	-4.28	-3.41	-7.66	-4.35	-8.84	-3.56	-5.32	-6.87
R8	-3.63	-0.56	-3.30	-3.03	-6.37	-0.59	-1.97	-5.50
R9	0.31	2.57	-0.63	-0.23	-3.33	1.39	0.12	-1.52
R10	0.40	2.66	-0.48	-0.15	-3.21	1.46	0.20	-1.28
R11	3.18	5.17	1.95	2.74	-0.37	4.10	2.84	0.95
R12	3.01	5.30	2.36	2.86	-0.11	4.06	2.90	1.53
R13	0.46	-1.76	-5.31	-0.10	-7.86	1.53	-4.18	-5.64
R14	6.60	9.15	6.48	6.02	3.33	7.62	6.52	5.06
R15	0.04	2.61	-0.20	-0.41	-3.22	1.11	-0.04	-0.94
R16	3.82	7.07	4.19	4.22	1.07	5.37	4.19	1.13
R17	-4.04	-3.30	-7.67	-4.10	-8.71	-3.35	-5.16	-6.75
R18	-3.36	-2.75	-7.16	-3.43	-8.13	-2.65	-4.50	-6.24

**Table A.45:**  $\Delta G$  TS-I<sub>2</sub> without standard state shift in toluene at 373.15 K in kcal/mol.

	BP86	B3-LYP	BH-LYP	PBE	PBE0	TPSS	TPSSH	M06
R1	18.92	28.65	33.73	20.78	25.11	21.94	23.93	28.04
R2	21.44	31.96	37.66	23.73	28.48	24.65	26.87	31.13
R3	16.31	25.33	29.99	17.67	21.86	19.18	21.02	26.26
R4	19.57	29.32	34.68	21.26	25.99	22.54	24.65	30.23
R5	20.29	28.90	33.37	21.01	25.26	22.37	24.23	29.96
R6	29.12	37.19	40.55	30.15	33.24	31.33	32.76	37.59
R7	32.19	39.66	43.10	32.83	35.86	33.31	34.69	40.66
R8	31.47	42.76	48.69	33.94	38.92	35.33	37.54	42.20
R9	26.81	35.01	38.70	27.80	31.29	28.99	30.59	35.76
R10	30.17	38.43	41.79	31.23	34.32	32.60	34.02	38.89
R11	22.21	31.57	36.76	23.13	27.92	24.35	26.46	32.80
R12	30.55	39.42	43.64	31.72	35.54	32.79	34.54	40.07
R13	26.81	34.97	38.63	27.84	31.29	29.02	30.60	35.79
R14	35.22	43.49	45.97	36.27	38.46	37.78	38.83	43.28
R15	35.92	44.63	47.24	37.15	39.55	38.61	39.79	44.73
R16	21.10	31.48	36.46	24.06	27.93	24.62	26.54	29.79
R17	32.61	40.05	43.39	33.22	36.15	33.77	35.10	40.82
R18	31.38	38.73	41.97	32.01	34.84	32.50	33.79	39.65

**Table A.46:**  $\Delta G$  (TS-I<sub>2</sub>)-TS with standard state shift in toluene at 373.15 K in kcal/mol.

\*: Optimized using the m5 grid.

	BP86	B3-LYP	BH-LYP	PBE	PBE0	TPSS	TPSSH	M06
R1*	-6.84	-3.89	-1.12	-5.71	-2.97	-6.26	-4.96	-3.07
R2	-6.89	-3.41	-0.31	-5.54	-2.51	-6.13	-4.68	-2.23
R3	-6.59	-3.79	-1.09	-5.80	-3.01	-6.28	-4.98	-1.85
R4	-6.84	-3.86	-1.13	-5.79	-2.96	-6.34	-5.01	-1.70
R5	-7.49	-4.52	-1.83	-6.60	-3.86	-7.05	-5.76	-2.97
R6	-4.40	-2.35	-0.06	-3.40	-1.00	-4.26	-3.10	-1.01
R7	-7.08	-3.70	-0.61	-6.81	-3.41	-7.28	-5.79	-1.98
R8	-5.00	-2.68	-1.41	-3.78	-2.33	-4.11	-3.40	-1.86
R9	-5.06	-2.85	-0.44	-4.09	-1.55	-4.88	-3.66	-1.30
R10	-3.95	-1.93	0.22	-2.89	-0.65	-3.72	-2.62	-0.62
R11	-6.22	-2.95	0.01	-5.08	-2.14	-5.61	-4.23	-1.07
R12	-5.69	-3.42	4.30	-4.52	-2.01	-5.48	-4.26	2.87
R13	-4.83	-2.65	-0.28	-3.82	-1.33	-4.62	-3.41	-1.08
R14	-2.30	-0.96	0.26	-1.20	-0.03	-2.22	-1.57	-0.67
R15	-2.54	-1.10	0.37	-1.39	0.07	-2.59	-1.81	-0.81
R16	-6.33	-3.06	-0.22	-4.94	-2.18	-5.58	-4.24	-2.12
R17	-6.73	-3.32	-0.20	-6.49	-3.05	-6.92	-5.42	-1.77
R18	-8.04	-4.54	-1.41	-7.78	-4.31	-8.24	-6.73	-2.71

**Table A.47:**  $\Delta G$  TS with standard state shift in toluene at 373.15 K in kcal/mol.

	BP86	B3-LYP	BH-LYP	PBE	PBE0	TPSS	TPSSH	M06
R1	21.03	27.80	30.10	21.74	23.34	23.45	24.15	26.37
R2	23.59	30.63	33.23	24.53	26.25	26.05	26.81	28.63
R3	18.15	24.39	26.35	18.74	20.13	20.71	21.27	23.36
R4	21.67	28.44	31.06	22.31	24.21	24.14	24.92	27.20
R5	23.04	28.68	30.45	22.87	24.38	24.68	25.26	28.20
R6	28.78	34.81	35.87	28.81	29.50	30.85	31.12	33.87
R7	36.90	40.99	41.34	37.28	36.90	38.22	38.11	40.26
R8	31.73	40.70	45.36	32.98	36.51	34.70	36.19	39.31
R9	27.13	33.12	34.40	27.15	28.10	29.13	29.50	32.31
R10	29.38	35.62	36.82	29.38	30.23	31.58	31.90	34.77
R11	23.69	29.78	32.02	23.47	25.32	25.23	25.95	29.13
R12	31.50	38.11	34.60	31.50	32.81	33.53	34.06	32.46
R13	26.90	32.89	34.17	26.92	27.87	28.90	29.27	32.13
R14	32.79	39.71	40.97	32.73	33.74	35.26	35.67	39.21
R15	33.73	40.99	42.13	33.80	34.74	36.46	36.86	40.80
R16	22.68	29.80	31.94	24.26	25.38	25.46	26.04	27.17
R17	36.97	40.99	41.22	37.34	36.83	38.31	38.15	40.22
R18	37.05	40.91	41.01	37.42	36.78	38.37	38.15	40.00

**Table A.48:**  $\Delta G$  products with standard state shift in toluene at 373.15 K in kcal/mol.

	BP86	B3-LYP	BH-LYP	PBE	PBE0	TPSS	TPSSH	M06
R1	-1.93	0.91	-2.06	-2.29	-5.23	-0.60	-1.80	-4.45
R2	0.47	3.50	0.93	0.53	-2.19	1.85	0.78	-1.91
R3	-7.04	-4.64	-7.77	-7.28	-10.40	-5.43	-6.72	-9.64
R4	-3.83	-1.53	-4.62	-3.73	-6.87	-2.19	-3.44	-6.14
R5	-2.39	-0.31	-3.63	-3.13	-6.28	-1.35	-2.67	-5.03
R6	-1.94	0.33	-2.82	-2.49	-5.56	-0.88	-2.14	-3.65
R7	-4.28	-3.41	-7.66	-4.35	-8.84	-3.56	-5.32	-6.87
R8	-6.00	-2.93	-5.67	-5.40	-8.74	-2.96	-4.34	-7.87
R9	-2.06	0.20	-3.00	-2.60	-5.70	-0.98	-2.25	-3.89
R10	-1.97	0.29	-2.85	-2.52	-5.58	-0.91	-2.17	-3.65
R11	0.81	2.80	-0.42	0.37	-2.74	1.73	0.47	-1.42
R12	0.64	2.93	-0.01	0.49	-2.48	1.69	0.53	-0.84
R13	-1.91	-4.13	-7.68	-2.47	-10.23	-0.84	-6.55	-8.01
R14	4.23	6.78	4.11	3.65	0.96	5.25	4.15	2.69
R15	-2.33	0.24	-2.57	-2.78	-5.59	-1.26	-2.41	-3.31
R16	1.45	4.70	1.82	1.85	-1.30	3.00	1.82	-1.24
R17	-4.04	-3.30	-7.67	-4.10	-8.71	-3.35	-5.16	-6.75
R18	-3.36	-2.75	-7.16	-3.43	-8.13	-2.65	-4.50	-6.24



**Table A.49:**  $\Delta G$  TS-I<sub>2</sub> with standard state shift in toluene at 373.15 K in kcal/mol.

	BP86	B3-LYP	BH-LYP	PBE	PBE0	TPSS	TPSSH	M06
R1	14.18	23.91	28.99	16.04	20.37	17.20	19.19	23.30
R2	16.70	27.22	32.92	18.99	23.74	19.91	22.13	26.39
R3	11.57	20.59	25.25	12.93	17.12	14.44	16.28	21.52
R4	14.83	24.58	29.94	16.52	21.25	17.80	19.91	25.49
R5	15.55	24.16	28.63	16.27	20.52	17.63	19.49	25.22
R6	24.38	32.45	35.81	25.41	28.50	26.59	28.02	32.85
R7	29.82	37.29	40.73	30.46	33.49	30.94	32.32	38.29
R8	26.73	38.02	43.95	29.20	34.18	30.59	32.80	37.46
R9	22.07	30.27	33.96	23.06	26.55	24.25	25.85	31.02
R10	25.43	33.69	37.05	26.49	29.58	27.86	29.28	34.15
R11	17.47	26.83	32.02	18.39	23.18	19.61	21.72	28.06
R12	25.81	34.68	38.90	26.98	30.80	28.05	29.80	35.33
R13	22.07	30.23	33.89	23.10	26.55	24.28	25.86	31.05
R14	30.48	38.75	41.23	31.53	33.72	33.04	34.09	38.54
R15	31.18	39.89	42.50	32.41	34.81	33.87	35.05	39.99
R16	16.36	26.74	31.72	19.32	23.19	19.88	21.80	25.05
R17	30.24	37.68	41.02	30.85	33.78	31.40	32.73	38.45
R18	29.01	36.36	39.60	29.64	32.47	30.13	31.42	37.28



# List of Figures

3.1	Orbital characters (top) and configuration contributions (bottom) of cerocene at the CASSCF level. . . . .	39
3.2	CASSCF(4,4)/RSPT2 optimized ground state structures of the $D_{2d}$ (left) and $D_{2h}$ (right) symmetric bis( $\eta^8$ -pentalene)cerium. . . . .	43
3.3	Orbital rotation of bis( $\eta^8$ -pentalene)cerium compared to a hydrogen dimer. . . . .	46
3.4	Occupation number fluctuation and local spin derived from CASSCF wavefunctions for bis( $\eta^8$ -pentalene)cerium and various reference systems. The $H_2$ reference curve is given in blue. . . . .	48
3.5	Different conformations of the $Cp_2CeO$ complex. . . . .	53
3.6	Illustration of the possible $C_{2v}$ structures of the $Cp_2CeCH_2$ complex. . . . .	54
3.7	Optimized $C_{2v}$ structures of all investigated $Cp_2CeZ$ compounds. . . . .	55
3.8	Force constants for the Ce-Z bond computed at the HF and RSPT2 level using the basis set given in a.u. for the $Cp_2CeZ$ compounds compared to the Hf-O bond in $Cp_2HfO$ and the C-C bonds of the molecular series $C_2H_n$ ( $n=2, 4, 6$ ). . . . .	57
3.9	Orbital characters determined by Mulliken population analysis (top) and configuration contributions to the CASSCF(2,2) wavefunction (bottom) for $Cp_2CeCH_2$ using the VTZ <sub>b</sub> basis sets. The vertical line shows the rotation angle where the f character of orbital a is maximized . . . . .	73
3.10	As Figure 3.9 but for the $Cp_2CeO$ compound using $a_1$ symmetric orbitals. The p character of orbital b was maximized. . . . .	74
3.11	Charge fluctuation and local spin computed for the Ce-Z bonds of the $Cp_2CeZ$ complexes ( $Z = CH_2, CH^-, NH, O, F^+$ ) at their HF geometries from CASSCF(2,2) calculations in comparison to corresponding results for the $H_2$ molecule. Filled symbols are used for $\sigma$ bonds and empty symbols for $\pi$ bonds. . . . .	76
3.12	HF/RS2C optimized ground state geometries using the VTZ basis sets for $CH_2CeF_2$ (left) and $OCeF_2$ (right). . . . .	81

3.13	Orbital characters determined by Mulliken population analysis (top) and configuration contributions to the CASSCF(2,2) wavefunction (bottom) for $\text{CH}_2\text{CeF}_2$ using the VTZ basis sets. The vertical line shows the rotation angle where the f character of orbital b is maximized . . . . .	89
3.14	As Figure 3.13, but for the $\text{OCeF}_2$ complex. . . . .	90
3.15	Occupation number fluctuations and local spin from CASSCF(2,2) calculations of $\text{OCeF}_2$ and $\text{CH}_2\text{CeF}_2$ using the VTZ basis set in comparison to corresponding results for the $\text{H}_2$ molecule (the dots correspond to $\text{H}_2$ bond distances from 0.75 to 3.0 Å in steps of 0.25 Å). . . . .	91
3.16	The four former investigated iodine catalyzed reactions [72]. . . . .	97
3.17	Investigated iodine catalyzed reactions. . . . .	109
3.18	Transition states for reaction 5 (TS, TS- $\text{I}_2$ for $\text{R5}^*$ , TS- $\text{I}_2$ for R5). . . . .	112
A.1	As Figure 3.13 but for a CASSCF(2,2) optimized geometry. . . . .	135

# List of Tables

3.1	Selected bond distances and bond angles of the optimized bis( $\eta^8$ -pentalene)cerium structures in $D_{2h}$ and $D_{2d}$ symmetry compared to averaged experimental values from a crystal structure ( $D_{2d}$ ). The atom numbering is according to IUPAC. C atoms 1,3,4,6 are equivalent as well as 2 and 5. C atoms 3a and 6a are common to the ring ligands. X describes the middle of C(3a)-C(6a).	44
3.2	Configuration contributions [%] to the CASSCF(4,4) and CASSCF(2,2) singlet ground state wavefunction. Localized orbitals: nearly pure cerium 4f and ligand $\pi$ orbitals.	45
3.3	Energy differences of the optimized $C_{2v}$ and $C_1$ structures in kJ/mol.	52
3.4	Energy differences $\Delta E(G_i - G_1)$ in kJ/mol of the optimized $C_{2v}$ geometries of the $Cp_2CeCH_2$ compound.	54
3.5	Ce-Z bond distances of the optimized structures given in Å.	56
3.6	Energy differences of the CASSCF states (unrestricted) of the $CeCp_2CH_2$ complex compared to the RHF singlet state.	59
3.7	As Table 3.6 but for the $CeCp_2CH^-$ complex.	59
3.8	As Table 3.6 but for the $CeCp_2NH$ complex.	59
3.9	As Table 3.6 but for the $CeCp_2O$ complex.	60
3.10	As Table 3.6 but for the $CeCp_2F^+$ complex.	60
3.11	Energy differences of the $^1A_1$ state of the $CeCp_2CH_2$ complex compared to the RHF singlet state using the VDZ basis.	61
3.12	As Table 3.11 but for the $CeCp_2CH^-$ complex.	61
3.13	As Table 3.11 but for the $CeCp_2NH$ complex.	61
3.14	As Table 3.11 but for the $CeCp_2O$ complex.	61
3.15	Energy differences of the $^1A_1$ state of the $CeCp_2CH_2$ complex in comparison of the different performed CASSCF computations.	63
3.16	As Table 3.16 but for the $CeCp_2CH^-$ complex.	63
3.17	As Table 3.16 but for the $CeCp_2NH$ complex.	64

3.18	As Table 3.16 but for the $\text{CeCp}_2\text{O}$ complex using the HOMO-1 instead of the HOMO. . . . .	64
3.19	Cerium 4f and 5d populations for the $^1\text{A}_1$ CASSCF (HF) ground state of all investigated compounds. . . . .	66
3.20	Energy differences of the $^1\text{A}_1$ ground state at the CASSCF(2,2) level and the closed-shell HF ground state of the $\text{Cp}_2\text{CeCH}_2$ and $\text{Cp}_2\text{CeCH}^-$ complex. $\Delta E$ values are given in eV. . . . .	67
3.21	As Table 3.20 but for the $\text{Cp}_2\text{CeZ}$ ( $Z = \text{NH}, \text{O}, \text{F}^+$ ) compounds. . . . .	68
3.22	Configuration contributions (in %) to the $^1\text{A}_1$ ground state wavefunction at the CASSCF(2,2) level for the $\text{Cp}_2\text{CeCH}_2$ and $\text{Cp}_2\text{CeCH}^-$ compounds based on their HF optimized $\text{C}_{2v}$ symmetric structure. The rotation angle with maximized f character of orbital a is shown for each complex and the corresponding results for the CASSCF(6,10) optimized geometry are written in parentheses. . . . .	71
3.23	As Table 3.22 but for the $\text{Cp}_2\text{CeZ}$ ( $Z = \text{NH}, \text{O}, \text{F}^+$ ) compounds. The rotation angle leading to a maximized Z p character using the VTZ <sub>b</sub> basis are shown. . . . .	72
3.24	Lowest singlet and triplet state energies obtained by CASSCF/RS2C computations using the VTZ basis sets, based on the optimized HF/RS2C structures. . . . .	83
3.25	Electronic energies [a.u.] of the $^1\text{A}$ ground state for $\text{CH}_2\text{CeF}_2$ and $\text{OCeF}_2$ at the HF, CASSCF(2,8) and CASSCF(2,2) level using the VTZ basis set, based on the HF/RS2C optimized geometries. Energy differences to the HF energy are given in eV. . . . .	84
3.26	Mulliken 4f populations for HF, UHF, CASSCF and several DFT methods. For $\text{CH}_2\text{CeF}_2$ computed values arising from the difference of $\alpha$ and $\beta$ spin density matrices are presented in parentheses. . . . .	85
3.27	Configuration contributions [%] to the $^1\text{A}_1$ ground state of the CASSCF(2,2) wavefunction based on HF/RS2C optimized geometries. In the upper line the rotation angle leading to an orbital with maximized f character is presented, whereby in the lower line the most compact wavefunction in the sense of contributing configurations is shown. The different orbital characters were obtained from a Mulliken population analysis. . . . .	87

3.28	Ce-C and Ce-O stretching frequencies in $\text{cm}^{-1}$ (singlet ground states) computed by various DFT and wavefunction-based methods compared to experimental frequencies measured in a solid argon (neon) matrix ( $\text{CH}_2\text{CeF}_2$ : Wang <i>et al.</i> [60] and $\text{OCeF}_2$ : Mikulas <i>et al.</i> [61]). The reported computed (B3LYP/DZVP2) frequency for the methylene complex is given in square brackets. . . . .	92
3.29	Results of the iodine catalysis for the investigated reactions 1-4 using COSMO( $\text{CH}_2\text{Cl}_2$ ), dispersion (D3), quasiharmonic and standard state correction (+: calculation confirms the experiment, -: calculation does not confirm the experiment). . . . .	101
3.30	Results of the iodine catalysis for the investigated reactions 1-4 using COSMO( $\text{CH}_2\text{Cl}_2$ ), quasiharmonic and standard state correction (+: calculation confirms the experiment, -: calculation does not confirm the experiment). . . . .	101
3.31	Electronic energy differences ( $\Delta E_{\text{Disp}} = E_{\text{COSMO+D3}} - E_{\text{COSMO}}$ ) of $\text{I}_2$ in kcal/mol. The def2-TZVP basis set was used. . . . .	102
3.32	Free-energies $\Delta G$ for the transition states and the following intermediates in kcal/mol for reaction 3 and 4. . . . .	103
3.33	$\Delta G$ values in kcal/mol for several carbonyl compounds with iodine, recently published[72]. . . . .	105
3.34	Maximum signed error compared to the experimental $\Delta G$ values in kcal/mol of the five test systems calculated with COSMO( $\text{CCl}_4$ ) including dispersion correction, free-energy correction without standard state correction. The def2-X basis sets were used. . . . .	107
3.35	Maximum signed error compared to the experimental $\Delta G$ values in kcal/mol of the five test systems calculated with COSMO( $\text{CCl}_4$ ) including dispersion correction, free-energy correction and standard state correction. The def2-X basis sets were used. . . . .	108
3.36	$\Delta G$ in kcal/mol computed for $\text{CH}_2\text{Cl}_2$ at 298.15 K computed by TPSSH-D3/def2-TZVP/COSMO//TPSSH/def2-TZVP using standard state correction. (Experiments for R8[84], R1-R5 and R16[85]) . . . . .	110
3.37	$\Delta G$ in kcal/mol computed for $\text{CH}_2\text{Cl}_2$ at 298.15 K computed by TPSSH-D3/def2-TZVP/COSMO//TPSSH/def2-TZVP using standard state correction. (Experiments for R8[84], all other[85]) . . . . .	113

3.38	DFT performance on similar reactions in $\text{CH}_2\text{Cl}_2$ at 298.15 K. (+: calculation confirms the experiment, -: calculation does not confirm the experiment). Geometry optimizations and free-energy corrections were computed using TPSSH/def2-TZVP. Electronic energies were computed by the given functionals including D3 correction and a COSMO correction for $\text{CH}_2\text{Cl}_2$ . Standard state correction was used. . . . .	115
3.39	DFT performance on the prediction of reactions in $\text{CH}_2\text{Cl}_2$ at 298.15 K. (+: calculation confirms the experiment, -: calculation does not confirm the experiment). Geometry optimizations and free-energy corrections were computed using TPSSH/def2-TZVP. Electronic energies were computed by the given functionals including D3 correction and a COSMO correction for $\text{CH}_2\text{Cl}_2$ . Standard state correction was not used. . . . .	115
3.40	$\Delta G$ for the catalyzed transition states TS-I <sub>2</sub> using dispersion (D3) and standard state correction in $\text{CH}_2\text{Cl}_2$ at 298.15 K. . . . .	117
3.41	As Table 3.38 including height consistency for reaction 6. . . . .	117
3.42	As Table 3.39 but for toluene at 343.15 K. . . . .	118
3.43	DFT performance on the prediction of reactions in toluene at 343.15 K. (+: calculation confirms the experiment, -: calculation does not confirm the experiment). Geometry optimizations and free-energy corrections were computed using TPSSH/def2-TZVP. Electronic energies were computed by the given functionals including D3 correction and a COSMO correction for toluene. Standard state correction was used. †: Reaction outcome is implicitly given. . . . .	119
3.44	As Table 3.43 including height consistency. . . . .	120
3.45	As Table 3.43 for toluene at 373.15 K. . . . .	122
3.46	Computed $\Delta G$ values using the PBE0-D3/COSMO/def2-TZVP method based TPSSH/def2-TZVP optimized structures using the standard state correction in dichlormethane at 25 °C. . . . .	123
3.47	Computed $\Delta G$ values using the PBE0-D3/COSMO/def2-TZVP method based TPSSH/def2-TZVP optimized structures using the standard state correction in toluene at 70 °C. . . . .	124
3.48	Free-energy $\Delta G$ of catalyzed and uncatalyzed transition states using COSMO, D3 and standard state correction for dichlormethane at 25 °C in kcal/mol. . . . .	125
3.49	Standard Deviation using COSMO( $\text{CCl}_4$ ) and D3 at 25 °C. . . . .	127
3.50	Averaged error to the experimental results without using standard state correction in kcal/mol. . . . .	128



3.51	Averaged error to the experimental results using standard state correction kcal/mol. . . . .	128
3.52	Catalyzed transition states including the experimentally derived shift compared to unshifted values for all reactions in $\text{CH}_2\text{Cl}_2$ at 25 °C in kcal/mol. . . . .	129
A.1	CASSCF(6,10) for $\text{Cp}_2\text{CeCH}_2$ in $\text{C}_{2v}$ symmetry. CI coefficients of leading determinants for NO basis. . . . .	131
A.2	CASSCF(6,10) for $\text{Cp}_2\text{CeCH}_2$ in $\text{C}_{2v}$ symmetry. NO occupation numbers (orbital.irrep). . . . .	131
A.3	CASSCF(6,10) for $\text{Cp}_2\text{CeCH}^-$ in $\text{C}_{2v}$ symmetry. CI coefficients of leading determinants for NO basis. . . . .	132
A.4	CASSCF(6,10) for $\text{Cp}_2\text{CeCH}^-$ in $\text{C}_{2v}$ symmetry. NO occupation numbers (orbital.irrep). . . . .	132
A.5	CASSCF(6,10) for $\text{Cp}_2\text{CeNH}$ in $\text{C}_{2v}$ symmetry. CI coefficients of leading determinants for NO basis. . . . .	132
A.6	CASSCF(6,10) for $\text{Cp}_2\text{CeNH}$ in $\text{C}_{2v}$ symmetry. NO occupation numbers (orbital.irrep). . . . .	133
A.7	CASSCF(6,10) for $\text{Cp}_2\text{CeO}$ in $\text{C}_{2v}$ symmetry. CI coefficients of leading determinants for NO basis. . . . .	133
A.8	CASSCF(6,10) for $\text{Cp}_2\text{CeO}$ in $\text{C}_{2v}$ symmetry. NO occupation numbers (orbital.irrep). . . . .	133
A.9	CASSCF(6,10) for $\text{Cp}_2\text{CeF}^+$ in $\text{C}_{2v}$ symmetry. CI coefficients of leading determinants for NO basis. . . . .	134
A.10	CASSCF(6,10) for $\text{Cp}_2\text{CeF}^+$ in $\text{C}_{2v}$ symmetry. NO occupation numbers (orbital.irrep). . . . .	134
A.11	Error compared to the experimental results in kcal/mol. SVP basis set was applied without using standard state correction. . . . .	136
A.12	Error compared to the experimental results in kcal/mol. SVPD basis set was applied without using standard state correction. . . . .	136
A.13	Error compared to the experimental results in kcal/mol. TZVP basis set was applied without using standard state correction. . . . .	136
A.14	Error compared to the experimental results in kcal/mol. TZVPP basis set was applied without using standard state correction. . . . .	137
A.15	Error compared to the experimental results in kcal/mol. TZVPD basis set was applied without using standard state correction. . . . .	137

A.16 Error compared to the experimental results in kcal/mol. QZVP basis set was applied without using standard state correction. . . . .	137
A.17 Maximal signed error to the experimental results without using standard state correction. . . . .	137
A.18 Averaged error to the experimental results without using standard state correction. . . . .	138
A.19 Error compared to the experimental results in kcal/mol. SVP basis set was applied without using standard state correction. . . . .	138
A.20 Error compared to the experimental results in kcal/mol. SVPD basis set was applied without using standard state correction. . . . .	138
A.21 Error compared to the experimental results in kcal/mol. TZVP basis set was applied with using standard state correction. . . . .	138
A.22 Error compared to the experimental results in kcal/mol. TZVPP basis set was applied with using standard state correction. . . . .	139
A.23 Error compared to the experimental results in kcal/mol. TZVPD basis set was applied with using standard state correction. . . . .	139
A.24 Error compared to the experimental results in kcal/mol. QZVP basis set was applied with using standard state correction. . . . .	139
A.25 Averaged error compared to the experimental results with using standard state correction in kcal/mol. . . . .	139
A.26 $\Delta G$ (TS-I <sub>2</sub> )-TS without standard state shift in CH <sub>2</sub> Cl <sub>2</sub> at 298.15 K in kcal/mol. *: Optimized using the m5 grid. . . . .	140
A.27 $\Delta G$ TS-I <sub>2</sub> without standard state shift in CH <sub>2</sub> Cl <sub>2</sub> at 298.15 K in kcal/mol.	141
A.28 $\Delta G$ TS without standard state shift in CH <sub>2</sub> Cl <sub>2</sub> at 298.15 K in kcal/mol. .	142
A.29 $\Delta G$ products without standard state shift in CH <sub>2</sub> Cl <sub>2</sub> at 298.15 K in kcal/mol. . . . .	143
A.30 $\Delta G$ (TS-I <sub>2</sub> )-TS with standard state shift in CH <sub>2</sub> Cl <sub>2</sub> at 298.15 K in kcal/mol. *: Optimized using the m5 grid. . . . .	144
A.31 $\Delta G$ TS-I <sub>2</sub> with standard state shift in CH <sub>2</sub> Cl <sub>2</sub> at 298.15 K in kcal/mol. .	145
A.32 $\Delta G$ TS with standard state shift in CH <sub>2</sub> Cl <sub>2</sub> at 298.15 K in kcal/mol. . .	146
A.33 $\Delta G$ products with standard state shift in CH <sub>2</sub> Cl <sub>2</sub> at 298.15 K in kcal/mol.	147
A.34 $\Delta G$ (TS-I <sub>2</sub> )-TS without standard state shift in toluene at 343.15 K in kcal/mol. *: Optimized using the m5 grid. . . . .	148
A.35 $\Delta G$ TS without standard state shift in toluene at 343.15 K in kcal/mol. .	149
A.36 $\Delta G$ products without standard state shift in toluene at 343.15 K. . . . .	150
A.37 $\Delta G$ TS-I <sub>2</sub> without standard state shift in toluene at 343.15 K. . . . .	151

A.38 $\Delta G$ (TS-I <sub>2</sub> )-TS with standard state shift in toluene at 343.15 K in kcal/mol.	
*: Optimized using the m5 grid. . . . .	152
A.39 $\Delta G$ TS with standard state shift in toluene at 343.15 K in kcal/mol. . . .	153
A.40 $\Delta G$ products with standard state shift in toluene at 343.15 K in kcal/mol.	154
A.41 $\Delta G$ TS-I <sub>2</sub> with standard state shift in toluene at 343.15 K in kcal/mol. .	155
A.42 $\Delta G$ (TS-I <sub>2</sub> )-TS without standard state shift in toluene at 373.15 K in	
kcal/mol. *: Optimized using the m5 grid. . . . .	156
A.43 $\Delta G$ TS without standard state shift in toluene at 373.15 K in kcal/mol. .	157
A.44 $\Delta G$ products without standard state shift in toluene at 373.15 K in kcal/mol.	158
A.45 $\Delta G$ TS-I <sub>2</sub> without standard state shift in toluene at 373.15 K in kcal/mol.	159
A.46 $\Delta G$ (TS-I <sub>2</sub> )-TS with standard state shift in toluene at 373.15 K in kcal/mol.	
*: Optimized using the m5 grid. . . . .	160
A.47 $\Delta G$ TS with standard state shift in toluene at 373.15 K in kcal/mol. . . .	161
A.48 $\Delta G$ products with standard state shift in toluene at 373.15 K in kcal/mol.	162
A.49 $\Delta G$ TS-I <sub>2</sub> with standard state shift in toluene at 373.15 K in kcal/mol. .	163



# References

- [1] A. Szabo, N. S. Ostlund, *Modern Quantum Chemistry*, Dover Publications, Mineola, NY, **1996**.
- [2] F. Jensen, *Introduction to Computational Chemistry*, John Wiley & Sons, Ltd., Chichester, 2. Edition, **2007**.
- [3] I. N. Levine, *Quantum Chemistry*, Prentice Hall, Upper Saddle River, NJ, 6. Edition, **2009**.
- [4] J. C. Slater, *Phys. Rev.* **1929**, *34*, 1293–1322.
- [5] T. D. Crawford, H. F. Schaefer, *An Introduction to Coupled Cluster Theory for Computational Chemists*, John Wiley & Sons, Inc., **2007**, pp. 33–136.
- [6] K. G. Dyall, K. Faegri Jr., *Introduction to Relativistic Quantum Chemistry*, Oxford University Press, New York, NY, **2007**.
- [7] M. Dolg, X. Cao, *Chem. Rev.* **2012**, *112*, PMID: 21913696, 403–480.
- [8] I. V. Abarenkov, V. Heine, *Philos. Mag.* **1965**, *12*, 529–537.
- [9] W. Schwarz, *Theoret. Chem. Acta* **1968**, *11*, 307–324.
- [10] L. R. Kahn, W. A. Goddard III, *J. Chem. Phys.* **1972**, *56*, 2685–2701.
- [11] L. R. Kahn, P. Baybutt, D. G. Truhlar, *J. Chem. Phys.* **1976**, *65*, 3826–3853.
- [12] W. C. Ermler, Y. S. Lee, P. A. Christiansen, K. S. Pitzer, *Chem. Phys. Lett.* **1981**, *81*, 70–74.
- [13] R. S. Mulliken, *J. Chem. Phys.* **1955**, *23*, 1833–1840.
- [14] C. J. Cramer, *Essentials of Computational Chemistry*, John Wiley & Sons, Ltd., Chichester, **2002**.
- [15] A. Greco, S. Cesca, G. Bertolini, *J. Org. Chem.* **1976**, *113*, 321–330.
- [16] A. Streitwieser, U. Mueller-Westerhoff, *J. Am. Chem. Soc.* **1968**, *90*, 7364–7364.
- [17] A. Streitwieser, S. A. Kinsley, J. T. Rigsbee, I. L. Fragala, E. Ciliberto, *J. Am. Chem. Soc.* **1985**, *107*, 7786–7788.

- [18] C. S. Neumann, P. Fulde, *Z. Phys. B Condens. Matter* **1989**, *74*, 277–278.
- [19] M. Dolg, P. Fulde, W. Kchle, C. Neumann, H. Stoll, *J. Chem. Phys.* **1991**, *94*, 3011–3017.
- [20] M. Dolg, P. Fulde, H. Stoll, H. Preuss, A. Chang, R. Pitzer, *Chem. Phys.* **1995**, *195*, 71–82.
- [21] N. M. Edelstein, P. G. Allen, J. J. Bucher, D. K. Shuh, C. D. Sofield, N. Kaltsoyannis, G. H. Maunder, M. R. Russo, A. Sella, *J. Am. Chem. Soc.* **1996**, *118*, 13115–13116.
- [22] H.-D. Amberger, H. Reddmann, F. T. Edelmann, *J. Org. Chem.* **2005**, *690*, 2238–2242.
- [23] C. H. Booth, M. D. Walter, M. Daniel, W. W. Lukens, R. A. Andersen, *Phys. Rev. Lett.* **2005**, *95*, 267202.
- [24] M. D. Walter, C. H. Booth, W. W. Lukens, R. A. Andersen, *Organomet.* **2009**, *28*, 698–707.
- [25] A. Streitwieser, S. A. Kinsley, C. H. Jenson, J. T. Rigsbee, *Organomet.* **2004**, *23*, 5169–5175.
- [26] G. Balazs, F. G. N. Cloke, J. C. Green, R. M. Harker, A. Harrison, P. B. Hitchcock, C. N. Jardine, R. Walton, *Organomet.* **2007**, *26*, 3111–3119.
- [27] A. Kerridge, R. Coates, N. Kaltsoyannis, *J. Phys. Chem. A* **2009**, *113*, 2896–2905.
- [28] A. Kerridge, *Dalton Trans.* **2013**, *42*, 16428–16436.
- [29] E. Kurras, C. Krüger, *Cambridge Structural Database deposit number CCDC 256935* **2004**.
- [30] O. Moossen, M. Dolg, *Chem. Phys. Lett.* **2014**, *594*, 47–50.
- [31] H.-J. Werner, P. J. Knowles, G. Knizia, F. R. Manby, M. Schütz, P. Celani, T. Korona, R. Lindh, A. Mitrushenkov, G. Rauhut, K. R. Shamasundar, T. B. Adler, R. D. Amos, A. Bernhardsson, A. Berning, D. L. Cooper, M. J. O. Deegan, A. J. Dobbyn, F. Eckert, E. Goll, C. Hampel, A. Hesselmann, G. Hetzer, T. Hrenar, G. Jansen, C. Köppl, Y. Liu, A. W. Lloyd, R. A. Mata, A. J. May, S. J. McNicholas, W. Meyer, M. E. Mura, A. Nicklass, D. P. O’Neill, P. Palmieri, D. Peng, K. Pflüger, R. Pitzer, M. Reiher, T. Shiozaki, H. Stoll, A. J. Stone, R. Tarroni, T. Thorsteins-son, M. Wang, MOLPRO, version 2012.1, a package of ab initio programs, see, Cardiff, UK, **2012**.
- [32] M. Douglas, N. M. Kroll, *Ann. Phys.* **1974**, *82*, 89–155.

- [33] B. A. Hess, *Phys. Rev. A* **1986**, *33*, 3742–3748.
- [34] G. Jansen, B. A. Hess, *Phys. Rev. A* **1989**, *39*, 6016–6017.
- [35] R. A. Kendall, T. H. Dunning Jr., R. Harrison, *J. Chem. Phys.* **1992**, *96*, 6796–6806.
- [36] D. E. Woon, T. H. Dunning Jr., *J. Chem. Phys.* **1993**, *98*, 1358–1371.
- [37] M. Dolg, *J. Chem. Theor. Comput.* **2011**, *7*, 3131–3142.
- [38] G. Balazs, F. G. N. Cloke, J. C. Green, R. M. Harker, A. Harrison, P. B. Hitchcock, C. N. Jardine, R. Walton, *Organomet.* **2007**, *26*, 3111–3119.
- [39] A. Ashley, G. Balazs, A. Cowley, J. Green, C. H. Booth, D. O’Hare, *Chem. Commun.* **2007**, 1515–1517.
- [40] M. Dolg, O. Moossen, *Journal of Organometallic Chemistry* **2015**, *794*, 17–22.
- [41] T. H. Dunning Jr., *J. Chem. Phys.* **1989**, *90*, 1007–1023.
- [42] W. A. de Jong, R. J. Harrison, D. A. Dixon, *J. Chem. Phys.* **2001**, *114*, 48–53.
- [43] P. Celani, H.-J. Werner, *J. Chem. Phys.* **2000**, *112*, 5546–5557.
- [44] M. Mödl, M. Dolg, P. Fulde, H. Stoll, *J. Chem. Phys.* **1996**, *105*, 2353–2363.
- [45] D. L. Clark, J. C. Gordon, P. J. Hay, R. Poli, *Organomet.* **2005**, *24*, 5747–5758.
- [46] K. Aparna, M. Ferguson, R. G. Cavell, *J. Am. Chem. Soc.* **2000**, *122*, 726–727.
- [47] H.-S. Chan, H.-W. Li, Z. Xie, *Chem. Commun.* **2002**, 652–653.
- [48] O. T. Summerscales, J. C. Gordon, *RSC Adv.* **2013**, *3*, 6682–6692.
- [49] O. Moossen, M. Dolg, *Comput. Theor. Chem.* **2015**, *1073*, 34–44.
- [50] R. Ahlrichs, M. Bär, M. Häser, H. Horn, C. Kölmel, *Chem. Phys. Lett.* **1989**, *162*, 165–169.
- [51] K. A. Peterson, D. Figgen, E. Goll, H. Stoll, M. Dolg, *J. Chem. Phys.* **2003**, *119*, 11113–11123.
- [52] F. Weigend, R. Ahlrichs, *Phys. Chem. Chem. Phys.* **2005**, *7*, 3297–3305.
- [53] H.-J. Werner, P. J. Knowles, *J. Chem. Phys.* **1985**, *82*, 5053–5063.
- [54] P. J. Knowles, H.-J. Werner, *Chem. Phys. Lett.* **1985**, *115*, 259–267.
- [55] H.-J. Werner, P. J. Knowles, *J. Chem. Phys.* **1988**, *89*, 5803–5814.
- [56] P. J. Knowles, H.-J. Werner, *Chem. Phys. Lett.* **1988**, *145*, 514–522.
- [57] T. H. Dunning, *J. Chem. Phys.* **1989**, *90*, 1007–1023.

- [58] W. J. Hehre, R. Ditchfield, J. A. Pople, *J. Chem. Phys.* **1972**, *56*, 2257–2261.
- [59] M. Mödl, M. Dolg, P. Fulde, H. Stoll, *J. Chem. Phys.* **1997**, *106*, 1836–1846.
- [60] X. Wang, H.-G. Cho, L. Andrews, M. Chen, D. A. Dixon, H.-S. Hu, J. Li, *J. Phys. Chem. A* **2011**, *115*, 1913–1921.
- [61] T. Mikulas, M. Chen, D. A. Dixon, K. A. Peterson, Y. Gong, L. Andrews, *Inorg. Chem.* **2014**, *53*, 446–456.
- [62] O. Moossen, M. Dolg, *J. Phys. Chem. A* **2016**, *120*, 3966–3974.
- [63] M. Dolg, H. Stoll, H. Preuss, *J. Chem. Phys.* **1989**, *90*, 1730–1734.
- [64] R. Gulde, P. Pollak, F. Weigend, *J. Chem. Theor. Comput.* **2012**, *8*, 4062–4068.
- [65] A. D. Becke, *Phys. Rev. A* **1988**, *38*, 3098–3100.
- [66] J. P. Perdew, *Phys. Rev. B* **1986**, *33*, 8822–8824.
- [67] A. D. Becke, *J. Chem. Phys.* **1993**, *98*, 5648–5652.
- [68] C. Lee, W. Yang, R. G. Parr, *Phys. Rev. B* **1988**, *37*, 785–789.
- [69] Y. Zhao, D. Truhlar, English, *Theo. Chem. Acc.* **2008**, *120*, 215–241.
- [70] C. Hampel, K. Peterson, H.-J. Werner, *Chem. Phys. Lett.* **1992**, *190*, 1–12.
- [71] M. J. O. Deegan, P. J. Knowles, *Chem. Phys. Lett.* **1994**, *227*, 321–326.
- [72] M. Breugst, E. Detmar, D. von der Heiden, *ACS Catalysis* **2016**, *6*, 3203–3212.
- [73] D. Rappoport, F. Furche, *J. Chem. Phys.* **2010**, *133*, 134105.
- [74] A. D. Becke, *J. Chem. Phys.* **1993**, *98*, 1372.
- [75] J. P. Perdew, K. Burke, M. Ernzerhof, *Phys. Rev. Lett.* **1996**, *77*, 3865–3868.
- [76] C. Adamo, V. Barone, *J. Chem. Phys.* **1999**, *110*, 6158.
- [77] J. Tao, J. P. Perdew, V. N. Staroverov, G. E. Scuseria, *Phys. Rev. Lett.* **2003**, *91*, 146401.
- [78] V. N. Staroverov, G. E. Scuseria, J. Tao, J. P. Perdew, *J. Chem. Phys.* **2003**, *119*, 12129–12137.
- [79] A. Klamt, G. Schramm, *J. Chem. Soc. Perkin Trans.* **1993**, *2*, 799–805.
- [80] S. Grimme, J. Antony, S. Ehrlich, H. Krieg, *J. Chem. Phys.* **2010**, *132*, 154104.
- [81] R. F. Ribeiro, A. V. Marenich, C. J. Cramer, D. G. Truhlar, *J. Phys. Chem. B* **2011**, *115*, 14556–14562.
- [82] S. Kozuch, J. M. L. Martin, *J. Chem. Theory and Comput.* **2013**, *9*, 1918–1931.



- 
- [83] C. Laurence, G. Guiheneuf, B. Wojtkowiak, *J. Am. Chem. Soc.* **1979**, *101*, 4793–4801.
- [84] D. von der Heiden, S. Bozkus, M. Klussmann, M. Breugst, *J. Org. Chem.* **2017**, *82*, 4037–4043.
- [85] K. J. Borah, M. Phukan, R. Borah, *Synth. Commun.* **2010**, *40*, 2830–2836.
- [86] J. Schmauck, M. Breugst, *Org. Biomol. Chem.* **2017**.



# Danksagung

- Ich danke vor allem Prof. Dr. Michael Dolg für die jahrelange Unterstützung und die Möglichkeit meine Doktorarbeit in seiner Arbeitsgruppe angefertigt haben zu dürfen.
- PD Dr. Michael Hanrath möchte ich ebenfalls für die jahrelange Unterstützung danken, für alle hitzigen und nicht hitzigen, fachlichen und nicht fachlichen Diskussionen, sowie den großen und kleinen Hilfestellungen bei meiner Forschung. Ganz besonders möchte ich mich für den zusätzlich angebotenen Programmierkurs bedanken.
- Ich danke zudem Prof. Dr. Axel Klein für die Übernahme des Prüfungsvorsitzes und Dr. Xiaoyan Cao-Dolg für die Übernahme des Prüfungsbeisitzes.
- Meinen ehemaligen Arbeitskollegen Jan Ciupka, Tim Hangele und Daniel Weißmann, sowie den aktuellen Arbeitskollegen Sascha Bubeck, Nils Herrmann, Nikolas Nowak und Mad Max Mörechen möchte ich mich ebenfalls für die schöne Zeit im Arbeitskreis Dolg danken.
- Ich möchte mich ganz herzlich bei Linda Jütten, Yannic Falke, Nikolas Nowak, Sascha Bubeck und Nils Herrmann für das Korrekturlesen meiner Dissertation bedanken.
- Ein großer Dank gilt meinen Eltern Christel und Hans-Joachim Mooßen, die mich mein ganzes Leben tatkräftig unterstützt haben und die mir das Studium in Köln erst ermöglicht haben.
- Ein besonderes Dankeschön möchte ich an meine Schwester Sandra Mooßen richten, die nicht nur seit Kindheitstagen meine beste Freundin ist, sondern mir auch als WG-Mitbewohnerin in Köln eine grandiose Zeit geschenkt hat.
- Desweiteren danke ich meiner kompletten Familiensippe für die tollen Jahre in meiner Heimatstadt Hagen und den überragenden Familienzusammenhalt. Ich werde selbstverständlich jeden namentlich aufzählen:

- meine tollen Großeltern: Ruth Mooßen, Doris und Ewald Scheene
- meine tollen Tanten und Onkel: Marina Kuper, Angelika und Josef Zarnke, Doris und Matthias Titze, Andrea und Dirk Scheene, sowie Marc und Claudia Scheene
- meine tollen Cousins und Cousinen: Christian und Lisa Titze, Sven und Björn Kuper, Jennifer Zarnke, Tim und Jan Scheene
- Ich danke meinen Studiumsleidensgenossen und langjährigen Freunden Nikolas Nowak, Marco Klein und Moritz Vollmer, die mich seit meinem ersten Semester im Chemiestudium begleitet haben.
- Ich bedanke mich bei allen, die auch über die fachlichen Aspekte einer Promotion hinaus, die Arbeit im Departement für Chemie bereichert und unvergessen gemacht haben:
  - AK Goldfuß: Falco Fox, Florian Wolf, Eric Brüllingen, Florian Dato und Vanessa Grote
  - AK Griesbeck: Moritz Vollmer, Margarethe Kleczka, Murat Atar, Angelika Eske, Florian Gaida, Diana But, Wolfram Schulze, Banu Öngel und Melissa Renner
  - Marco Klein, Julia Westphal, Daniel von der Heiden, Katrin Peckelsen, Yannic Falke, Flore Mees, Nikolas Nowak, Katharina von Schoeler
- Einen eigenständigen Dankesabschnitt widme ich natürlich Linda Jütten, die mich seit Jahren beruflich wie privat begleitet, aufrichtet und unterstützt. Diese Arbeit, wie auch mein Studium erfolgreich zu absolvieren wäre ohne sie nicht möglich gewesen und das Leben ist mit ihr ist als ohne sie. Daher danke ich im wesentlichen für alles.

# Erklärung

Ich versichere, dass ich die von mir vorgelegte Dissertation selbstständig angefertigt, die benutzten Quellen und Hilfsmittel vollständig angegeben und die Stellen der Arbeit - einschließlich Tabellen, Karten und Abbildungen -, die anderen Werken im Wortlaut oder dem Sinn nach entnommen sind, in jedem Einzelfall als Entlehnung kenntlich gemacht habe; dass diese Dissertation noch keiner anderen Fakultät oder Universität zur Prüfung vorgelegen hat; dass sie - abgesehen von unten angegebenen Teilpublikationen - noch nicht veröffentlicht worden ist sowie, dass ich eine solche Veröffentlichung vor Abschluss des Promotionsverfahrens nicht vornehmen werde. Die Bestimmungen der Promotionsordnung sind mir bekannt. Die von mir vorgelegte Dissertation ist von Prof. Dr. Michael Dolg betreut worden.

Nachfolgend genannte Teilpublikationen liegen vor:

- O. Mooßen, M. Dolg, *Chem. Phys. Lett.* **2014**, 594, 47-50.
- M. Dolg, O. Mooßen, *J. Organomet. Chem.* **2015**, 794, 17-22.
- O. Mooßen, M. Dolg, *Comput. Theor. Chem.* **2015**, 1073, 34-44.
- O. Mooßen, M. Dolg, *J. Phys. Chem. A* **2016**, 120(22), 3966-3974.

Ich versichere, dass ich alle Angaben wahrheitsgemäß nach besten Wissen und Gewissen gemacht habe und ich verpflichte mich, jedmögliche, die obigen Angaben betreffenden Veränderungen, dem Dekanat unverzüglich mitzuteilen.

---

(Datum)

---

(Unterschrift)



# Lebenslauf

## Persönliche Daten

Name: Oliver Mooßen  
Geburtsdatum: 19.02.1989 in Hagen  
Staatsangehörigkeit: deutsch  
Familienstand: ledig

## Promotion

November 2014 - Mai 2018: Promotion bei Prof. Dr. Michael Dolg im Bereich Theoretische Chemie zum Thema „Interpretation of ab initio Calculations of Cerium Compounds and Predictive Power of Density Functional Theory Calculations for Iodine Catalysis “

## Hochschulstudium

Oktober 2012 - September 2014: Masterstudium in Chemie an der Universität zu Köln  
Oktober 2009 - Oktober 2012: Bachelorstudium in Chemie an der Universität zu Köln  
Oktober 2008 - September 2009: Bachelorstudium in Wirtschaftsmathematik an der Universität zu Köln

## Schulbildung

1999 - 2008: Theodor-Heuss-Gymnasium in Hagen  
1995 - 1999: Meinolfschule in Hagen

## **Beruflicher Werdegang**

April 2013 - Juli 2018:	Wissenschaftliche Hilfskraft im Institut für Theoretische Chemie für Forschung und Lehre
März 2013 - Februar 2014:	Wissenschaftliche Hilfskraft als Tutor für Physik und Physikalische Chemie
Juni 2012 - Februar 2013:	Studentische Hilfskraft als Tutor für Physik und Physikalische Chemie

---

(Datum)

---

(Unterschrift)